USGS
science for a changing world

Geologic Investigations in the Lake Valley Area, Sierra County, New Mexico

U.S. Geological Survey Professional Paper 1644

U.S. Department of the Interior
U.S. Geological Survey

Front and back cover. Lake Valley mines and mill, Sierra County, New Mexico.

Geologic Investigations in the Lake Valley Area, Sierra County, New Mexico

By J.M. O'Neill, *Editor*

U.S. Geological Survey Professional Paper 1644

Chapter titles and authors are listed on volume contents page

U.S. Department of the Interior
U.S. Geological Survey

U.S. Department of the Interior
Gale A. Norton, Secretary

U.S. Geological Survey
Charles G. Groat, Director

Version 1.0

First Printing 2002

For sale by U.S. Geological Survey, Information Services
Box 25286, Federal Center
Denver, CO 80225

This report is also available online at:
http://geology.cr.usgs.gov/pub/ppapers/p1644/

Published in the Central Region, Denver, Colorado
Manuscript approved for publication March 30, 2001
Graphics by authors and Gayle M. Dumonceaux
Photocomposition by Gayle M. Dumonceaux
Edited by Lorna Carter

Any use of trade, product, or firm names in this publication
is for descriptive purposes only and
does not imply endorsement by the U.S. Government

Library of Congress Cataloging-in-Publication Data

Geologic investigations in the Lake Valley area, Sierra County, New Mexico / by J.M. O'Neill, editor.
p. cm.—(U.S. Geological Survey professional paper ; 1644)
Includes bibliographical references.
1. Geology—New Mexico—Lake Valley Region (Sierra County). 2. Mines and mineral resources—New Mexico—Lake Valley Region (Sierra County). I. O'Neill, J. Michael. II. Series.

QE144.L33 G46 2002
557.3 s—dc21
[557.89′67]

2001033355

ISBN: 0-607-96957-1

Volume Contents

(Letters designate chapters)

PREFACE

The Caballo Resource Area is a Bureau of Land Management (BLM) designated region that includes all of Sierra and Otero Counties, south-central New Mexico. Within this resource area of more than 33,790 square kilometers, nearly one-fourth of the land is administered by the BLM. At the request of the BLM, the area of the historic Lake Valley mining district and townsite, at the southeastern margin of the Black Range of western Sierra County, New Mexico, was evaluated for its potential for undiscovered mineral resources (Nutt and others, 1998). The BLM-designated study area, called the Lake Valley Area of Critical Environmental Concern (ACEC), is located in the northern part of the Lake Valley $7^1/_2'$ quadrangle, New Mexico. An area of more than 195 square kilometers in the area of the Lake Valley ACEC was mapped to increase understanding of ore controls and to effectively assess mineral potential. The geology of this map area is described in this Professional Paper.

This report is divided into four chapters whose themes and content inform each other in contributing to a complete discussion of the area; each chapter is also designed to stand alone as an individual report. The first chapter describes the geology of the northern part of the Lake Valley quadrangle and the adjacent McClede Mountain $7^1/_2'$ quadrangle to the north. The second chapter presents the results of geophysical investigations, carried out to assist in the interpretation of the subsurface geology of the map area. The third chapter describes the mining history of Lake Valley and the character of its ore deposits. The fourth chapter is a geochemical study, undertaken to determine the potential for contamination of the surrounding area from abandoned mine dumps in the mining district.

Note that because the four chapters cite many of the same references, all references from the four have been combined into a single listing that is located at the end of the volume, beginning on page 76.

Geology of the Lake Valley Area

By J.M. O'Neill, D.A. Lindsey, D.C. Hedlund, C.J. Nutt, *and* J.C. Ratté

U.S. Geological Survey Professional Paper 1644–A

Description of the geologic framework of Lake Valley and the surrounding area

GEOLOGIC INVESTIGATIONS IN THE LAKE VALLEY AREA, SIERRA COUNTY, NEW MEXICO

U.S. Department of the Interior
U.S. Geological Survey

Contents

Plate

Figures

Tables

Note: Combined references list begins on page 76.

Geology of the Lake Valley Area

By J.M. O'Neill, D.A. Lindsey, D.C. Hedlund, C.J. Nutt, *and* J.C. Ratté

Abstract

The historic Lake Valley townsite and silver-manganese mining district lies along the southeastern margin of the Black Range of western Sierra County, New Mexico. At the request of the Bureau of Land Management, the U.S. Geological Survey assessed the Lake Valley Area of Critical Environmental Concern (ACEC) for undiscovered mineral resources. As part of the study, an area surrounding the Lake Valley ACEC was mapped to understand ore controls and to assess mineral-resource potential. Prior production from the Lake Valley district exceeded 6,000,000 troy ounces of silver. Time of mineralization is middle to late Tertiary.

Lake Valley is located in a structurally elevated fault block underlain mainly by Ordovician through Pennsylvanian sedimentary rocks; ore deposits are stratabound and confined to Lower Mississippian Lake Valley Formation carbonate rocks. Much of the terrane surrounding the mining district consists of middle Tertiary volcanic rocks of the Mogollon-Datil volcanic field. Specifically, the mining district is situated near the southeast edge of the Emory cauldron, one of the largest volcanic centers within the field. Volcanic rocks include flows, breccias, ash-flow tuffs, and intrusive-extrusive rhyolites.

Faulting within the Lake Valley area is largely confined to three major episodes: an older northwest-trending normal fault episode that in part restricted the deposition of the oldest volcanic flows in the area; an intermediate period of ring fracture faulting related to volcanism and collapse of the Emory cauldron; and a younger episode of deformation related to the formation of the Rio Grande rift.

The Lake Valley and Berrenda faults are the major structural features in the study area. Geologic and geophysical data suggest that the Lake Valley fault is composed of two segments: a southern, northwest-striking segment that may have a pre-Tertiary history and that is now joined with a northerly-striking segment that is part of the Emory cauldron ring fracture zone. The mining district is bounded by the southern, northwest-striking segment of the fault, which may have acted as the conduit for late-stage intrusion of a rhyolite dome adjacent to the mining district. The Berrenda fault does not appear to be related to the collapse of the Emory cauldron; rather, the fault bounds the Animas basin, the westernmost Rio Grande rift-related structure in the Lake Valley area.

Introduction

The discovery of gold deposits in the vicinity of Hillsboro, 32 km north of Lake Valley (fig. 1), and the mining of rich silver deposits in the Kingston district west of Hillsboro and at Lake Valley from 1882 to 1896 led to early geologic investigations in the area by Lindgren and others (1910). Their descriptions of the geology, mines, and structural and stratigraphic controls of ore deposition provided a framework for later studies. The decline of silver prices in 1893, which accompanied the abandonment of silver as a monetary standard, greatly diminished mining activity in the southern Black Range.

Many of the silver workings were reopened during World War II for production of low-grade manganese, which occurs in the oxidized parts of the silver and base-metal deposits in this region. Detailed district and mine maps of the Lake Valley manganese district were completed by the U.S. Geological Survey in 1953 (Creasey and Granger, 1953).

The geology of the Lake Valley 15′ quadrangle was mapped and discussed by Jicha (1954). Hedlund (1977a, b) mapped the geology and described the mineral resources of the Hillsboro and San Lorenzo 15′ quadrangles north of the Lake Valley quadrangle. A regional geologic map of the northwest part of the Las Cruces 1°× 2° sheet (Seager and others, 1982) includes both the Lake Valley and Hillsboro quadrangles. Seager (1986) also published a geologic map of the Hillsboro and adjacent San Lorenzo 15′ quadrangles. These geologic maps have greatly aided in the resolution of the complex volcanic stratigraphy in this region.

The Emory cauldron, from which significant parts of the volcanic rocks in the map area were erupted, underlies the western parts of both the Lake Valley and Hillsboro 15′ quadrangles and lies just west of the western margin of the study area. The volcanic center, first recognized by Ericksen and others (1970), is one of the largest Tertiary volcanic vents in the Mogollon-Datil volcanic field of southwestern New Mexico and underlies most of the southern and central Black Range.

Regional Geology

The Black Range is on the northeast edge of the Late Cretaceous to early Tertiary (Laramide) volcanic-plutonic arc of southwestern United States. The west- to northwest-trending, arc-related porphyry copper belt of Arizona and southwestern New Mexico is represented by the Tyrone and Santa Rita intrusions south and west of Lake Valley; the easternmost of these intrusions, the 75.1 ± 2.5 Ma copper porphyry (Hedlund, 1974) at Hillsboro (fig. 2), crops out just north of Lake Valley.

Lake Valley is near the crest of the now buried, northwest-trending Rio Grande uplift of Laramide age and directly south of the associated Love Ranch basin (fig. 2). Scattered outcrops of Love Ranch Formation are preserved in the Lake Valley area (Seager and others, 1986).

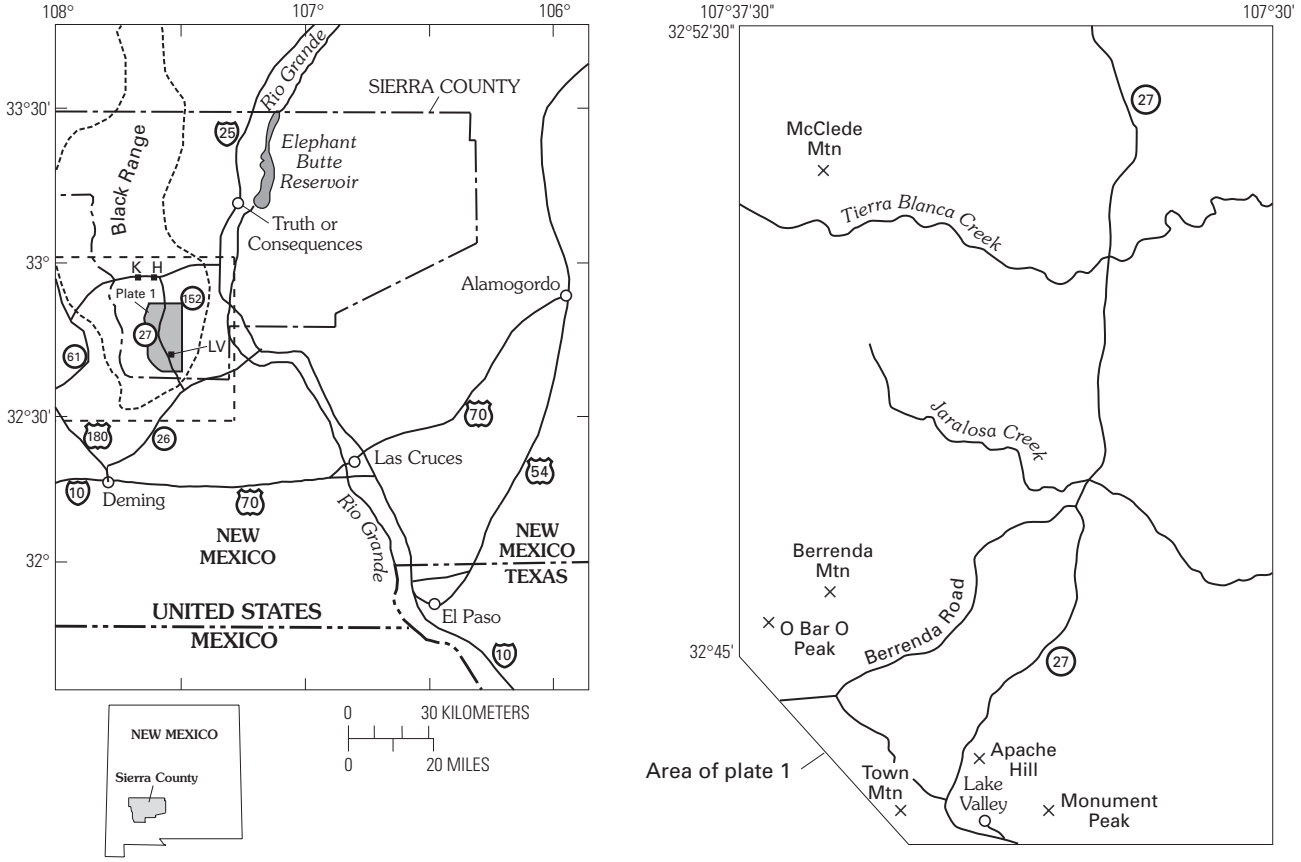

Figure 1. Index map of Lake Valley area, Sierra County, N. Mex. LV, Lake Valley; H, Hillsboro; K, Kingston. Dashed line, area of geophysical study, Chapter B; dotted line, outline of Black Range.

The geology of the Black Range is dominated by Tertiary volcanic rocks, many associated with the Oligocene Emory cauldron, which is located just northwest of the study area (fig. 2). The Mogollon-Datil volcanic field of southwestern New Mexico, of which the Emory cauldron is a part, consists in the Lake Valley area of Eocene and Oligocene volcanic rocks. Eocene (40–36 Ma) intermediate volcanism was followed by Eocene to Oligocene (36–24 Ma) basaltic to andesitic and silicic volcanism. The Emory cauldron in the Black Range, first recognized by Ericksen and others (1970) and later briefly described by Elston and others (1975), is one of the largest cauldrons in the Mogollon-Datil volcanic field. The cauldron is an elongate, north-northeast-trending structure that measures about 48×19 km and is cut by north-trending normal faults of Oligocene and younger age. Formation of the cauldron commenced with the eruption of the Kneeling Nun Tuff. Coeval with this eruption was the intrusion of numerous rhyolite plugs best exposed in the central part of the cauldron along the crest and western slopes of the Black Range (Hedlund, 1977a); many clasts from these plugs were incorporated in the basal parts of the ash flow. The cauldron collapsed during eruption of the 34.9 Ma Kneeling Nun Tuff. Cauldron resurgence was accompanied by eruption of the 34.5 Ma Mimbres Peak Formation (McIntosh and others, 1991, 1992). Whereas the Kneeling Nun is a widespread ignimbrite unit, the Mimbres Peak occurs largely in domes and intrusions along the edges and within the ring fracture zone of the cauldron (fig. 2). The 36–24 Ma volcanic activity of the Mogollon-Datil volcanic field was associated with multiple cauldron development and included at least four pulses of silicic magmatism (McIntosh and others, 1992).

The central Black Range was also the focus of local, noncaldera-related magmatism during a major episode of volcanism at 29.0–27.4 Ma (McIntosh and others, 1992; Harrison, 1990), represented by emplacement of rhyolite domes and flows. On their regional map, Seager and others (1982) showed intrusions of this younger age along the southwest edge of the Emory cauldron, but had difficulty in distinguishing rhyolites of this age from Mimbres Peak rhyolites.

Paleozoic sedimentary rocks of the southeast Black Range crop out in uplifted and eroded fault blocks. They consist of predominantly carbonate rocks and lesser clastic rocks deposited on a shallow, stable, south-dipping platform present in much of southern and central New Mexico.

The Palomas basin is east of the Lake Valley study area; the basin is part of the vast Rio Grande rift, a system of basins and ranges bounded by extensional faults that has been intermittently active since late Oligocene time, but most notably in Miocene and Pliocene time (Seager and others, 1984). The Miocene and Pliocene faults have appreciable displacement (1,525–3,050 m) and have served as conduits for the eruption of

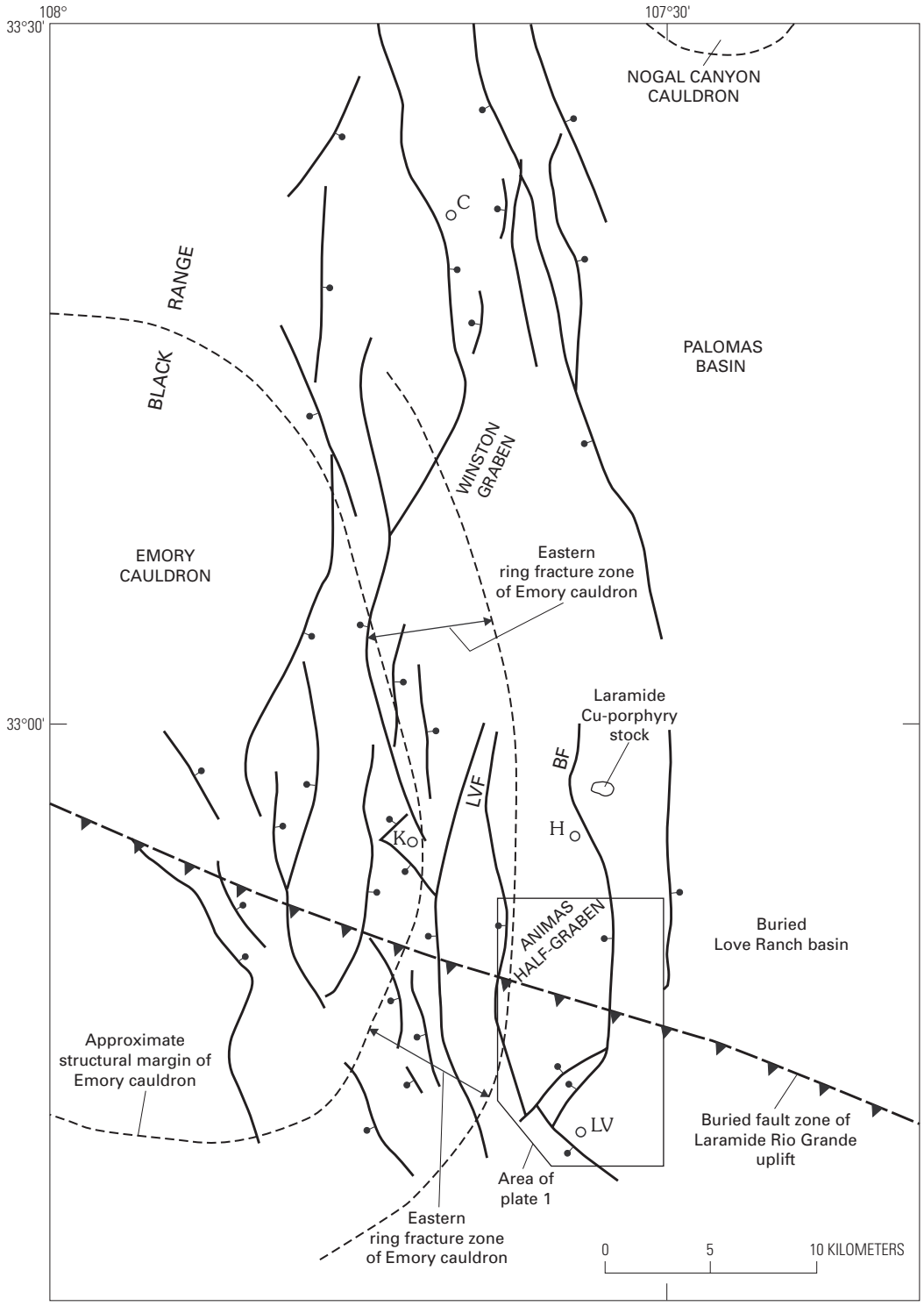

Figure 2. Major volcanic and tectonic features of Lake Valley and adjacent area (simplified from Callender and others, 1983). C, Chloride; H, Hillsboro; K, Kingston; LV, Lake Valley; LVF, Lake Valley fault; BF, Berrenda fault. Bar and ball on fault show downthrown side where known; sawteeth are on upthrown block of Laramide Rio Grande uplift.

numerous basalt flows in the Hillsboro area north of Lake Valley (Hedlund, 1977a). The Animas half-graben north of the Lake Valley study area (fig. 2) is the southern part of the 80 km long Winston graben, the westernmost extensional basin of the Rio Grande rift at this latitude.

The map area of plate 1 is near the southeast edge of the Emory cauldron and includes the Rio Grande rift-related Animas half-graben (Animas basin) (Seager and others, 1982; Harrison, 1990). Rocks exposed in the map area include Paleozoic carbonate and clastic rocks, scattered thin outcrops

of Paleocene to Eocene Love Ranch Formation sedimentary rocks, a complex sequence of Eocene to Oligocene volcanic rocks and interbedded sedimentary rocks of the Mogollon-Datil volcanic field, and Miocene and younger Santa Fe Group sedimentary and interlayered volcanic rocks. Mesozoic strata are not present and were apparently removed by erosion during and after uplift of this area in Laramide time (Seager and others, 1986).

The principal structural features of the map area are east- to southeast-dipping fault blocks cut by north-, northeast-, and northwest-striking normal faults (pl. 1). The Berrenda and Lake Valley faults divide the map area into separate tilted blocks. The Berrenda fault is the southeast and east boundary of the Animas basin; the northern part of the Lake Valley fault is the easternmost of the ring fracture faults of the Emory cauldron (Elston, 1989). The north-trending blocks or half-grabens in this area appear to have formed initially after deposition of the Kneeling Nun Tuff inasmuch as mappable basin-fill deposits of coarse sand, arkose, and gravel are interlayered with overlying volcanic flows. The Animas basin is filled with thick deposits of Santa Fe Group rocks indicating major faulting and subsidence in Miocene and Pliocene time.

Paleozoic Sedimentary Rocks

Ordovician to Pennsylvanian sedimentary rocks crop out in the map area (pl. 1). Middle Cambrian strata that rest unconformably on Precambrian basement rocks in this region are, in the study area, covered by volcanic rocks or downdropped and concealed along normal faults. Carbonate strata of dominantly shallow marine origin constitute most of the Paleozoic section; siliciclastic strata include the Upper Devonian Percha Shale, discontinuous exposures of the Middle Ordovician Cable Canyon Sandstone Member of the Second Value Dolomite, and the arenaceous Lower Mississippian Caballero Formation.

Ordovician

The oldest sedimentary rocks exposed in the map area consist of the Lower Ordovician El Paso Group, which is divided into (ascending) the Sierrita Limestone and Bat Cave Formation (Kelly and Silver, 1952). Thickness of the group in the Lake Valley–Hillsboro region is about 146 m (Hedlund, 1977a); however, only rocks correlative with the Bat Cave Formation are exposed in the study area. The Bat Cave consists of medium-light-gray, poorly fossiliferous limestone beds that are laminated to thin to medium bedded and finely crystalline. Some beds are pelletal and locally are brown weathering and silty. Intraformational breccias are common, and nodular to ropy chert is especially common in the upper 21 m.

The Middle and Upper Ordovician Montoya Group consists of three formations that were not mapped separately (ascending): the Second Value Dolomite (Middle Ordovician) and the Aleman Formation and Cutter Dolomite (both Upper Ordovician). All formations in the Hillsboro area have an aggregate thickness of 140 m (Hedlund, 1977a), whereas the group aggregates only 61.5 m in the Lake Valley area (Jicha, 1954). The Second Value Dolomite consists of two members: the basal Cable Canyon Sandstone Member is a discontinuous, medium- to coarse-grained, well-cemented thick-bedded and crossbedded sandstone with a maximum thickness of about 10 m. The upper part of the formation consists of medium-gray, thick-bedded, finely crystalline dolomite, which grades upward into light-gray dolomite that contains abundant disseminated rounded and frosted quartz grains as much as 4 mm across. The uppermost part of the formation is medium-gray to black, massive, sugary textured dolomite. Total thickness is about 26 m.

The overlying Aleman Formation consists of laminated chert layers 1–3 cm thick alternating with medium-gray, very fine crystalline dolomite beds about 2–3 cm thick. The chert beds are more continuous in the lower part of the section. Average thickness of the unit is about 12 m.

The Cutter Dolomite, in the uppermost part of the Montoya, is laminated to thinly bedded in the lower part, becoming thickly bedded to massive in the upper part. The formation is poorly fossiliferous except for a few silicified colonial corals (*Mesofavosites* sp.). Scattered jasperoid in the Montoya Group fills what we interpret as small karst-related collapse features.

Silurian

The Lower Silurian (Poole and others, 1992) Fusselman Dolomite is a distinctive cliff-forming, thick-bedded, medium-gray to dark-olive-gray dolomite in its lower part; it grades upward into ledge-forming, medium-gray dolomite that contains locally abundant brown-weathering chert and siliceous crusts, stringers, and lenses. This silicified rock, or jasperoid, is most prominent at the upper contact between the Fusselman and overlying Percha Shale. The jasperoid commonly shows brecciated textures that predate silicification. In the map area, Quartzite Ridge is a dip slope of Fusselman jasperoid. We suggest that the jasperoid is concentrated in the upper Fusselman because of slippage and brecciation along the contact between competent Fusselman and ductile Percha Shale and because the Percha Shale served as a cap to fluids that moved out along the brecciated contact.

Devonian

The Upper Devonian Percha Shale is typically poorly exposed, forming gentle slopes beneath the overlying Mississippian carbonate rocks. The formation has been divided into the Ready Pay Member and the overlying Box Member. The Ready Pay Member consists of black to olive-black, highly fissile shale, 30–33 m thick. The Box consists of about 9 m of dark-gray to medium-gray to pale-yellowish-green silty shale with limestone nodules especially common in the lowest 6 m.

Mississippian

Most of the Mississippian strata in the southern Black Range are Osagean in age, but in the map area, the Caballero Formation is of Kinderhookian age. In the map area the Mississippian strata include the Caballero Formation, the lowermost formation, and the overlying Lake Valley Limestone, named for exposures near the Lake Valley mining district. The Lake Valley Limestone, divided into six members by Laudon and Bowsher (1949), is about 73.5 m thick in the map area (Jicha, 1954). Because most of the mineralized rock in the Lake Valley mining district is restricted to certain members of the Lake Valley, four members in the study area were mapped separately.

The Caballero Formation consists of a basal arenaceous, crossbedded limestone overlain by thin-bedded, marly limestone beds that contain abundant crinoidal columnals and minor black, ropy chert. Thin interbeds of black and gray chert-pebble conglomerate are locally present in the upper part. Thickness is variable, ranging from 1–2 m in the north to as much as 11 m near Lake Valley.

The overlying Lake Valley Formation consists of four members in the study area. The lowermost Andrecito Member consists of medium-light-gray, thin-bedded argillaceous limestone with undulose bedding surfaces. The slope-forming limestone contains abundant fenestelloid bryozoa and minor crinoid columnals.

The overlying Alamogordo Member is a distinctive ledge-forming limestone unit. It consists of evenly spaced beds 0.5–1 m thick and contains minor, distinctive dark-gray chert nodules in the lowest 1.5 m. The limestone is medium gray to light gray, very finely crystalline, and nonfossiliferous.

The Nunn Member consists of medium-gray, thin-bedded, slope-forming, marly, coarse-crystalline limestone that commonly contains abundant crinoid fragments. Minor amounts of ropy black chert occur in the upper 15 m of the member.

The uppermost Tierra Blanca Member consists of medium-light-gray limestone that contains distinctive and abundant white to very light gray chert nodules and lenses. The member is medium bedded and medium to coarsely crystalline and commonly forms ledges that weather to abundant white chert rubble.

Pennsylvanian

The Magdalena Group carbonate rocks are incompletely exposed in the map area due to faulting and concealment by younger Tertiary volcanic rocks. The Magdalena consists of two formations—the Middle and Upper Pennsylvanian Oswaldo and the overlying Upper Pennsylvanian Syrena Formations—that were not mapped separately during this study. The group consists mostly of medium-gray, medium- to thick-bedded, fine-grained to very fine grained crystalline limestone. The unit commonly contains silty limestone laminae that weather to a yellowish gray and a rubble of light-brown plates as much as 2.5 cm thick. The group contains locally abundant brachiopods, gastropods, fusulinids, and horn corals. Maximum exposed thickness of the group in the map area is less than about 60 m.

Cenozoic Sedimentary Rocks

Paleocene and Eocene

Discontinuous exposures of the Paleocene to Eocene Love Ranch Formation overlie the Paleozoic carbonate rocks in the map area (pl. 1). The Love Ranch is a basin-fill deposit shed from the adjacent Laramide Rio Grande uplift (Seager and others, 1986). In the map area, the Love Ranch consists mostly of locally derived pebble to cobble conglomerate and minor red siltstone and shale, and is mapped only locally, north of Lake Valley.

Oligocene

Oligocene fluvial and alluvial deposits (Tt on pl. 1) locally are interlayered with volcanic rocks in the area south of McClede Mountain. These deposits, tentatively correlated with the Oligocene part of the Thurman Formation, are the oldest sedimentary fill in the Animas basin. The alluvial-fluvial deposits separate Kneeling Nun Tuff (Tk, pl. 1) from the overlying trachyandesite (Tta, pl. 1) and the trachyandesite from andesitic and rhyolitic deposits (Tsa and Tvp, pl. 1). All of the volcanic rocks interlayered with the sedimentary deposits are interpreted to be younger than the 34.5 Ma Mimbres Peak Formation; thus the clastic sedimentary lenses that separate them are no older than 34.5 Ma.

Sedimentary basin-fill deposits have been described from the Caballo Mountains 20 mi (32 km) east of the Lake Valley area. These rocks include the Eocene Palm Park Formation and the Oligocene and Miocene Thurman Formation (Seager and Hawley, 1973). The Thurman Formation at its type locality is interlayered with middle Oligocene basaltic volcanic rocks and also includes a basal ash-flow tuff that has yielded a K-Ar age of 34 Ma (Seager and Hawley, 1973, p. 9). Seager and Hawley interpreted the Thurman Formation as a broad alluvial apron that was periodically inundated by basaltic andesites from vents of the Sierra de Las Uvas volcanic center. The thin alluvial and fluvial deposits south of McClede Mountain are similar in age to basal Thurman strata and are interlayered with Oligocene volcanic rocks. Based on these similarities, the deposits in the map area are tentatively correlated with the lower part of the Thurman Formation.

The Oligocene air-fall tuff which overlies Thurman-like strata pinches out on the south within strata that we suspect also are lower Thurman. Seager (1986) correlated these deposits with the upper Miocene Rincon Valley Formation of the Santa Fe Group. We do not dispute the presence of Santa Fe Group rocks in this area, but suggest that lowermost rocks included in the Santa Fe by Seager likely include Thurman Formation. Poor exposures and concealment of strata by younger pediment gravels do not permit the accurate mapping of the contact between the Thurman and the Santa Fe Group Rincon Valley Formation; the contact between the two units shown on plate 1 separates moderately east dipping and indurated alluvium and fanglomerate, resting directly on moderately east dipping upper Oligocene volcanic rocks, from very poorly exposed, finer grained and less well cemented basin-fill deposits of the Rincon Valley Formation.

Miocene

Within the map area the Santa Fe Group is largely restricted to an east-tilted half-graben directly west of Sibley Mountain and poorly exposed consolidated deposits on the east side of Sibley Mountain. Deposits west of Sibley Mountain were mapped as upper Miocene Rincon Valley Formation of the Santa Fe by Seager and others (1986). As discussed just preceding, we map the Thurman Formation as the basal part of the basin-fill deposits of the Animas basin.

Pliocene and Quaternary

Quaternary surficial deposits are common in the map area. Older Pliocene and Pleistocene pediment deposits (QTpo) were shed eastward from block-faulted mountain fronts along the eastern margin of the Black Range. Pediment gravels are commonly incised by contemporary stream systems and locally overlain by alluvial fan deposits directly adjacent to mountain fronts.

Included with Quaternary deposits is an elongate north-northeast-trending zone of coalescing landslide deposits or earth flows of Quaternary age (Qls). The deposits parallel the eastern foot of Quartzite Ridge between Lake Valley and Jaralosa. The earth flows consist mostly of brecciated fragments of Fusselman Dolomite and the Lake Valley Limestone; clasts larger than 1–2 m across are common.

The deposits consist of three types.

1. Chaotically mixed, poorly sorted, randomly oriented, angular blocks of limestone and dolomite in a finer grained, lithologically similar matrix constitute the bulk of the deposit on the south and west. The debris consists almost exclusively of Fusselman Dolomite and Lake Valley Formation and everywhere rests directly on Percha Shale. The base of the deposits, where exposed, is a mixture of carbonate clasts in a matrix of strongly contorted Percha Shale.

2. A second type of deposit occupies the area directly southeast of Berrenda Creek. This area is marked by huge slabs of randomly oriented Lake Valley Limestone that are complexly interlayered with younger, Tertiary Rubio Peak Formation volcanic rocks.

3. The third type, characterized by deposits preserved on the low mesas directly north of Berrenda Creek, consists of large, semi-coherent slabs of Fusselman Dolomite that rest directly on younger Percha Shale. So deceiving is this exposure that it has been repeatedly identified as in-place bedrock of the Lake Valley Limestone (Seager and others, 1982; data of Hedlund, 1997).

The landslide deposits appear to occupy a paleovalley of late Quaternary age carved by Berrenda Creek and its tributaries into the Devonian Percha Shale. The creek cut a narrow gap through the resistant, east-dipping, silicified Fusselman Dolomite that underlies Quartzite Ridge on the west (pl. 1). East of the ridge, the creek carved a broad valley into the younger, overlying Percha Shale. Two main orthogonal tributaries of Berrenda Creek, east of and parallel to Quartzite Ridge, flowed into this valley from the north and south. The larger of these tributaries was on the south and was bounded by abrupt bedrock highlands on both sides (Quartzite Ridge on the west and Apache Hill on the east). The broad lowland along the creek and directly east of Quartzite Ridge was apparently dammed, and a lake of unknown duration was formed (Ql, pl. 1). Bedrock units from the adjacent high areas were shed into the valley of the southern tributary feeding the lake and apparently "flowed" down the tributary toward the lake and Berrenda Creek. A large slab of Fusselman Dolomite was apparently dislodged from the north end of Quartzite Ridge and displaced eastward into the northern tributary and the broad lake valley, sliding on the incompetent Percha Shale. Bedrock exposures of Lake Valley Limestone and overlying Rubio Peak volcanic rocks south of Berrenda Creek apparently were structurally unstable in this shaly, water-saturated lowland. The shale on the south, overlain by a rigid carapace of carbonate and volcanic rocks, apparently failed to support the overburden, flowed laterally, and disrupted the stratigraphic layering in the overlying rocks such that a complex mixing of semi-rigid blocks ensued. Hydrologic saturation of this area may have been the driving force for failure and extreme disruption of adjacent bedrock exposures.

The age of the landslide deposits appears to be Quaternary. The area drained by Berrenda Creek and its tributaries and now occupied by the landslide and earth flow deposits was overlain by a continuous pediment surface of late Quaternary age (Qpy, pl. 1) that extended from McClede Mountain southeastward to Berrenda Creek and the south end of Sibley Mountain and beyond. The gravels of this pediment surface are now preserved as isolated remnants on flat, bedrock mesas directly north and south of the landslide deposits. The paleovalley that was infilled with landslide deposits is being exhumed today and appears to have been an integral part of the incised stream system that is inset into the pediment surface (Qpy). Nowhere did we observe pediment gravels overlying the landslide deposits or incorporated in the deposits; the deposits appear to be younger than the development of the pediment surface. Some slides and flows may be active today.

Tertiary Igneous Rocks

Ignimbrites, lava flows, and rhyolite intrusive-extrusive domes of late Eocene to Miocene (?) age constitute about 50 percent of bedrock exposures in the map area (pl. 1). The stratigraphic nomenclature for the various volcanic units is largely based on the previous work of Elston (1957) in the Dwyer 15′ quadrangle directly west of the Lake Valley 15′ quadrangle and that of Jicha (1954) for the Lake Valley 15′ quadrangle.

Rubio Peak Formation

The Rubio Peak Formation is the oldest volcanic rock in the map area. The age of the Rubio Peak Formation is probably about 36 Ma. Flow rocks of the Rubio Peak underlie the Sugarlump Tuff, which is dated at 35.17 ± 0.12 Ma (McIntosh and others, 1991). Two other K-Ar ages of 36.4 ± 2.3 Ma and 32.6 ± 2.1 Ma for the Sugarlump Tuff were acquired by R.F. Marvin and others (written commun. to Hedlund, 1975).

The Rubio Peak Formation unconformably overlies limestone of Paleozoic age and, northeast of the junction of Berrenda Road and New Mexico Route 27, it overlies jasperoid hills of pre-Rubio Peak age. East of the Lake Valley townsite, Rubio Peak overlies Love Ranch Formation. The Rubio Peak Formation consists of trachyandesitic to trachydacitic flow rocks and volcaniclastic rocks. Following Seager and others (1982), we include the Macho Andesite, mapped near Lake Valley townsite by Jicha (1954), in the Rubio Peak Formation map unit. Maximum preserved thickness of the Rubio Peak Formation, mapped and measured north of Jaralosa Creek, is about 500 m.

North and west of the Berrenda fault zone, the Rubio Peak Formation was divided into five discontinuous informal members. From bottom to top (maximum thickness shown in parentheses), these are conglomerate (about 25 m), a lower member of flows and breccias (375 m), a small area of scoriaceous vent breccia, volcaniclastic rocks (180 m), and an upper member of flows and breccias (210 m), which is marked by a prominent scarp at its base that can be traced throughout the map area. The upper member including its basal scarp was mapped as far south as Berrenda Mountain, where it rests on the lithologically similar lower flow and breccia member. South of Berrenda fault zone, flows and breccias indistinguishable from the lower member compose the entire Rubio Peak Formation.

Conglomerate (Trpc) is known only from an area about 3 km long, northwest of Decker Draw. It underlies and is intercalated with the lower flow and breccia member. The conglomerate contains abundant angular to subrounded pebbles and cobbles of red sandstone and siltstone from the Abo Formation, rounded limestone from the Magdalena Group, and andesite. It crops out poorly but forms rounded hills covered with conspicuous red clasts from the Abo.

The lower member of flows and breccias (Trpl) extends south from the northern boundary of the map to Jaralosa Creek. Similar flows and breccias south of Jaralosa Creek, including the Macho Andesite of Jicha (1954) at Lake Valley townsite, are tentatively included in the lower member. Andesitic flows, flow breccias, and laharic breccias dominate the lower member. North of Jaralosa Creek, the lower member is interbedded with the overlying volcaniclastic rocks. At the head of Jaralosa Creek, where the conglomerate member is missing, coarse breccias of limestone and andesitic rock of the lower member lie directly on a red, weathered surface of Magdalena Group limestone.

At the southwest base of McClede Mountain, vent deposits (Trs) of reddish-brown, scoriaceous lava, cinders, and bombs crop out in a small area within the lower flow and breccia member; they probably represent an exhumed cinder cone (Elston and others, 1975, 1989).

Volcaniclastic rocks north of Jaralosa Creek (Trv) may represent part of the outflow apron of the cinder cone on Tierra Blanca Creek. They consist of light-gray to light-brown, greenish-gray, and reddish-gray volcaniclastic sandstone, tuffaceous sand, tuff breccia, and blocky debris flows. Some of the sandstone beds are crossbedded. Individual beds may be biotite- or hornblende-rich. Volcaniclastic rocks are best exposed in Trujillo Park and in cliffs and steep slopes south of Tierra Blanca Creek.

Flows and breccias of dark-gray trachyandesite and hornblende trachydacite (Trpu) compose the upper member of the Rubio Peak Formation from Tierra Blanca Creek to Berrenda Mountain. A prominent cliff-forming flow marks the base of the upper member. Most of the breccias of the upper member were formed by shattering and ramping of flow margins.

Although interlayered volcaniclastic deposits and lava flows characterize the Rubio Peak Formation in the northwest part of the map area, thick successions of trachyandesitic flow rocks are the most abundant rock type of the Rubio Peak elsewhere in this part of the Black Range. These flows are medium gray, dark greenish gray to olive gray. The trachyandesite is typically porphyritic with as much as 30 percent phenocrysts of zoned andesine ($An_{32–43}$), oxyhornblende, clinopyroxene, and accessory dusky-brown oxybiotite. Zoned augite makes up as much as 4 percent of the rock. Accessory minerals include primary apatite and secondary iron oxide minerals, epidote, celadonite, calcite, and chlorite. Hornblende trachydacite porphyry is generally olive gray to dark purplish gray and contains conspicuous aligned black hornblende prisms up to 5 mm long that locally make up about 15 percent of the rock. Oligoclase-andesine ($An_{23–33}$) phenocrysts are strongly zoned and compose as much as 5 percent of the dacite. Quartz phenocrysts with irregular, resorbed boundaries are locally present; accessory minerals include oxybiotite, iron oxides, and apatite. Two chemical analyses of Rubio Peak flow rocks are slightly alkali-rich and intermediate in silica composition (table 1, fig. 3). Sample 1 represents typical upper member Rubio Peak trachyandesite flow rocks from the western part of the map area. Sample 2 is a trachydacite from directly south of Lake Valley townsite, originally mapped as Macho Andesite by Jicha (1954).

Sugarlump Tuff

The Sugarlump Tuff unconformably overlies the Rubio Peak Formation throughout the southern Black Range (Seager and others, 1982), including the mapped area. The Sugarlump is of relatively small volume as compared to other lower Oligocene ignimbrites of the region (McIntosh and others, 1991, 1992). Its main eruptive center remains unknown, but breccias at O Bar O Peak indicate a small vent in the map area. The age of the Sugarlump Tuff is at least 35 Ma; an age of 35.17 ± 0.12 Ma by the $^{40}Ar/^{39}Ar$ method has been reported for an upper unit of the Sugarlump (McIntosh and others, 1991). The Sugarlump Tuff is 140 m thick on Sibley Mountain and as much as 100 m thick on Berrenda Mountain and McClede Mountain; at Jaralosa Creek, it has been removed by erosion prior to deposition of the overlying Kneeling Nun Tuff.

Two members are recognized in the map area: tuff, which makes up most of the Sugarlump, and breccia, which represents vent fill and proximal outflow.

Tuff consists chiefly of air-fall and ash-flow deposits, with thin beds of sandstone at scattered intervals. Tuff is very light gray, greenish gray, light yellowish gray, and grayish yellow green in color. It contains about 80–90 percent variably altered pumice lapilli. Welding is absent to locally moderate. Lithic fragments of pale-red to purple andesite and basaltic andesite locally compose as much as 15 percent of the tuff; phenocrysts

Table 1. Major-element geochemistry of extrusive and intrusive rocks of Lake Valley map area.

[Oxide analysis by X-ray fluorescence; analyst, Joseph Taggart. LOI = loss on ignition. Numbers in ( ) are LOI-free normalized values and are used in alkali-silica plots of figure 3]

Sample No.	1	2	3	4	5	6	7
	Rubio Peak Fm.	Rubio Peak Fm.	Kneeling Nun Tuff	Andesite of Sibley Mtn.	Trachydacite porphyry	Dacite of McClede Spring	Basaltic andesite, McClede Spring
Field No.	112MM	9LV	HL-5-71	100MM	144MM	4MM-3	104MM
Map unit	Trp	Trp	Tk	Tta	Tdp	Tsd	Tsa
SiO_2	59.0 (61.8)	63.0 (64.2)	72.0 (73.0)	60.8 (61.8)	66.8 (67.8)	64.0 (65.4)	52.7 (53.4)
TiO_2	0.79	0.72	0.28	0.91	0.35	0.60	1.27
Al_2O_3	16.4	16.4	14.6	16.4	16.0	16.1	16.0
Total Fe	5.39	4.09	1.76	5.42	3.46	3.61	8.08
MnO	0.04	0.05	0.04	0.06	0.14	0.05	0.11
MgO	1.95	1.48	0.38	2.40	0.62	1.60	5.72
CaO	3.24	3.50	1.20	4.77	2.13	3.76	8.73
Na_2O	2.90 (3.03)	4.20 (4.27)	3.40 (3.44)	3.85 (3.91)	4.63 (4.73)	3.69 (3.77)	3.39 (3.43)
K_2O	4.51 (4.72)	3.33 (3.39)	4.80 (4.86)	2.54 (2.58)	3.38 (3.43)	3.22 (3.29)	1.31 (1.32)
P_2O_5	0.34	0.33	0.10	0.40	0.24	0.28	0.59
LOI	4.68	1.86	1.45	1.74	1.49	2.24	1.29
Total	99.24	98.86	100.01	99.29	99.24	99.13	99.19

Sample No.	8	9	10	11	12	13
	Vicks Peak Tuff	Altered Vicks Peak Tuff	Intrusive trachy-andesite	Intrusive trachy-andesite	Basalt vent	Basalt flow
Field No.	24MM-1	109MM	48MM	14MM	186MM2	186MM1
Map unit	Tvp	Tvp	Ta2	Ta1	Tb	Tb
SiO_2	76.8 (76.8)	81.6 (83.1)	55.3 (56.8)	60.3 (61.0)	49.0 (49.4)	46.5 (47.5)
TiO_2	0.17	0.14	1.12	0.89	1.40	1.90
Al_2O_3	11.50	8.04	18.1	16.1	15.9	15.7
Total Fe	1.36	1.00	6.42	5.72	11.9	12.4
MnO	0.11	0.07	0.08	0.08	0.19	0.19
MgO	<0.10	<0.10	2.84	2.81	6.68	6.56
CaO	0.11	0.28	5.83	4.99	8.52	8.52
Na_2O	3.91 (3.91)	2.56 (2.60)	4.55 (4.67)	3.77 (3.81)	3.79 (3.82)	3.47 (3.54)
K_2O	4.54 (4.54)	3.19 (3.24)	1.80 (1.85)	3.02 (3.05)	1.03 (1.04)	1.68 (1.71)
P_2O_5	0.09	0.07	0.47	0.42	0.43	0.53
LOI	0.06	1.83	2.80	1.11	0.90	2.16
Total	99.19	98.78	99.31	99.21	99.74	99.61

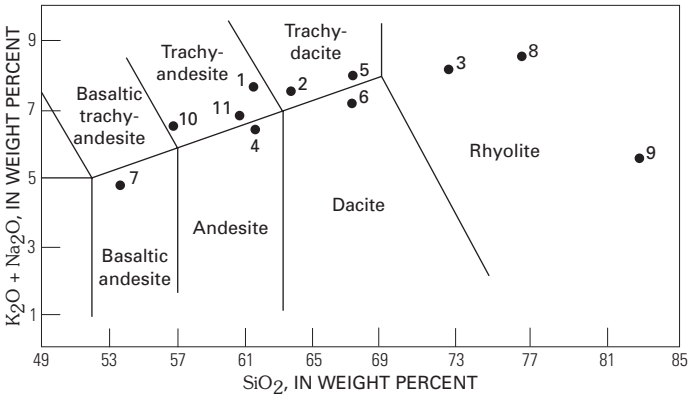

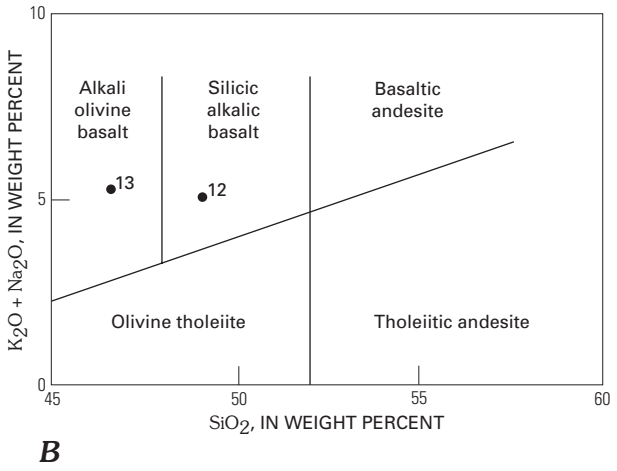

Figure 3. Alkali-silica plots from Lake Valley map area. *A*, Mid-Tertiary igneous rocks, classified according to I.U.G.S. (Le Bas and others, 1986). *B*, Upper Tertiary alkali basalts, classified according to McDonald and Katsura (1964). Numbers refer to samples listed in table 1.

make up only 5–10 percent of the tuff. Biotite is conspicuous, but broken phenocrysts of oligoclase ($An_{23–25}$), sanidine, and quartz are also present. Thin tuffaceous sandstone weathers platy and is locally crossbedded and burrowed; it consists of medium- to coarse-grained reworked pumice, crystals, and lithic fragments.

Breccia fills a vent on O Bar O Peak, and outflow breccia crops out south of Berrenda Mountain (fig. 4). The vent fill consists of massive breccia with angular blocks of andesitic Rubio Peak Formation as large as 1 m across in a densely welded tuffaceous matrix. Tuff beds and lenses measuring only a few centimeters in thickness are interspersed in the breccia; these beds dip gently east, in conformity with the regional dip of the surrounding volcanic rocks. The vent fill appears to rise plug-like from, and may intrude, Sugarlump Tuff that makes up the foot of O Bar O Peak. On the lower slopes south of Berrenda Mountain, proximal outflow from the vent at O Bar O Peak consists of moderately welded ash-flow tuff. The proximal outflow resembles other ash-flow tuff of the Sugarlump, except that it contains clasts of Rubio Peak Formation as much as 1 m across. The outflow is crudely bedded and contains sparse lenses of tuffaceous sandstone a few centimeters in thickness.

Kneeling Nun Tuff

The Kneeling Nun Tuff forms conspicuous escarpments in the map area and throughout the southeastern Black Range. It unconformably overlies the Sugarlump Tuff. At most localities, two or more cooling units are present as welded tuff with well-developed columnar joints underlain by poorly welded, slope-forming tuff. The Kneeling Nun was erupted from the Emory cauldron, located immediately west and northwest of the map area, and its eruption was accompanied by subsidence of the cauldron (Elston and others, 1975). The age of the Kneeling Nun is 34.89 ± 0.05 Ma by the $^{40}Ar/^{39}Ar$ method (McIntosh and others, 1991). The tuff is as much as 230 m thick from Berrenda Mountain to McClede Mountain and about 180 m thick on Sibley Mountain.

The Kneeling Nun Tuff consists entirely of rhyolitic ash-flow deposits. It is crystal rich but poor in lithic fragments and ranges in color from pale red and pinkish gray to medium light gray. Welded zones display well-developed eutaxitic texture. Typically, the tuff contains 35–40 percent broken crystals as large as 4 mm across, dispersed in a devitrified groundmass of ash. Crystals consist of about 18 percent oligoclase ($An_{20–28}$), 13 percent sanidine, 5–6 percent quartz, and 2–3 percent biotite. Accessory minerals include sphene, magnetite, oxyhornblende, clinopyroxene, apatite, zircon, and secondary calcite. Chemical analysis of the tuff at Berrenda Mountain shows it to be rhyolite (table 1, sample 3; fig. 3*A*).

Landslide Megabreccia

Megabreccia, as much as 120 m in thickness, forms the lower slopes west and north of McClede Mountain (fig. 5). The megabreccia probably formed as a paleo-landslide along the topographic wall of the Emory cauldron (Elston, 1989). Large blocks of Kneeling Nun Tuff, some measuring hundreds of feet across, are intermingled with smaller and fewer blocks of Sugarlump Tuff and Rubio Peak Formation. Many of the largest blocks of Kneeling Nun are shattered and brecciated.

The megabreccia overlies Sugarlump Tuff and Rubio Peak Formation and is in turn overlain by tuff of the Mimbres Peak Formation on McClede Mountain. North of McClede Mountain, the top of the megabreccia has been exhumed, revealing a hummocky paleosurface consistent with landslides.

Mimbres Peak Formation

The Mimbres Peak Formation forms rhyolite domes at Town Mountain and directly west of McClede Mountain. The domes west of McClede Mountain are herein called the Deer Hill dome complex, which is named for exposures on both sides of Tierra Blanca Creek immediately west of the mapped area of this report. The Deer Hill complex, of which McClede Mountain is also a part, is interpreted to have been erupted within the ring fracture zone of the Emory cauldron; Town Mountain was intruded along faults outside the cauldron. In ascending order, the domes are composed of tuff, vitrophyre, and rhyolite flow,

Figure 4. Central part of vent breccia of Sugarlump Tuff on O Bar O Peak, west of Berrenda Mountain. Large clasts in breccia are Rubio Peak Formation (Trp) as much as 1 m across. Height of outcrop about 25 m. View to north.

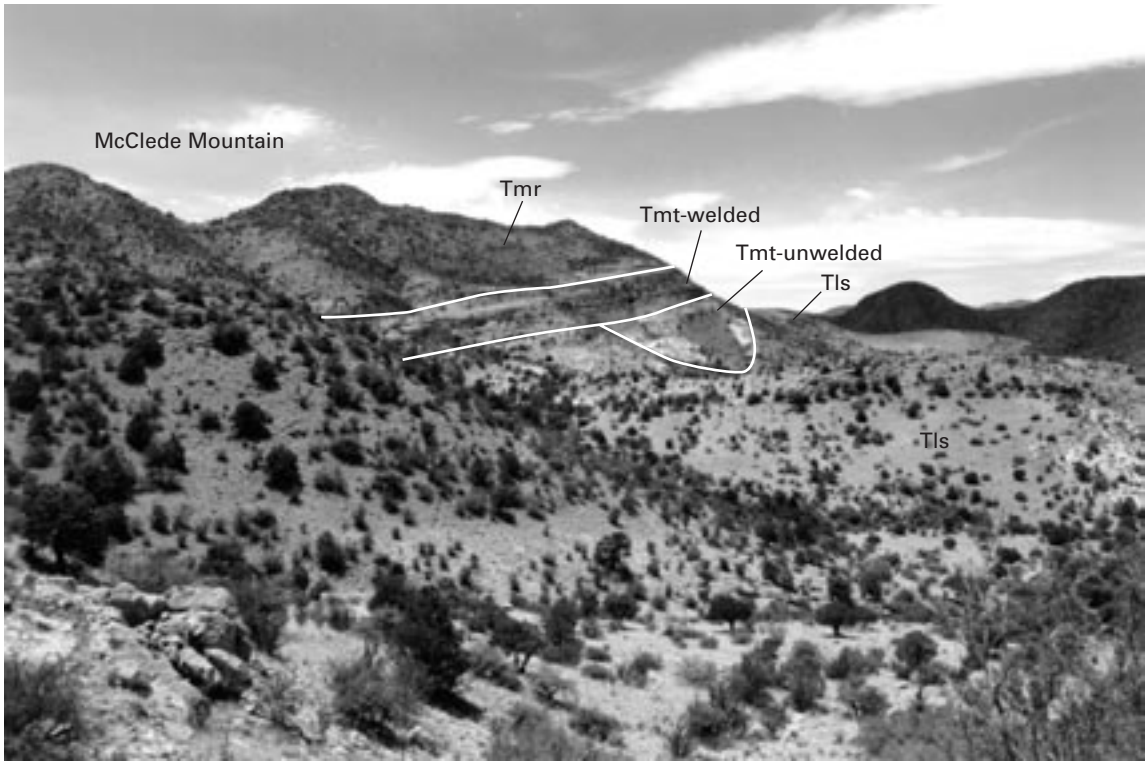

Figure 5. Megabreccia landslide and Mimbres Peak Formation, north side of McClede Mountain. Megabreccia (Tls) displays hummocky topography of exhumed paleo-landslide surface. Megabreccia is overlain by gently east dipping tuff of Mimbres Peak Formation (Tmt), here consisting of lower, unwelded part and upper, welded part. Rhyolite flows of Mimbres Peak Formation (Tmr) overlie tuff.

with rhyolite flows making up most of the domes. Rhyolite breccia, dikes, and small, unmapped plugs were intruded along faults that bound the Town Mountain dome, near Lake Valley townsite. Mimbres Peak rhyolite and tuff collected from McClede Mountain has been dated at 34.32 ± 0.11 Ma and 34.22 ± 0.16 Ma by the $^{40}Ar/^{39}Ar$ method (W.C. McIntosh, written commun., 1999).

Brownish-pale-red to light-pinkish-gray pumice-and-lapilli tuff and breccia crop out on the slopes of hills cored by rhyolite domes. The tuff is bedded, vitric to altered, and crystal poor. Most beds are air-fall tuff, but unwelded ash flows, debris flows, and ground surge deposits are also present. On the north side of McClede Mountain, as much as 20 m of welded ash-flow tuff may indicate proximity to a vent. Typically, tuff of the Mimbres Peak Formation contains 5–10 percent broken crystals—mostly sanidine, oligoclase ($An_{28–30}$), and quartz—with accessory clinopyroxene, hornblende, biotite, and iron oxide minerals. Lithic fragments are sparse in air-fall tuff but abundant in individual breccia beds; north of McClede Mountain, blocks of Kneeling Nun Tuff as large as 1 m occur in tuff of the Mimbres Peak Formation. Tuff overlies and fills depressions in the pre-Mimbres Peak paleosurface. Thickness of the tuff varies from 6–12 m at Town Mountain to as much as 90 m at McClede Mountain.

Glassy to perlitic vitrophyre was mapped with overlying rhyolite; it represents the chilled basal zone of the rhyolite. Basal vitrophyre is typically lenticular and reaches as much as 12–15 m in thickness. Fresh surfaces of vitrophyre are vitreous with a conchoidal fracture and range in color from light bluish gray to dark gray; vitrophyre weathers light brown.

Rhyolite lava in domes is flow layered and foliated. Layers are locally folded and brecciated. Layers and foliation around the base of the Town Mountain dome dip gently toward the center of the dome, but layers in overlying lava are contorted and dip steeply in various directions. The base of the McClede Mountain dome dips gently east on all sides; the uniform eastward dip reflects regional tilting after Mimbres Peak time.

Rhyolite lava of the McClede Mountain dome is porphyritic, containing about 15 percent phenocrysts of sanidine and bipyramidal quartz and accessory biotite, sphene, iron oxide, and calcite. Rhyolite of the Town Mountain dome is aphanitic, having only about 1 percent phenocrysts. An inferred rhyolite dike at Lake Valley townsite, which underlies a low hill between two strands of the Lake Valley fault (pl. 1), is intruded by several small aphanitic rhyolite dikes similar to the Town Mountain rhyolite.

The inferred rhyolite dike at Lake Valley townsite, which alternatively could be a faulted sliver of a porphyritic phase of the dome itself, is steeply layered and foliated; along with adjacent rhyolite intrusion breccia, it is interpreted to have been intruded along the Lake Valley fault zone. The rhyolite dike contains clasts of Rubio Peak Formation, Kneeling Nun Tuff, and, rarely, gneiss. Although not strongly mineralized, the dike contains veinlets of manganese oxide minerals and quartz. The dike adjoins rhyolite intrusion breccia to the northwest. Along its northern contact, with Rubio Peak Formation, the dike contains vitrophyre.

Rhyolite intrusion breccia crops out adjacent to the rhyolite dike at Lake Valley townsite. The breccia contains large blocks of pre-Mimbres Peak volcanic rocks, Paleozoic rocks, and Precambrian crystalline rock.

Trachydacite Porphyry

Phenocryst-rich dacite (Tdp) at the northwest corner of Sibley Mountain occurs as a shallowly emplaced sill locally overlain by a carapace of intrusion breccia (Tdpb) composed of fragments and blocks of Kneeling Nun Tuff and Rubio Peak Formation. The intrusion was partly exhumed prior to eruption of trachyandesite flows (Tta) that rest unconformably on the intrusive and carapace rocks. In thin section the trachydacite is seen to contain phenocrysts of sodic andesine ($An_{30–32}$) as much as 3 mm across set in a patchy felsitic groundmass that shows various stages of alteration to calcite, sericite, and secondary quartz. Andesine phenocrysts constitute 30–40 percent of the dacite, and oxyhornblende, biotite, and iron oxides constitute less than 3 percent. Chemical analysis of the porphyry shows the rock to be a trachydacite (table 1, sample 5; fig. 3*A*).

$^{40}Ar/^{39}Ar$ age determinations of the porphyry attempted during this study have yielded spurious results suggesting contamination of the sill during emplacement. The sill has been interpreted to be older than Kneeling Nun Tuff (Seager and others, 1982; Hedlund, 1977a) and as Cretaceous in age by Kelley and Chapin (1997). Field relations observed in the map area (pl. 1) indicate that the sill is Oligocene in age; it intrudes the 34.9 Ma Kneeling Nun Tuff and is overlain unconformably by the 28 Ma andesite of Sibley Mountain.

Andesite of Sibley Mountain

Andesite flows (Tta) are a major, informal volcanic unit in the map area that underlies Sibley Mountain on the east and a ridge of hills that extend south from McClede Mountain on the west. The predominantly medium gray, aphanitic to slightly porphyritic flows characteristically have a platy weathering habit. In thin section, phenocryst content varies from 0 to 15 percent and includes about 10 percent zoned calcic oligoclase (An_{28}), 3–4 percent oxyhornblende, 0–4 percent bipyramidal quartz, and 0–2 percent oxybiotite. The pilotaxitic to felted groundmass consists of sanidine and oligoclase microlites with interstitial iron oxides and clinopyroxene granules. Chemical analysis of the rock shows composition borderline between andesite and trachyandesite (table 1, sample 4; fig. 3*A*).

The andesite of Sibley Mountain was originally mapped as Pollack Quartz Latite by Hedlund (1977a) and later correlated with the Bear Springs Basalt by Elston (1989). The flows bear little resemblance to the Pollack Quartz Latite of Jicha (1954) at the type locality in the Lake Valley quadrangle and are probably too old to be correlative with the upper Oligocene Bear Springs Basalt. Whole rock K-Ar age determination of 28.1 ± 0.6 Ma has been reported by Seager and others (1982) and Seager (1986) from a series of similar flows in the Hillsboro $7^1/_2'$ quadrangle; the flows described by Seager are located about 3 km west of Hillsboro and are the northward extension of flows mapped at McClede Mountain in this report.

Basalt, Dacite, and Rhyolite of McClede Spring

A series of discontinuous, basaltic and dacitic flows and rhyolite ash-flow tuff are exposed at McClede Spring southeast of McClede Mountain (fig. 6). The deposits rest directly on the andesite of Sibley Mountain. North of Tierra Blanca Creek basaltic andesite (Tsa) is separated from the underlying andesite of Sibley Mountain (Tta) by a lens-shaped dacitic ash-flow tuff (Tsd). Overlying the mafic flow north of Tierra Blanca Creek is a light-brown, crystal-poor ash-flow tuff (Tvp) that contains abundant, weakly welded, devitrified ash shards and minor amounts of pumice. The crystal fragments are generally less than 2 percent of the rocks and include sanidine and bipyramidal quartz. The rhyolite is lithologically and chemically similar to the crystal-poor, high-silica Vicks Peak Tuff erupted from the Nogal Canyon cauldron in the southern San Mateo Mountains to the north (fig. 2). W.C. McIntosh (written commun., 1999) reported a new mean $^{40}Ar/^{39}Ar$ spectra age of 28.4 ± 0.11 Ma for Vicks Peak Tuff at McClede Mountain. Chemical analyses of these volcanic units are shown in table 1, samples 6–9; alkali-silica variation plots of these rocks are shown in figure 3*A*.

South of Tierra Blanca Creek the mafic flow (Tsa) is underlain by a thin interval of tuffaceous sandstone and conglomerate correlated with the basal Thurman Formation (Tt) of Oligocene age.

Younger Intrusive Rocks

Trachyandesite also occurs as two small intrusive bodies in the east-central part of the map area. A basaltic trachyandesite plug (Ta2) intrudes the Rubio Peak Formation about 0.8 km east of State Highway 27 where it crosses Jaralosa Creek. A second trachyandesite body (Ta1) intrudes Sugarlump and younger volcanic flows as well as alluvial-fluvial deposits included with the Santa Fe Group rocks along Jaralosa Creek at the eastern margin of the map area.

The age of these intrusive rocks or even that they are the same or similar age is uncertain. Because the composition of these igneous bodies (table 1, samples 10 and 11, and fig. 3*A*) is similar to Eocene and Oligocene Mogollon-Datil volcanic rocks, we would not be inclined to include them with upper Tertiary alkali basalt flows and sills produced during younger Rio Grande rift igneous activity. However, the easternmost igneous body intruded alluvial-fluvial deposits that were mapped as Santa Fe Group rocks by us (pl. 1) and Seager (1982), and thus the intrusive could not be older than Miocene. We submit that misidentification of older, lithologically similar Thurman Formation at this locality as Santa Fe Group rocks is a distinct possibility; the Oligocene Thurman Formation is present above the andesite of Sibley Mountain in the extreme northeast corner of the map area where it clearly underlies, with angular

Figure 6. Northward-thinning flows of upper Oligocene andesite of Sibley Mountain (Tta) and Vicks Peak Tuff, a rhyolite ash-flow tuff (Tvp) along east flank of McClede Mountain. Sibley Mountain flows rest on Kneeling Nun Tuff (Tk) in middle ground and on Mimbres Peak Formation (Tmt and Tmr) in left background. View looking north across Tierra Blanca Creek at gravel-capped (Qpy) landscape underlain by Vicks Peak Tuff east of McClede Mountain. Tsa, basaltic andesite of McClede Spring; Tsd, dacite flows of McClede Spring.

unconformity, nearly flat lying Santa Fe Group rocks. A second possibility is that these intrusive rocks represent younger, post-caldera andesitic volcanism that is as young as early Miocene (Futa and Ratté, 1989).

Olivine Basalt

Olivine basalt flows and vent rocks crop out on the divide south of Trujillo Canyon, west of State Highway 27. The vent is exposed about 3.2 km north of McClede Mountain. The flows unconformably overlie an east-dipping sequence of rocks ranging from the Kneeling Nun Tuff to the Santa Fe Group. A thin layer of gravel, 1.5 m thick, not mapped separately, underlies basalt southwest of the vent. Similar basalt flows in the Hillsboro quadrangle were dated at 4.2 and 4.5 ± 0.1 Ma by the K-Ar method (Seager and others, 1984).

Erosional remnants of a flow, east of the vent, cap the ridge south of Trujillo Canyon. Not more than about 6 m of basalt remain. Vent rocks consist of scoria, which overlies the basal flow, and a central plug of basalt. The scoria weathers brown and forms gentle slopes and flat areas of rubble around the topographically prominent plug.

The basalt flow is dark gray, aphanitic, and contains phenocrysts of fresh, dark plagioclase (1–2 mm), pyroxene, and olivine (both, 3–4 mm). Rock of the vent-filling plug is mottled dark and light gray, weathers pock-marked, and has an aphanitic texture. Chemical analyses of both vent and flow facies of the basalt are listed in table 1, samples 12 and 13, and figure 3*B*. The vent and outflow rocks have alkalic, as opposed to tholeiitic affinities, characteristic of rift-related basaltic volcanism adjacent to the central axis of the rift.

Structural Geology

A homoclinal sequence of eastward-dipping volcanic and sedimentary rocks in the southeastern Black Range is cut by predominantly north trending, high-angle normal faults (Seager and others, 1982). The easterly dip of the rocks is interpreted as a response to the listric shape of normal faults that, although steeply dipping at the surface, must flatten at depth. Normal faults displace outflow from the Emory cauldron of early Oligocene age and sedimentary basin-fill rocks of Pliocene to late Oligocene age; locally, they are concealed beneath pediment gravels of Pliocene and Pleistocene age and by younger alluvial deposits and landslides. The faults were formed during regional extension in Oligocene time, which in part overlapped with explosive volcanism and caldera formation, and were reactivated during Rio Grande rifting.

Two major normal fault systems, here designated the Lake Valley and Berrenda fault systems, cut through the map area from Lake Valley to Tierra Blanca Creek (pl. 1; fig. 2; fig. 7). Both fault systems downdrop volcanic and sedimentary rocks on the west side and rotate strata about 10°–20° easterly (pl. 1, cross sections *A–A′*, *B–B′*, *C–C′*). Rocks east of the Berrenda fault are also rotated down-to-the-east, indicating a third, concealed, west-dipping fault beneath pediment gravels and Miocene (?) and Pliocene (?) basalt east of the mapped area (pl. 1, section *C–C′*). Northwest of Lake Valley townsite, the Lake Valley and Berrenda fault systems intersect; one splay of the Berrenda fault system trends westerly and offsets the Lake Valley fault system; another splay trends southwest and abuts the Lake Valley fault system. To the north, along the west side of Sibley Mountain, the Berrenda fault system forms the east side of the Animas half-graben, which is the southern terminus of the Winston graben (fig. 2). The half-graben or basin is filled with interlayered volcanics and associated sedimentary rocks of the Thurman Formation and the Santa Fe Group. The Winston-Animas structural depression (fig. 2) can be traced from Lake Valley almost 80 km north (Lovering and Heyl, 1989).

Movement along the Berrenda and Lake Valley faults reflects the regional Tertiary tectonism of the Black Range, from mid-Tertiary regional extension coeval with volcanism and cauldron collapse, to younger late Tertiary Rio Grande rifting. The Tertiary movement on the southern part of the Lake Valley fault also appears to have localized deposition of the oldest volcanic flows by the reactivation of an older fault or zone of weakness in the Precambrian basement that is of inferred Laramide age.

Lake Valley Fault System

The Lake Valley fault system is divisible into two major segments: (1) a north-striking segment that extends from west of Berrenda Mountain past the west side of McClede Mountain, and (2) a northwest-striking segment that extends from south of Lake Valley townsite to Berrenda Mountain; displacement along this segment is near 360 m (cross section *D–D′–D″*, pl. 1). Southwest of Berrenda Mountain, the two segments of the Lake Valley fault system are offset by small splays of the Berrenda fault system. Movement on the northern segment was dominantly dip slip; on the southern segment, movement was oblique-slip, with slickenlines on most fractures indicating a component of right-slip. Based on geophysical resistivity measurements (Chapter B, this report), the southern segment has a minimum displacement of about 50 m and a maximum of about 252 m. The southern segment passes northeast of Town Mountain and is paired with a parallel antithetic fault located south of Town Mountain. The graben in which the Town Mountain dome is located was also detected in geophysical resistivity studies across the Lake Valley fault (see geoelectric measurements, Chapter B of this report).

Analysis of gravity and magnetic surveys of the Lake Valley and surrounding area conducted during this study (Chapter B of this report) suggests that although the Lake Valley fault system is mapped as a continuous fault zone (pl. 1, fig. 2), two fundamentally different faults apparently have been tectonically linked in Tertiary time. The northern segment of the Lake Valley fault parallels the aeromagnetically defined structural margin of the Emory cauldron (Chapter B of this report), previously has been included in the ring fractures zone of the Emory cauldron (Elston, 1989), and appears to have partly controlled the intrusion of Mimbres Peak rhyolite intrusive-extrusive domes emplaced along the margins of the cauldron along Tierra Blanca Creek (pl. 1). The fault also clearly displaces the Mimbres Peak

Figure 7. Lake Valley fault at Lake Valley. View to northeast. The Lake Valley fault, down on the southwest, places Mimbres Peak Formation of Town Mountain dome (where photo was taken) against Silurian Fusselman Dolomite. Apache Hill and Monument Peak, held up by Lake Valley Limestone and Rubio Peak Formation, respectively, mark the northern and eastern limits of the Lake Valley mining district (LV).

rhyolite (pl. 1, section *A*-*A*″), suggesting reactivation of the fault during Neogene deformation related to Rio Grande rifting. The southern segment of the fault, oriented at a large angle to the cauldron margin, bounds a major northwest-trending depression filled mainly with pre-Emory cauldron volcanic rocks of the Rubio Peak Formation (see aeromagnetic and gravity measurements, Chapter B of this report); the northwest-trending southern segment may be related to early Paleogene Rio Grande rift tectonism postulated by Seager and others (1984). The southern segment of the fault is also within the postulated northwest-trending Laramide Rio Grande uplift of Seager and others (1986). Gravity and aeromagnetic anomaly maps presented in Chapter B of this report reveal permissive evidence for such an uplift and related fault systems. This uplift is characterized by a series of northwest-trending basement blocks which extend into the southeast Black Range (fig. 2), upon which was deposited a thin mantle of Love Ranch Formation postorogenic conglomerate that thickens dramatically to the northeast into the Love Ranch basin (Seager and others, 1986). The southern segment of the Lake Valley fault may possibly be a reactivated fault or fault splay related to the Late Cretaceous Laramide Rio Grande uplift.

A stereographic analysis of synthetic fractures and slickenlines in the Lake Valley fault zone near Town Mountain and the accompanying parallel antithetic fault south of Town Mountain indicates that both sets of fractures formed by near-horizontal northeast extensional stress that was accompanied by brittle fracture (fig. 8*A*).

Berrenda Fault Zone

The Berrenda fault zone consists of a north-trending segment along the west side of Sibley Mountain and two southern splays that trend southwesterly. North of the two splays, the major displacement on the north-trending segment of the Berrenda fault is best exposed at Sibley Mountain where it crosses Tierra Blanca Creek; the Santa Fe Group on the west side of the fault is downthrown against Pennsylvanian Magdalena Group on the east. Magnitude of displacement along this segment is unknown.

The north splay is a complex zone of down-to-the-north synthetic and down-to-the-south antithetic faults that extends from Sibley Mountain southwest past Berrenda Mountain. Overall displacement of about 600 m on the main fault of the splay is down to the northwest, placing rocks of the Thurman Formation against Kneeling Nun Tuff. An excellent example of an antithetic fault in the splay drops volcanic rocks down-to-the-south at Berrenda Mountain and O Bar O Peak (pl. 1).

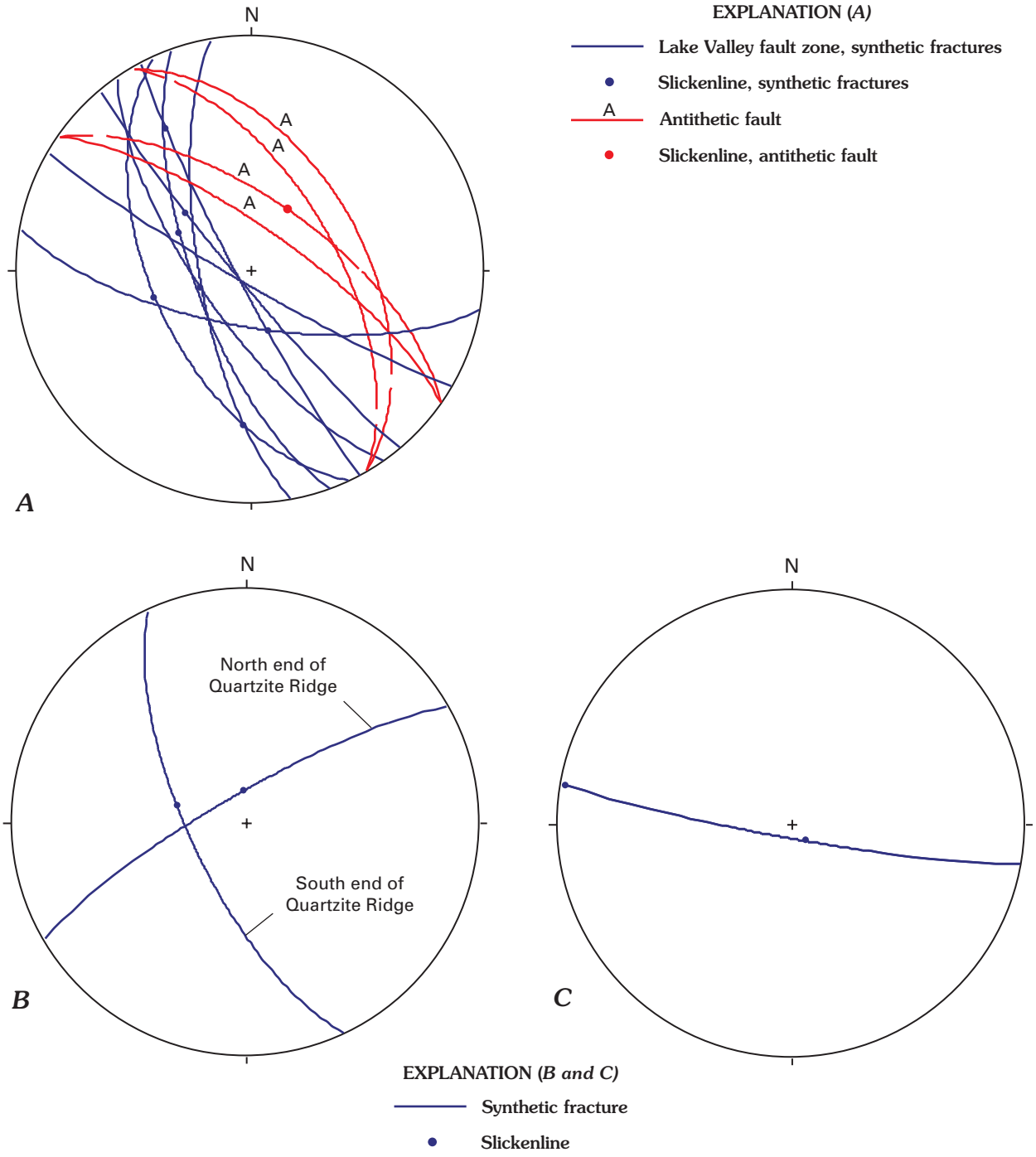

Figure 8. Lower hemisphere stereograms showing orientation of fractures and slickenlines in *A*, Lake Valley fault system (from Berrenda Mountain southeast) and parallel antithetic fault; *B*, southern splay of Berrenda fault zone; *C*, an east-trending fault at Quartzite Ridge.

The south splay of the Berrenda fault drops volcanic rocks down on the west about 300 m against Ordovician and Devonian rocks of Quartzite Ridge and ends where it abuts the southern segment of the Lake Valley fault system. It consists of several segments that range in trend from north to northeast and, where exposed, dip steeply west. Slickenlines (fig. 8*B*) reveal largely dip-slip motion.

East-Trending Faults North of Lake Valley Townsite

A system of closely spaced normal faults cuts Paleozoic rocks at and north of Lake Valley townsite. The closely spaced faults localize silver-manganese deposits at Lake Valley. Stratigraphic separation is small, and both down-to-the-north and -south separation is observed on individual faults. Although the

Figure 9. Hills of jasperoid in Fusselman Dolomite. Unaltered Trp (Rubio Peak Formation) and Ts (Sugarlump Tuff) overlie exhumed jasperoid hill. View looking east across State Highway 27 near Jaralosa Creek.

faults were mapped mainly in Paleozoic rocks, they cut outliers of Rubio Peak Formation on Apache Hill. Most of the faults could not be traced east or west of Apache Hill, but the two longest faults were traced across Quartzite Ridge. A large east-trending fault north of Apache Hill extends west across Quartzite Ridge and displaces a splay of the Berrenda fault zone and the Rubio Peak Formation. Slickenlines measured on Quartzite Ridge indicate both dip-slip and strike-slip movement (fig. 8*C*). A second east-trending fault south of Apache Hill crosses Quartzite Ridge and merges with or abuts the main strand of the Lake Valley fault system.

The origin of the east-tending faults is problematic. Their trend, as well as that of the adjacent southern segment of the Lake Valley fault system, is subparallel to the trend of Laramide faults postulated nearby by Seager and others (1986), suggesting the possibility that the east-trending faults may have first originated during Laramide thrusting. However, the observed offset of the Rubio Peak Formation and of the Berrenda fault zone reveals major movement on east-trending faults during Oligocene or later extension. The easterly trend may result from stress accommodation where the Berrenda fault zone ends, or it may represent development of en echelon fractures along the Lake Valley fault system, or it may have yet another explanation, unidentified by us. Other east-trending faults cut the northern segment of the Lake Valley fault system; their origin is also not understood by us.

Eocene and Oligocene Unconformities and Paleotopographic Features

Unconformities underlie and separate volcanic and sedimentary rocks of Eocene and Oligocene age. In ascending order, unconformities occur at the base of the Rubio Peak Formation (and, where present, the Love Ranch Formation), the base of the Sugarlump Tuff, and the base of the Mimbres Peak Formation and the base of the interlayered volcanic rocks of McClede Spring. Other, local unconformities may also occur in the complexly intertongued volcanic rocks of McClede Spring and Thurman Formation.

Unconformities at the base of the Love Ranch and Rubio Peak Formations may be of various ages, but they are discussed together because they cannot be distinguished in the map area. As reported by Seager and others (1986), the Love Ranch Formation overlies the Lake Valley Limestone north of Lake Valley townsite and west of the north end of Quartzite Ridge; it is in turn overlain by Rubio Peak Formation at these localities. At most localities, however, the Rubio Peak directly overlies rocks of Paleozoic age.

North of O Bar O Spring, in the western part of the map area, laharic breccia and flow rocks of the Rubio Peak Formation rest directly on limestone of the Pennsylvanian Magdalena Group. However, evidence of residual weathering prior to deposition of the Rubio Peak was observed locally. As seen in a gully cut by an ephemeral stream, surfaces on the Magdalena limestone beneath the Rubio Peak are coated with thick argillaceous deposits; cracks in limestone are likewise filled with the deposits, and unstratified breccia immediately overlying the limestone contains red matrix and abundant fragments of limestone as well as andesitic rock. Love Ranch Formation mapped there by Seager and others (1982) was found to consist of poorly exposed remnants of loosely consolidated gravel resting on Rubio Peak Formation.

Northeast of the junction of Jaralosa Creek and State Highway 27, paleohills of jasperoid in the Silurian Fusselman Dolomite, locally overlain by Rubio Peak and Sugarlump Formations, have been exhumed by present-day erosion (fig. 9). Jasperoid hills stand as much as 30 m above the base of the

Rubio Peak. In some places, tuff of the Sugarlump Tuff lies directly on jasperoid. At no place is the volcanic rock altered, indicating that the contacts with jasperoid are of neither intrusive nor hydrothermal replacement origin. These relationships date the jasperoid as pre-Rubio Peak.

The Sugarlump Tuff unconformably overlies Rubio Peak Formation on a surface of low relief throughout the map area. In the upper reaches of Jaralosa Creek, the outcrop of Sugarlump crosses the contact between flows and tuffaceous rocks of the Rubio Peak. Evidently, the Rubio Peak Formation was tilted slightly and eroded before deposition of the Sugarlump. Epiclastic rocks are not abundant at the base of the Sugarlump. On the west side of Berrenda Mountain, the Sugarlump Tuff rests directly on about 9 m of interbedded tuff and breccia. These deposits appear to be largely or entirely volcaniclastic in origin and do not indicate extensive erosion of the underlying volcanic rocks.

A landslide megabreccia composed largely of fragments of Kneeling Nun Tuff and Sugarlump Tuff unconformably overlies these formations and the Rubio Peak Formation at McClede Mountain (fig. 5). Fragments ranging up to tens of meters in size evidently slid off a west-facing escarpment in the Sugarlump and Kneeling Nun Tuffs. Scarps are exposed north and south of McClede Mountain, where megabreccia and the overlying basal tuff of the Mimbres Peak Formation abut Kneeling Nun and Sugarlump Tuffs along a steep, discordant surface. Foliation in some of the largest blocks of tuff is nearly horizontal, indicating little rotation during sliding. The megabreccia has been described in detail by Elston (1989), who interpreted it as a landslide deposit formed outside the Emory cauldron during collapse and erosion of the caldera wall. The landslide and associated scarp are part of the erosional surface on which the overlying Mimbres Peak Formation was deposited.

Note: A combined list of references for all chapters of this Professional Paper is located at the end of this volume, beginning on page 76.

Geophysical Investigations in the Lake Valley Area

By M.D. Kleinkopf, D.P. Klein, *and* R.A. Wise

U.S. Geological Survey Professional Paper 1644–B

An analysis of gravity, magnetic, and geoelectric measurements across major structural features in Lake Valley area

GEOLOGIC INVESTIGATIONS IN THE LAKE VALLEY AREA, SIERRA COUNTY, NEW MEXICO

U.S. Department of the Interior
U.S. Geological Survey

Contents

Figures

Tables

Note: Combined references list begins on page 76.

Geophysical Investigations in the Lake Valley Area

By M.D. Kleinkopf, D.P. Klein, *and* R.A. Wise

Abstract

This study is part of a U.S. Geological Survey investigation of the geology and mineral deposits for the Bureau of Land Management designated Lake Valley Area of Critical Environmental Concern. Analysis of aeromagnetic, gravity, and electrical data provided information about depths of burial and configurations of faults, igneous intrusions, calderas, and rift basins in the area of the Lake Valley mining district.

The boundary of the Emory cauldron is well expressed in the aeromagnetic anomaly data by highs and linear anomalies that reflect igneous intrusions and faults in the structural wall of the ring complex of the cauldron. A corresponding 30-mGal Bouguer gravity low narrows to the southeast, reflecting a trough or graben of volcanic rocks. The proposed graben extended to the northwest and may have been the precursor and structural control for emplacement of the Emory cauldron.

Of particular interest were investigations of the distribution of geologic units and structure associated with the Lake Valley fault that forms the southwestern boundary for silver-manganese mineralization. Interpretations were based largely on geologic models developed from resistivity and gravity profiles. Composite layered-earth inversions (one-dimensional) of audiomagnetotelluric measurements show discontinuities in the lateral distribution of resistivity units across the inferred projections of the Lake Valley fault southeast and northwest of the mining district. Steep gradients along three Bouguer gravity profiles across the study area suggest fault throws of about 300 meters at locations inferred from geologic mapping.

Introduction

Aeromagnetic and gravity anomaly maps provided information about the subsurface configuration and the areal distribution of geologic structure and lithology in the area of the Lake Valley mining district. Gravity modeling of three profiles across the area was used to prepare interpretive geologic sections showing faults, volcanic features, rift basins, and deep structure in the lower crust and upper mantle (figs. 4–6). Although the prominent aeromagnetic expressions associated with the Emory cauldron and the exposed igneous intrusions near Hillsboro appear to show a great deal of geologic information, it is beyond the scope of this report to make a detailed analysis of these anomalies.

Aeromagnetic and gravity anomalies result from juxtaposition of rocks of contrasting physical properties. Aeromagnetic anomaly data distinguish highly magnetic mafic rocks, such as basalts, from weakly to moderately magnetized rocks, such as granites, hydrothermally altered rocks, and most sedimentary rocks. Aeromagnetic anomaly data generally provide more detail about shallow structure and lithology than gravity data because of the nearly continuous measurement of magnetic responses along flight traverses compared with the generally randomly distributed points of gravity observations at spacings that often exceed 3.2 km. Aeromagnetic anomaly data commonly exhibit definitive signatures of intrusions and faults associated with ring structure and faulted volcanic rocks. Gravity anomaly data help identify large lithologic units and basins as well as major fault zones in the crust. For example, gravity lows may reflect granite plutons intruded into higher density terrane.

Results of earlier studies of magnetic and gravity anomaly data applied to geologic framework and mineral resource investigations that include the Lake Valley area have been reported by Adams and Keller (1994); Cordell (1983); Cordell and Grauch (1985), Kleinkopf (1997); and Schneider and Keller (1994).

Observations on Aeromagnetic and Gravity Anomalies

Aeromagnetic Anomaly Data

The aeromagnetic anomaly maps (figs. 1 and 2) were compiled from data purchased from the firm of Pearson, deRidder and Johnson, Inc. The survey was flown at line spacings of 0.53 km and at a mean terrane clearance of 152 m. The aeromagnetic maps in this report are at scales of 1:500,000 or smaller. Under the purchase agreement, the data cannot be published at scales larger than 1:500,000, or released in digital format. These data provide considerably more detail about the geology than the published data that were collected from surveys at higher altitude and wider line spacings (Cordell, 1983).

The total-intensity aeromagnetic anomaly data (fig. 1) were reduced to pole. The reduced-to-pole map corrects anomaly locations for inclination of the Earth's magnetic field and shifts anomaly centers over the causative sources. A residual total-intensity aeromagnetic anomaly map (fig. 2) was prepared by wave-length filtering (50 km high-pass) the reduced-to-pole magnetic data. The processing was done with software that uses fast Fourier transforms to convert aeromagnetic anomaly data in the space domain to the frequency domain (Hildenbrand, 1983). The filtering enhances definition of anomalies due to sources in the upper crust, on the assumption that anomaly wavelength is

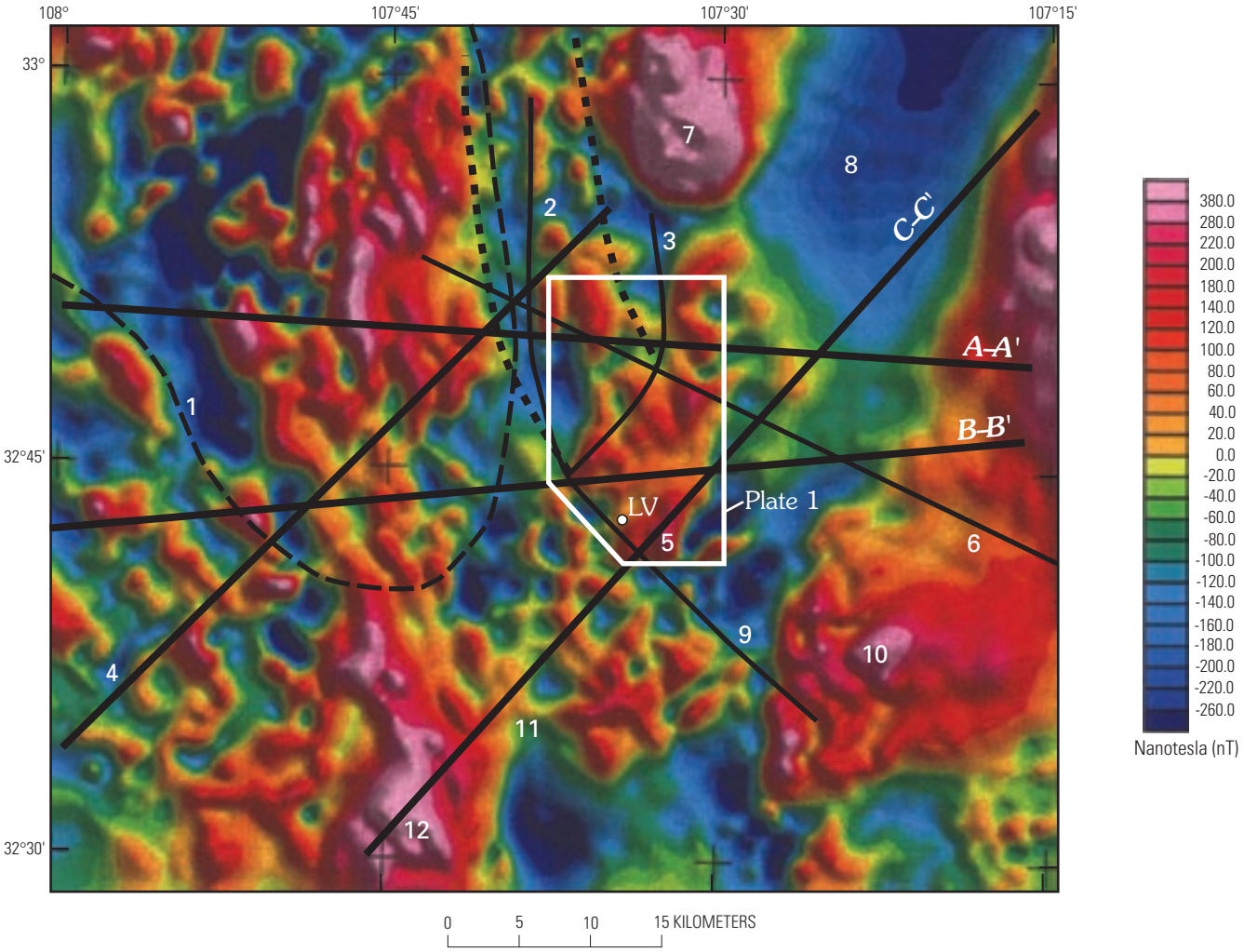

Figure 1. Total-intensity aeromagnetic anomaly map reduced to pole. *A–A'*, *B–B'*, and *C–C'*, profiles of crustal sections derived from gravity models (figs. 4, 5, 6). 1, outline of Emory cauldron; 2, Animas graben; 3, Berrenda fault; 4, Santa Rita lineament; 5, granitic intrusive rocks; 6, trace of regional thrust fault; 7, Copper Flat granitic intrusion; 8, Palomas basin; 9, Lake Valley fault; 10, granitic rocks of Rio Grande uplift; 11, graben of volcanic rocks, 12, granitic intrusion.

proportional to depth of source (Bankey and Kleinkopf, 1988). The traces of gradient midpoint (maxima) of the horizontal magnetic gradient (fig. 2) were calculated and plotted on the residual aeromagnetic anomaly map in order to enhance anomalies for geologic interpretation. The plots (fig. 2) help delineate magnetization boundaries (Cordell and Grauch, 1985) that may signify geologic contacts or linear geologic features.

Gravity Data

The complete Bouguer gravity anomaly map was compiled from nonproprietary data obtained from the National Imagery and Mapping Agency (NIMA). During field work in September 1996, 11 new gravity stations were read in the Lake Valley area to better constrain the gravity interpretations. The reference base used was DOD 3918-1 located at the Truth or Consequences Post Office. The gravity data were reduced using standard USGS procedures described by Bankey and Kleinkopf (1988). Gravity control for the map area consists of about 329 unevenly spaced stations mainly along roads and trails (fig. 3). The observed gravity values are referenced to the IGSN-71 gravity datum (Morelli and others, 1974) and are based on the 1967 ellipsoid (International Association of Geodesy, 1971). The digital gravity data may be obtained from the National Geophysical Data Center (NGDC), National Oceanic and Atmospheric Administration (NOAA), Boulder, CO 80303.

Gravity Models

Gravity models *A–A′*, *B–B′*, and *C–C′* provide information about the subsurface across the Lake Valley area (figs. 4–6). The models were produced using a 2.0-dimensional program (GM-SYS™, version 4.04) developed by Northwest Geophysical Associates, Inc. The Bouguer gravity anomaly data were used to calculate the models. As the topography is generally long wave length and less than 90 m in relief, the models were

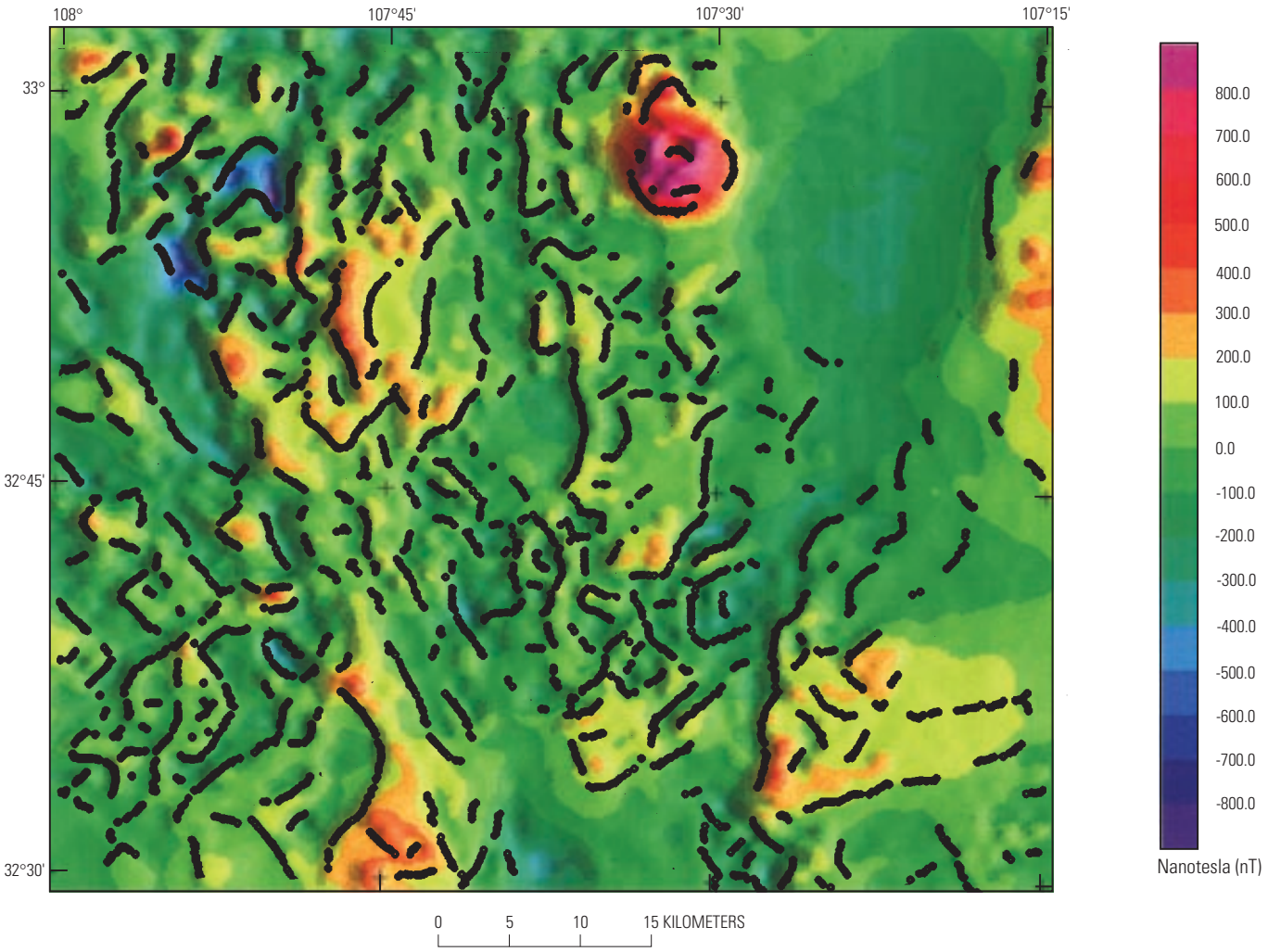

Figure 2. Residual total-intensity aeromagnetic anomaly map. Plots of small circle symbols denote maxima of the horizontal aeromagnetic gradient.

calculated assuming that the top of the model, or ground surface, was flat. Regional cross sections from gravity modeling described by Adams and Keller (1994) provided guidelines for preparing the models. The western quarter of Adams and Keller's profile *C–C′* passes across the Palomas basin about 50 km north of the Lake Valley area and is generally on geologic strike (see fig. 2, Chapter A of this report). Their gravity models were constrained by seismic profiles and some well data that penetrated Precambrian basement. Density values are from the tables of Dobrin and Savit (1988) and Telford and others (1990).

Discussion

The Lake Valley mining district is located in an area of diverse aeromagnetic signatures that reflect mainly the distribution of volcanic rocks having variable magnetization, and regional structures that reflect variable densities laterally and at depth. North of the Lake Valley townsite, the mapped segment of the Lake Valley fault is within the broad, prominent magnetic expression of the eastern boundary of the Emory cauldron (fig. 1, area 1) in the northwestern part of the study area (pl. 1). The fault curves south-southeastward west of the Lake Valley townsite (figs. 1, 2). The southeastern segment of the Lake Valley fault is poorly defined by the geologic mapping (see discussion of structural geology, Chapter A) and by the total-intensity aeromagnetic data (fig. 1). However, residual anomalies (fig. 2) do show discontinuous linear features that trend southeastward for nearly 10 km from locations where the Lake Valley fault is exposed and mapped in the geology. Definitive expression of the fault is likely masked by expressions of highly magnetic surface volcanic rocks. The gravity control is not sufficient at 5 mGal contour interval and 1:500,000 scale to map the southern segment of the Lake Valley fault (fig. 3).

The boundary of the Emory cauldron is well expressed in the aeromagnetic and gravity anomaly data (figs. 1 and 3). Aeromagnetic highs and linear anomalies reflect postcauldron igneous intrusions and faults in the structural wall and ring complex of the cauldron. The alignment of high gradient zones along the east and southeast cauldron boundary is depicted by plots of the maxima of the horizontal gradient (fig. 2). The diverse pattern of highs and lows within the cauldron reflects variable lithologies of the volcanic, plutonic, sedimentary, and crystalline rocks. The gravity expression of the Emory cauldron is a broad gravity low of about 30 mGal amplitude (fig. 3). The main part of the low corresponds well with the cauldron as outlined by the

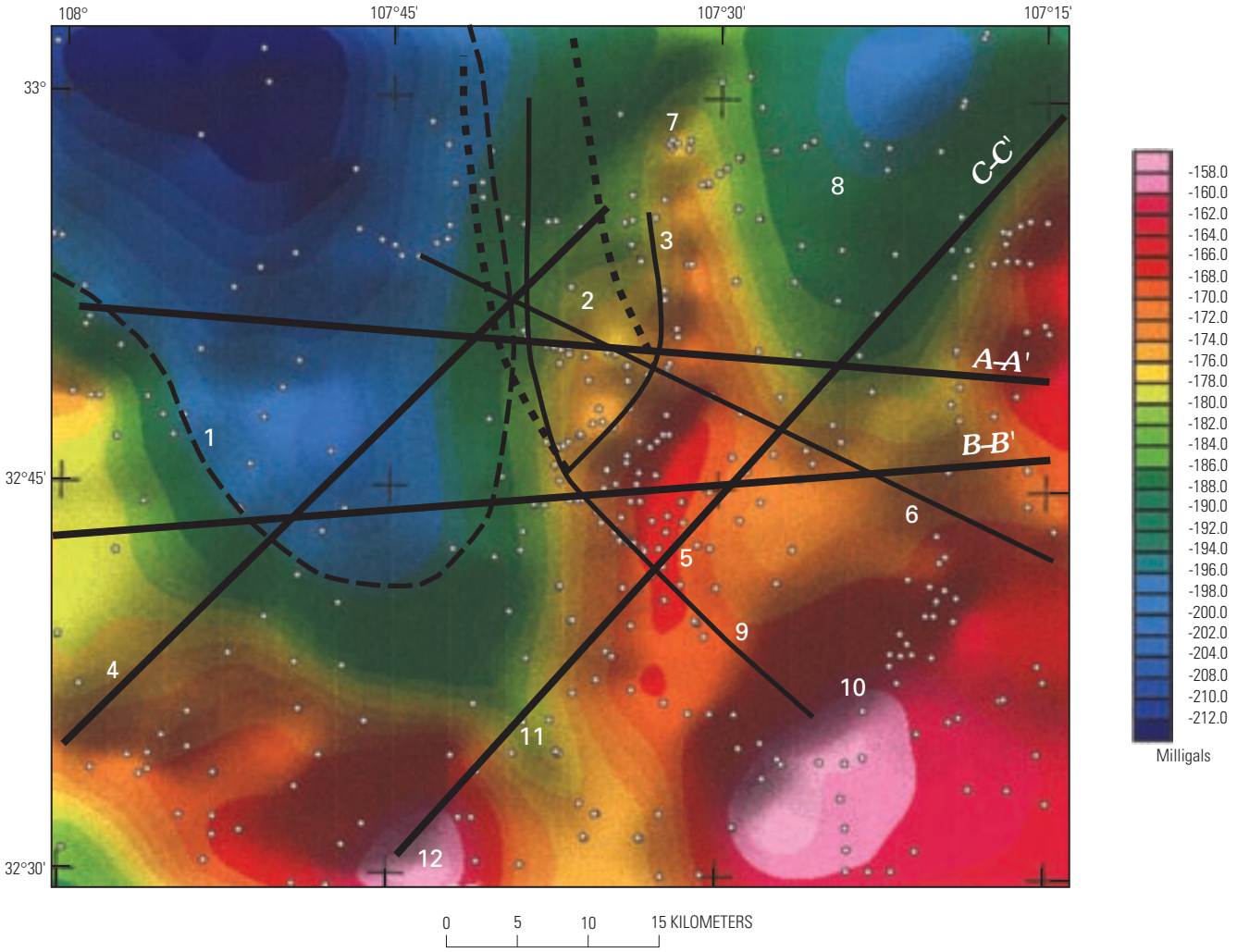

Figure 3. Complete Bouguer gravity anomaly map. Gravity station location (o). *A–A'*, *B–B'*, and *C–C'*, profiles of crustal sections derived from gravity models (figs. 4, 5, 6). 1, outline of Emory cauldron; 2, Animas half-graben; 3, Berrenda fault; 4, Santa Rita lineament; 5, granitic intrusive rocks; 6, trace of regional thrust fault; 7, Copper Flat granitic intrusion; 8, Palomas basin; 9, Lake Valley fault; 10, granitic rocks of Rio Grande uplift; 11, graben of volcanic rocks, 12, granitic intrusion.

aeromagnetics (fig. 1). However, the gravity low extends to the southeast and becomes a trough southeast of lat 32°40′ N. The gravity model across the trough (figs. 3 and 6) suggests preservation of nearly 3 km of pre-Emory cauldron Rubio Peak Formation volcanic rocks. The implication is that the proposed graben extended to the northwest and was the locus of emplacement of the Emery cauldron.

Structures associated with the main trend of the Rio Grande rift are well expressed on the aeromagnetic anomaly maps (figs. 1 and 2). The Animas half-graben or basin west of the Berrenda fault is expressed as a discrete magnetic domain characterized by prominent short wavelength highs and lows that exhibit strong north-south orientations parallel to the Rio Grande depression. Near-surface igneous rock, either intrusions or lava flows, is interpreted in gravity model *A–A′* to occur on both sides of the basin (fig. 4, unit gi). Volcanic rocks at the surface are assumed to be too thin to show in the model. The Palomas basin (figs. 1 and 3, area 8; and fig. 2, Chapter A) exhibits broad aeromagnetic and gravity lows that are nearly coincident. The gravity models suggest that the thickness of gravels and volcanic debris in the basin east of the postulated Palomas fault may exceed 6 km. Southwest of the Palomas basin, discontinuous linear residual aeromagnetic anomalies suggest that significant rift-related faults continue south-southwest (fig. 2) and are concealed by pediment gravels east of Lake Valley (near lat 32°45′ N. and long 107°30′ W.). In the central part of model *C–C′*, the long wavelength high of 25 mGal amplitude is associated with local crustal thinning and elevated mantle at the location of the Rio Grande uplift (Seager and others, 1986). In the modeling, thinning of the crust and inclusion of a high-density lower crust layer provided the best fit to the observed gravity.

Several other geologic features that extend into the study area have variable aeromagnetic and gravity expressions. The northwest-trending buried thrust fault interpreted by Seager and others (1986) to extend into the Lake Valley area has aeromagnetic support in the form of aeromagnetic anomalies aligned along the postulated trend (fig. 1, area 6) and in other places breaks in trends across the feature. South of the postulated thrust fault, the increase in gravity and aeromagnetic intensity

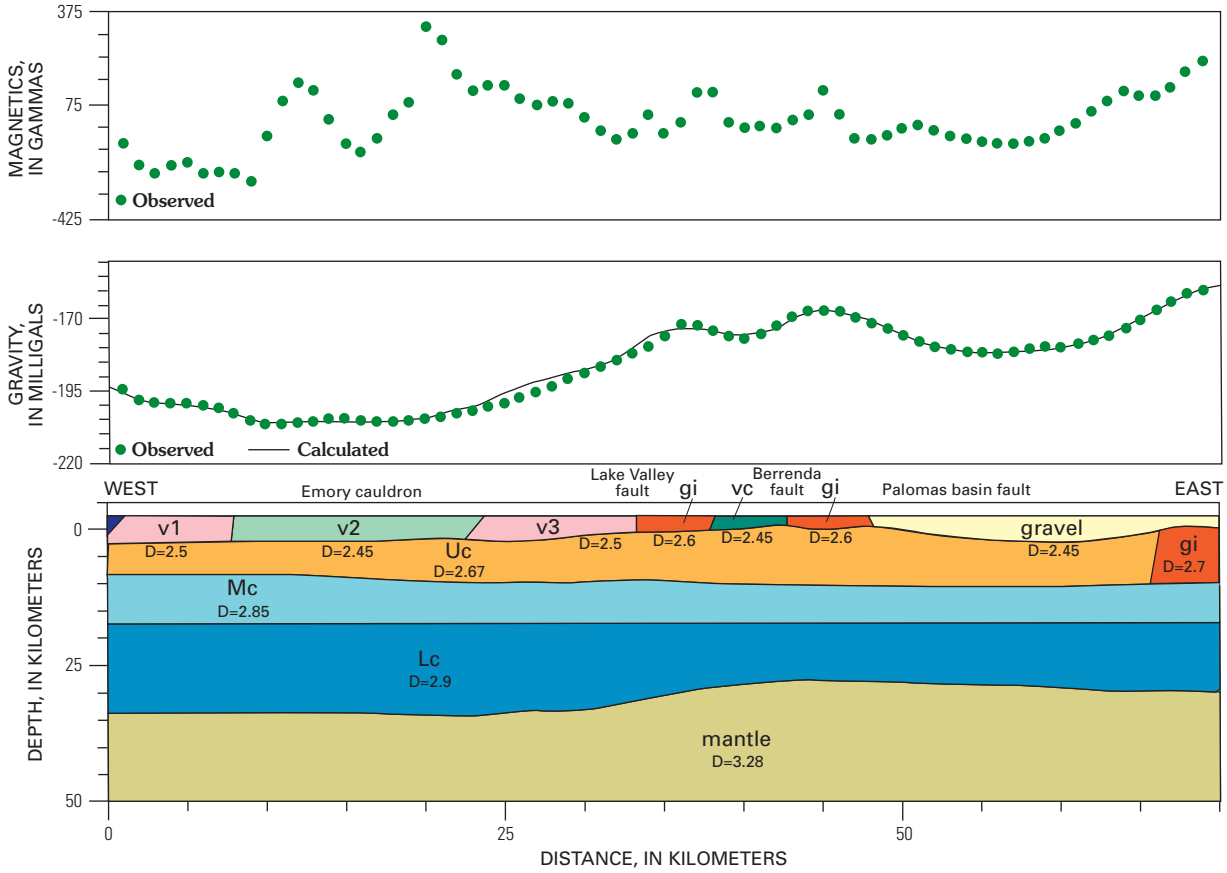

Figure 4. Gravity model of crustal section *A*–*A*' across study area. Numbers show densities assumed (D=2.67 g/cm^3). Zero depth in model represents sea level. Observed values are from reading in field. Calculated profile is mathematically derived from model. Geologic units of model are Uc, upper crust; Mc, middle crust; Lc, lower crust; mantle; gi, igneous intrusion; vn, volcanic rock; vc, possible volcanic center; gravel. Vertical exaggeration 0.35; scale 1:500,000.

and the presence of discontinuous aeromagnetic gradient zones along the trend suggest the presence of a thrust fault in the subsurface that brought crystalline basement rocks of the Laramide Rio Grande uplift (Seager and others, 1986) near the surface (figs. 1 and 3). The Santa Rita lineament (fig. 1, area 4), part of a regional alignment of Laramide intrusions, extends into the area from the southwest (Bartsch-Winkler, 1997). The structure exhibits a zone of linear aeromagnetic anomalies that trend northeast as far as the prominent magnetic high underlying the Cretaceous Copper Flat intrusion at Hillsboro.

A small magnetic high (fig. 1, area 5) of about 200 nT amplitude is present along a gravity ridge (fig. 3). Measurements of aeromagnetic gradients suggest the presence of granitic intrusive rocks, estimated to occur at a depth of 300–400 m. The anomalies are shown on model *C*–*C*′ and are closely coincident with an AMT high discussed in the following section.

Description of Lake Valley Fault from Geoelectric Measurements

Introduction

Measurements of electromagnetic fields using the tensor audiomagnetotelluric (AMT) method were made along traverses in the Lake Valley area in October 1997. The traverses were along northeast-southwest lines across the Lake Valley fault (fig. 7). Goals of the AMT survey were to investigate the distribution of geologic units and structure associated with the Lake Valley fault, which forms the western boundary for silver-manganese mineralization in the Lake Valley mining district. The AMT method (Vozoff, 1972, 1991; Strangway and others, 1973) uses electromagnetic fields across a range of frequencies to map the distribution of

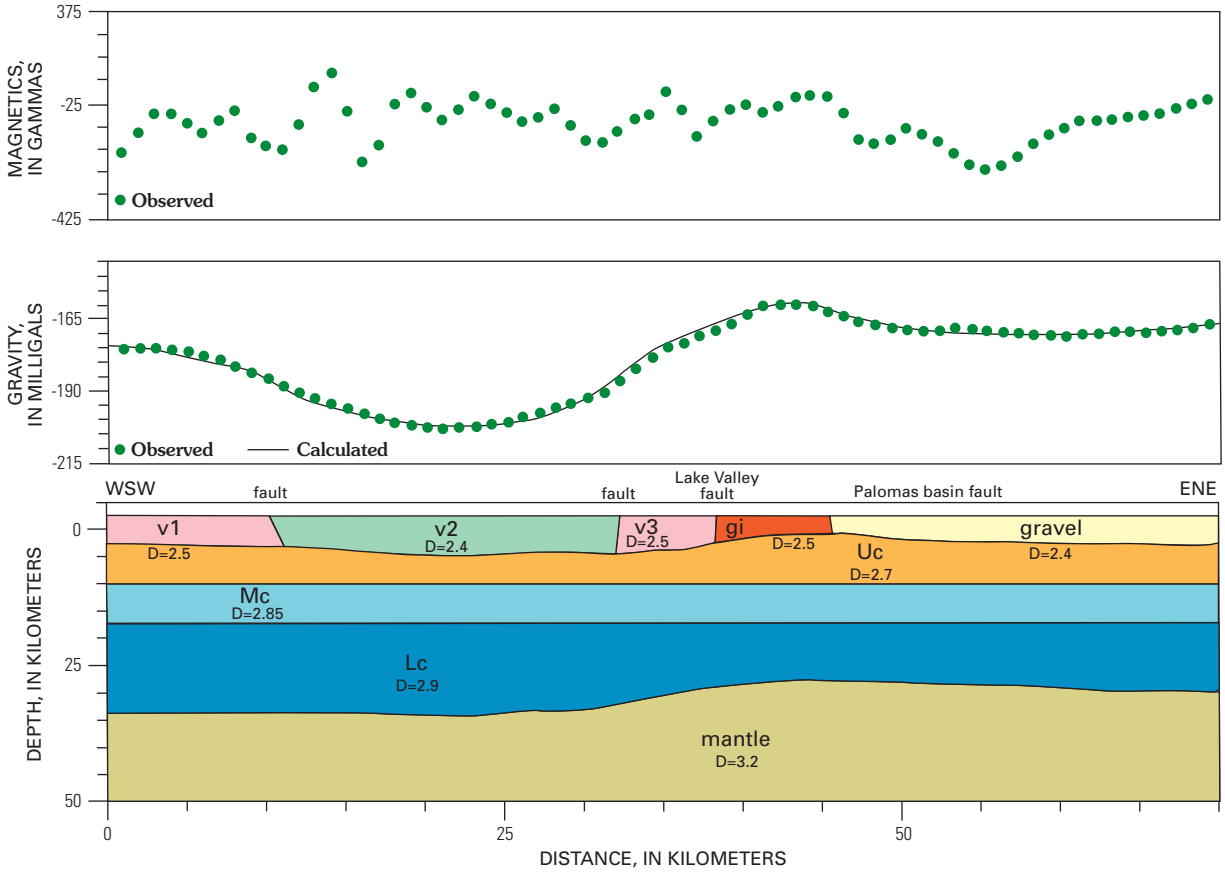

Figure 5. Gravity model of crustal section *B*–*B*' across study area. Numbers show densities assumed (D=2.67 g/cm^3). Zero depth in model represents sea level. Observed values are from reading in field. Calculated profile is mathematically derived from model. Geologic units of model are Uc, upper crust; Mc, middle crust; Lc, lower crust; mantle; gi, igneous intrusion; vn, volcanic rock; gravel. Vertical exaggeration 0.35; scale 1:500,000.

Table 1. Resistivity ranges of geologic materials in the southwest U.S.

[Keller and Frischknecht, 1966, p. 1–55; Brant, 1966; Klein, 1996. The lower 1/3 (approximate) of these ranges takes into account saturation by ground water (10–50 ohm-m). The upper 2/3 of these ranges represent low-porosity, dry and unaltered rock. Ranges shown may not account for the presence of conductive metallic sulfide minerals and hot saline water (0.1–10 ohm-m) or resistive alteration such as silicification. Single geologic units may exhibit a range in resistivity caused by a variation in weathering, alteration, and pore-fluid content]

Geologic material	Resistivity range (ohm-m)
Alluvium	10–100
Gravel and conglomerate	20–400
Argillite and shale	20–500
Tertiary volcanic rock	20–1,000
Sandstone	40–1,000
Mesozoic-Tertiary intrusions	50–2,000
Proterozoic schist	50–5,000
Limestone and dolomite	200–5,000
Quartzite and Proterozoic granite and gneiss	200–5,000

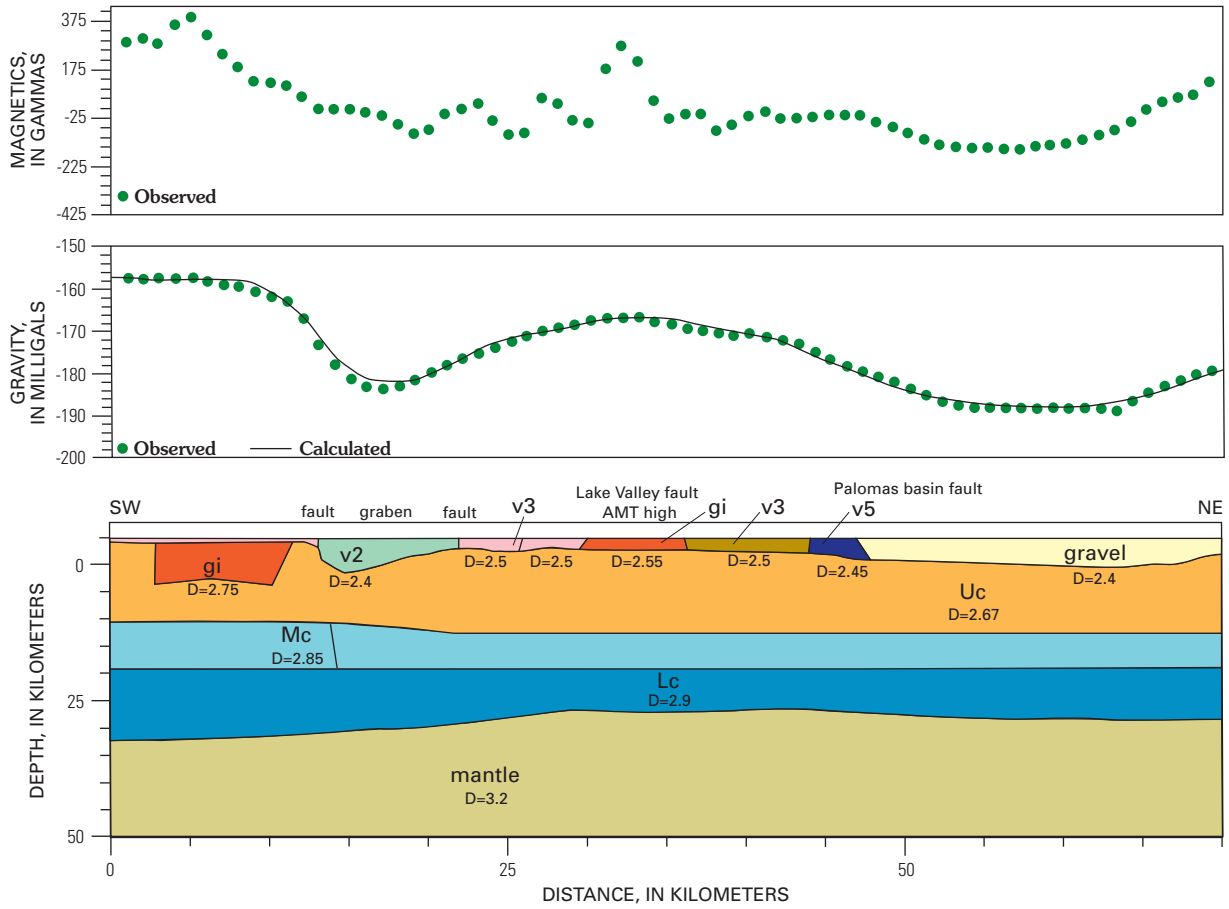

Figure 6. Gravity model of crustal section *C–C'* across study area. Numbers show densities assumed (D=2.67 g/cm^3). Zero depth in model represents sea level. Observed values are from reading in field. Calculated profile is mathematically derived from model. Geologic units of model are Uc, upper crust; Mc, middle crust; Lc, lower crust; mantle; gi, igneous intrusion; vn, volcanic rock; gravel. Vertical exaggeration 0.35; scale 1:500,000.

Table 2. Generalized sequence of chief lithologic units in vicinity of Lake Valley mining district, shown with typical thickness and relative resistivity.

[Refer to table 1 and text for actual ranges of resistivity encountered in various lithologies]

Gravel, float and alluvium (Tertiary and Quaternary): variable thickness, probably less than 30 m; low resistivity
Tertiary volcanic rock (Tertiary, mainly Rubio Peak Formation, lumped with about 20 m of various Mississippian calcareous rocks east of Lake Valley fault): 100 m thick east of Lake Valley fault; unknown thickness west of Lake Valley fault; moderate resistivity
Percha Shale (Devonian): 40 m thick; low resistivity
Dolomites and limestone (Ordovician and Silurian): 300 m thick; high resistivity
Granite and gneiss (Proterozoic): high resistivity

electrical resistivity versus depth in the Earth. Geologic inferences from this information are based on the relationships between electrical resistivity and lithology (table 1). Details of the acquisition and analysis of data are described in Klein and Wise (1998).

Observation sites and their projection onto lines are shown in figure 7. A cross section south of Lake Valley (southeast of Monument Peak) is based on sites 111 to 124 that are projected onto line 100. Line 300 (sites 324 (124), 325, and 326), northeast of Monument Peak, is discussed in the context of the

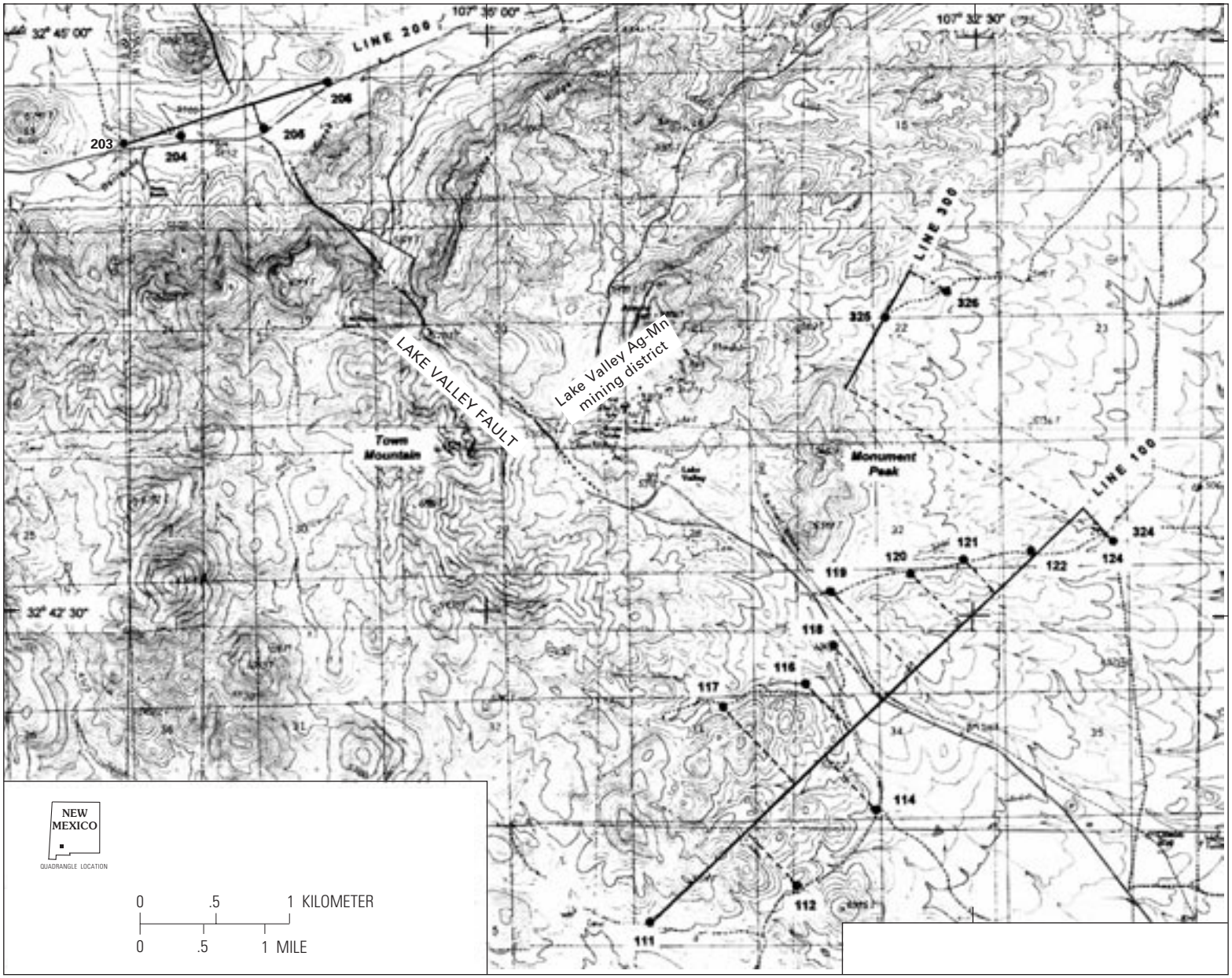

Figure 7. Map of AMT observation sites. Location of observation sites shown as filled circles with site designation. Dashed lines project to lines along which resistivity models were developed. Measurement at site 124 was used for both line 100 and line 300. Base from U.S. Geological Survey 1:24,000 Lake Valley (1989) and McClede Mountain (1985).

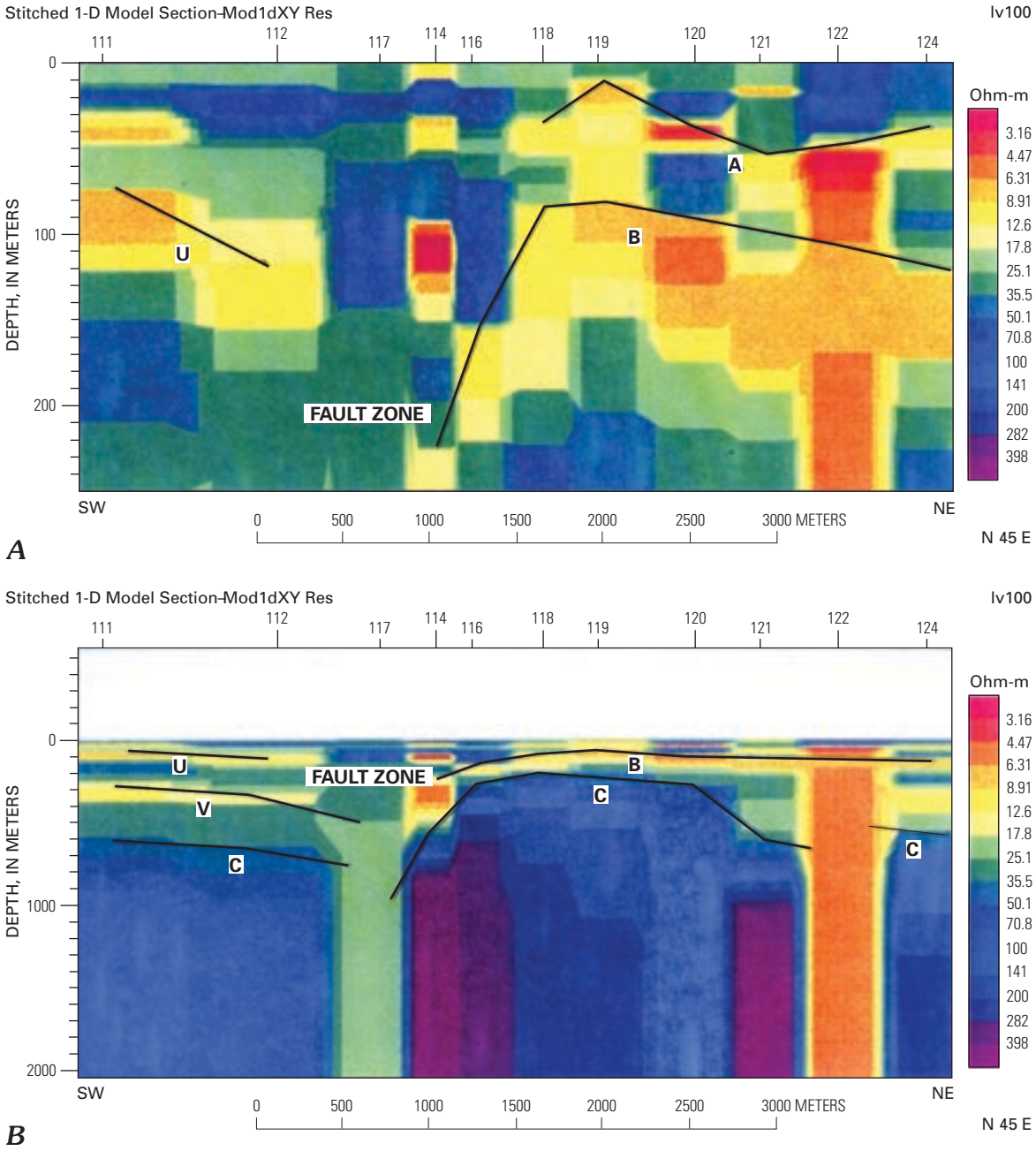

Figure 8. Resistivity model for line 100. Model is composite of layered strata inversions for each site based on error-weighted apparent resistivity (Rxy) and phase (Pxy). X rotated approximately perpendicular to Lake Valley fault. Resistivity values are color coded as shown on bars. *A*, Model to 250 m depth with vertical exaggeration of 10; *B* , Model to 2,000 m depth with no vertical exaggeration. Labeled ticks along top of models show projected location of AMT sites. Lines labeled A, B, C, U, and V show interpreted top of geoelectric units.

resistivity structure associated with line 100. A cross section northwest of Town Mountain uses sites 203 to 206 projected onto line 200. The succession of generalized lithologic units of the study area is listed in table 2, showing their typical thickness and relative resistivity. Depths and distances in the following discussion are in meters and kilometers.

Results

Cross Section South of Lake Valley

Geologic units in the Lake Valley mining district (table 2) have been mapped with a dip of about 20° SE. Such a dip

may result in a differential depth to units of about 350 m for each 1 km of separation between the mining area and the AMT sites. Actual locations of the sites, rather than their projection to a cross-section line, are considered when accounting for the dip.

Figure 8 shows a resistivity section for line 100. Resistivity is color coded as shown on the color bar with lower to higher resistivity corresponding to the color progression of various hues of red-yellow-green-blue-purple. The model was formed as a composite of layered-Earth (one-dimensional or 1-D) inversions (Constable and others, 1987). Therefore, the model is portrayed with a block of layers beneath each site. The model shows a transition zone between the layers of adjacent sites that is arbitrarily plotted midway between sites and spans a distance of 30 percent of the separation between sites. Figure 8*A* shows the upper 250 m of the model with a vertical exaggeration of about 10; figure 8*B* shows the section to 2,000 m with no vertical exaggeration. The depth of resolution for the data is about 1,200 m. Vertical bands for the deepest layer beneath each site are an artifact. Only depth and resistivity are resolved for the deepest layer detected; thickness is unknown and physically indistinguishable from being infinite in thickness.

In figure 8, interpretive lines labeled as A, B, C, U, V mark interfaces between electrical resistivity units. These units may differ from geologic units. Site 118 (fig. 8*A*) is near the inferred southward extension of the Lake Valley fault. The discontinuity in various lines on the model (fig. 8) is an expression of this fault. To the west of the fault, where geologic mapping (pl. 1) indicates an sequence of andesitic volcanic rock (Trp) of unknown thickness, there are electrical units that are as well defined as those to the east of the fault where a thin cover of volcanic rock (Trp) overlies a succession of Paleozoic formations.

Northeast of site 118, line A (fig. 8*A*) is at 10 to 50 m depth to mark the top of a low-resistivity unit (3–10 ohm-m). This low resistivity is interpreted to represent the bottom of unconsolidated gravel, float, and alluvium, a zone that is or has been conducive to weathering, and the collection of wet silts or clays.

Line B (fig. 8), at a depth of 80 to 110 m northeast of site 118, appears to be dipping west between sites 118 and 114. It marks a conductive unit (10–15 ohm-m) that is interpreted to represent the top of the Percha Shale. The westward dip indicates possible vertical offset of this unit amounting to about 140 m between sites 118 and 114. Site 114 is about 1 km southeast of station 118 (fig. 8), and the offset of the unit could be accounted for by a 7° SE. dip of the unit. Likewise, apparent dip on B northeast of 118 (fig. 8A) may in part be related to the differential southeast offsets of sites over dipping stratigraphy. The location of the fault, as indicated by the resistivity model along section line 100, is consistent with the southeast projection of the Lake Valley fault beneath alluvial cover as shown on the geologic map (pl. 1).

Line C (fig. 8*B*) marks the top of resistive units (50–300 ohm-m). The true resistivity within this unit is probably 300 ohm-m or greater, inasmuch as the inversion creates a smoothly varying resistivity model. The average depth of C is about 600 m southwest of site 117 compared to about 200 m to the northeast from sites 116 to 120. Northeast of site 120, C deepens to an average depth of about 500 m. On the average, C is about 150 m deeper than B, which was inferred to mark the top of the Percha Shale. Using a geologic estimate of thickness of the Percha Shale as 40 m, C is about 100 m into the Ordovician and Silurian dolomites and limestone, which have an estimated combined thickness of 300 m (table 2). Line C probably presents a boundary over a resistive unit in the sequence of Paleozoic carbonates. Line C shows a likely disruption of the carbonate units between sites 118 and 112 across a distance of about 1.5 km with an apparent cumulative downthrow of the carbonate units of 400 m. Correcting for an assumed maximum regional dip of 20° SE., and using an average offset between sites east and west of site 117 as 1 km, the interpreted fault throw would be about 50 m. Resistivity values extending downward from about 600 m beneath site 117 can be ignored because the data here are incomplete at low frequencies.

Apparent deepening of C by about 300 m northeast of site 120 may be partially accounted for by a 20° SE. dip of beds, but the largest downthrow occurs between sites 120 and 121, suggesting fault displacement down to the east. In conjunction with this postulated displacement, low resistivity (3–8 ohm-m) beneath site 122 suggests increased porosity, pore-fluid content, and altered rock that might be found along a fault. A north-trending fault beneath site 122 would be along the east edge of Monument Peak. At shallow depth, B shows a smaller displacement of about 50 m from sites 120 to 124 (fig. 8*A*); if a fault zone exists below 122, it must have had recurrent motion during deposition of the Paleozoic rocks. Beneath site 124 lies a conductive geoelectric layer between B and C (fig. 8*B*) that has no counterpart west of site 122. This localized conductive layer might reflect an eastward slump block or deposition of conglomerate formed during the hypothesized faulting.

West of Lake Valley fault, low-resistivity zones (8–10 ohm-m, fig. 8) indicated by U and V at depths of about 100 and 300 m are probably indicating higher fluid fraction and clay content due to weathering and alteration at interfaces between different episodes of Rubio Peak Formation flows or at intervals of epiclastic rock deposition. An indication of faulting, or dip of the lava units, is present in the apparent northeast deepening of V and C beneath 112. The vertical offset of these markers is 50–100 m. Dips on the outcropping volcanic rock west of the Lake Valley fault are generally northerly. Therefore, we conclude that these offsets are not likely to be reduced by the relations of site location and stratigraphic dip; rather, they may be increased. The resistivity section thus suggests graben development along the fault zone.

Proterozoic basement is not identified in the present results. Geologic consideration of the thickness of the Paleozoic rocks and their dip indicates that the Proterozoic rocks are probably present at a depth of 1,100–1,700 m beneath the profile. The nearest outcrops of Proterozoic rocks (granite and gneiss) are about 15 km southwest, in the vicinity of Cooks Range. Granitic and carbonate rocks may have overlapping resistivity (table 1); thus, if basement is within reach of the electromagnetic fields, it is indistinguishable from the overlying carbonates.

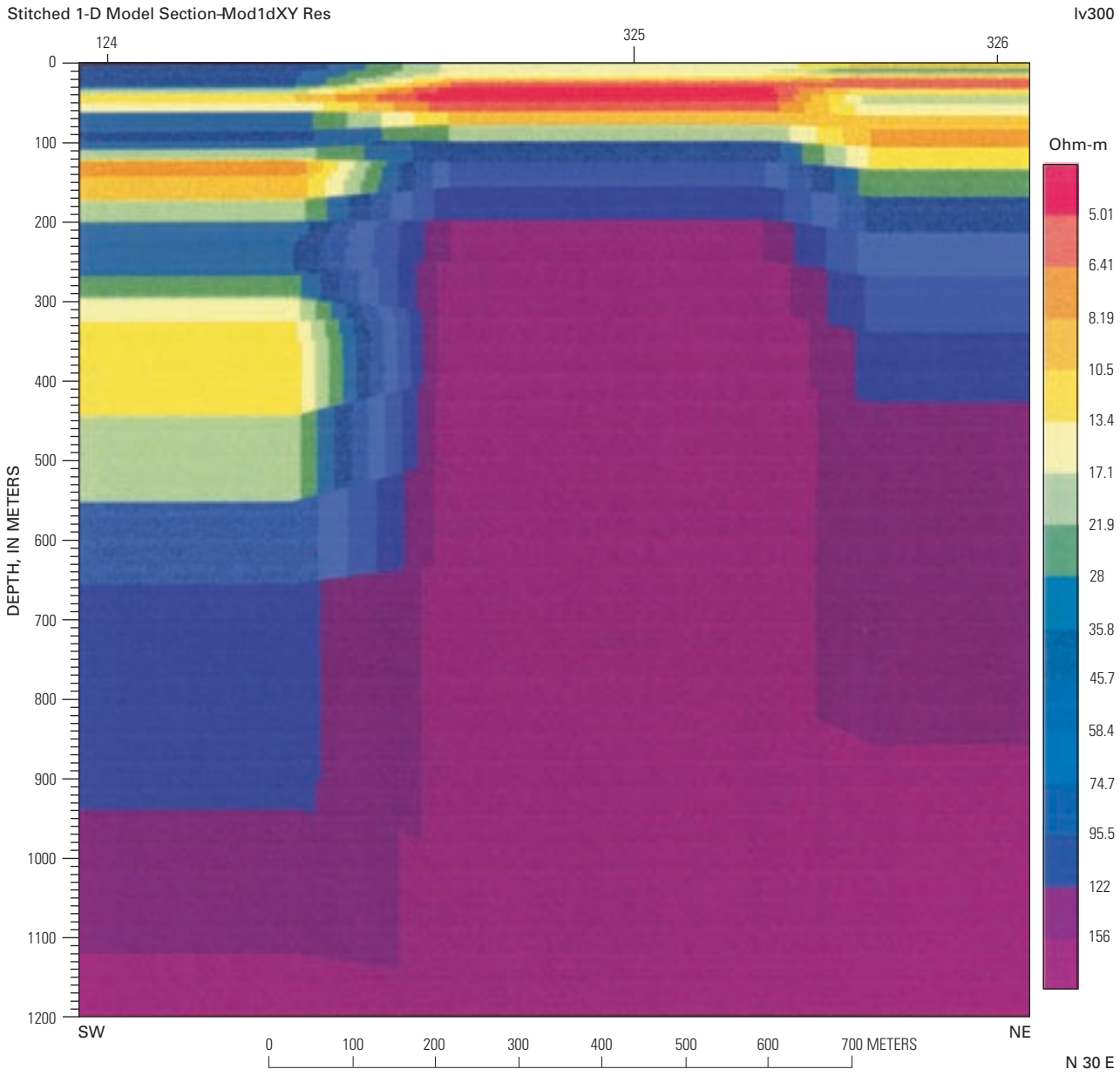

Figure 9. Resistivity model for line 300. This model is intended to show the vertical offset of correlative resistivity layers between sites 325 (and 326) with respect to 124. This offset is inferred to be related to the dip of strata between sites 325 and 124 (see text). Model is composed of layered strata inversions for each site based on error-weighted apparent resistivity (Rxy) and phase (Pxy). X rotated approximately perpendicular to Lake Valley fault. Model resistivity versus depth and horizontal separation has no vertical exaggeration. Labeled ticks along top of section show projected location of AMT sites. Resistivity values are color coded as shown on bars.

Apparent Dip of Resistivity Units

Sites 325 and 326, northeast of Monument Peak (fig. 7), along with site 324 (124), provide insight into the average apparent dip of geoelectric units in the survey area. Line 300 was established to show the projection of sites 324 (124), 325, and 326 as approximately equally spaced (fig. 9). This does not represent a realistic horizontal perspective; the line was constructed to provide a visual correlation of electrical units.

The upper two layers of low resistivity at site 324 (124) are at depths of about 30 m and 120 m respectively; these layers have been interpreted as the base of overburden and the Percha Shale (fig. 8 and accompanying discussion). A deeper conductive layer starting at about 300 m beneath site 324 (124) was unique to this site on line 100. It is apparently missing at sites 325 and 326. At site 325, the shallower conductive layers converge at a depth of less than 100 m implying that the basin cover and volcanic rocks may be thinner here than at line 100. Both conductive units and deeper resistive units (about 50 ohm-m or greater) at sites 325 and 326 indicate an apparent eastward dip.

The geoelectric marker within the carbonate section used for inferring throw across Lake Valley fault on line 100 was the top of resistivity greater than about 50 ohm-m, located at a depth of about 500 m beneath site 124 (C, fig. 8 and accompanying

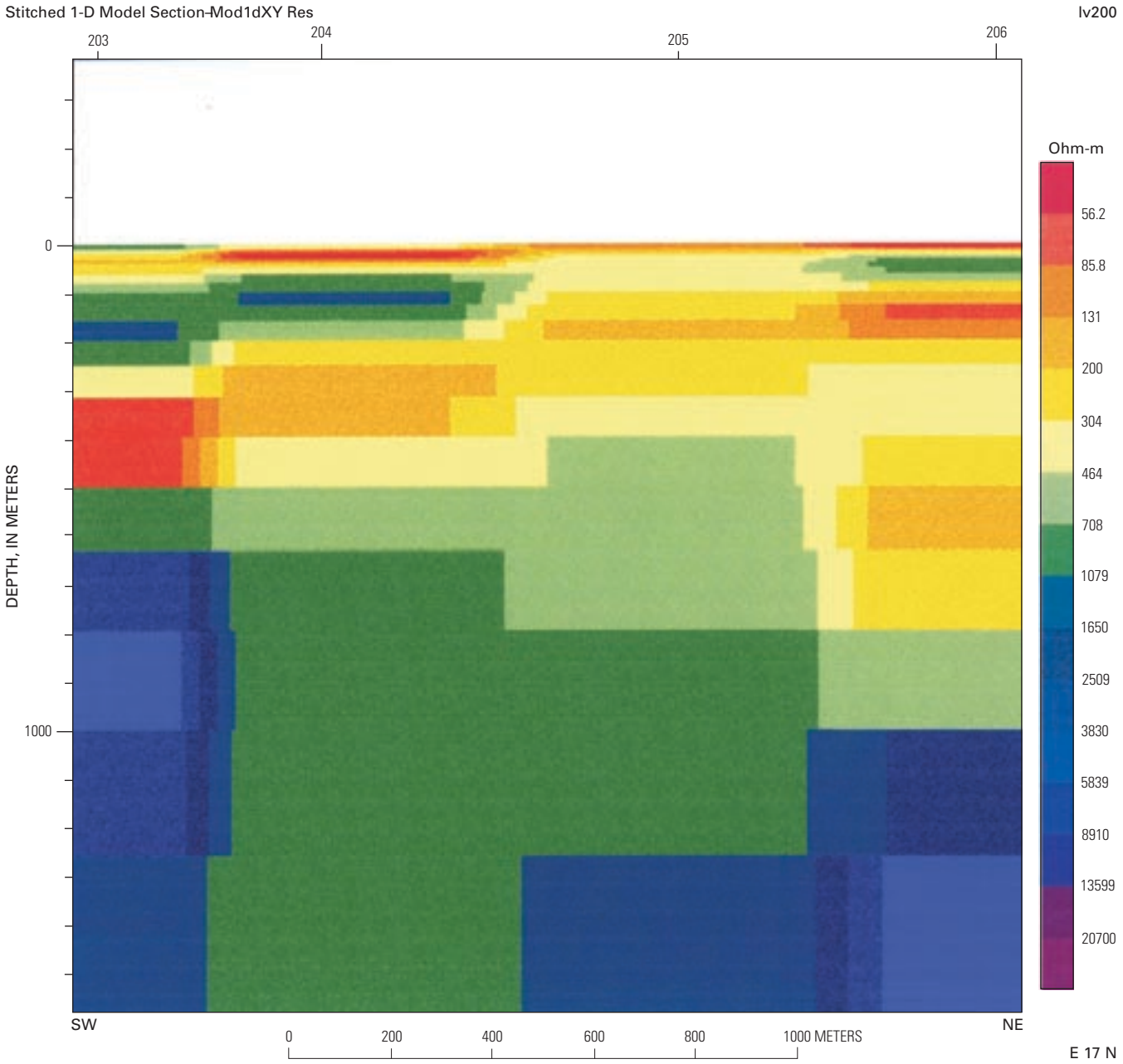

Figure 10. Resistivity model for line 200. Model is composite of layered strata inversions for each site based on error-weighted apparent resistivity (Rxy) and phase (Pxy). X rotated approximately perpendicular to Lake Valley fault. Model resistivity versus depth and distance has no vertical exaggeration. Labeled ticks along top of section show projected location of AMT sites. Resistivity values are color coded as shown on bars.

discussion). At station 325, the top of geoelectric units with resistivity greater than 50 ohm-m is at a depth of about 120 m. This apparent vertical offset of 380 m between 325 and 124 is consistent with an average south apparent dip of 8° from site 325 to 124. The previously estimated minimum throw, using a dip of 20° for strata beneath the measurements of line 100 is about 50 m. Using an 8° dip, a maximum throw of about 250 m is possible.

Cross Section North of Town Mountain

Line 200, located northwest of Town Mountain (fig. 7), is composed of four AMT sites acquired along Berrenda Creek. The line should intersect the northwest extension of Lake Valley fault near site 205. The Lake Valley fault disappears beneath cover about 1 km southeast of line 200 and reappears in outcrop again about 1 km to the northwest. Measurements lay on the Berrenda fault system that is bounded by two mapped northeast-trending splays roughly orthogonal to the Lake Valley fault (fig. 7).

A factor that weighs on the accuracy and interpretation of the AMT data on line 200 is a power line about 1 km northwest of sounding 206 that is subparallel to the line of sites. In the vicinity of sites 203 and 204, this power line is tapped to provide electricity to a ranch southeast of line 200. The subsidiary power line is about 150 m from site 204, and about 50 m from

site 203. Power line signals at 60 Hz and harmonics of those signals can produce deterioration of the signal-to-noise ratio for nearby measurement at frequencies less than a few thousand hertz. Power lines may also carry induced electric currents that distort the electromagnetic response of the Earth.

Figure 10 shows the resistivity section for line 200 based on the layered inversions. The basic data (Klein and Wise, 1998) indicate a three-dimensional geometry that is particularly pronounced west of site 204. Lateral changes in the 3-dimensional indications between sites 205 and 204 (fig. 10) may be in part due to the orthogonal intersection of the Lake Valley fault with the Berrenda fault system. Because of probable 3-D geoelectric structure and the noise generated by the power lines, only the higher frequency part of the section that penetrates to less than about 500 m will be considered.

The cross section (fig. 10) appears comparable in part to the segment of line 100 northeast of the Lake Valley fault (fig. 8) in that both lines detect alternating conductive and resistive zones inferred to be a reflection of Paleozoic sedimentary rocks at depth. A conductive zone near the surface in this cross section along line 200 is consistent with the conductive alluvium along Berrenda Creek. There is also a conductive zone (about 50 ohm-m) starting at about 100 m depth, possibly associated with the Percha Shale. Increased resistivity with depth is probably associated with the Paleozoic carbonates and Proterozoic basement. The conductive zone inferred to be Percha Shale appears to have a vertical offset (down to the southwest) between sites 204 and 205, and again between sites 203 and 204. The apparent offsets may be an indication of faulting, or a westerly dip of the strata. The former is considered probable because the Lake Valley fault can be geologically inferred to pass beneath the line. A throw of nearly 100 m down-to-the-west for the Lake Valley fault between 204 and 205, along with a splay of the Lake Valley fault with a throw of about 50 m between 203 and 204, seems likely.

Note: A combined list of references for all chapters of this Professional Paper is located at the end of this volume, beginning on page 76.

Discussion

South of Monument Peak, the northeast half of traverse 100 identified two widespread conductive units. The upper conductive unit (3–10 ohm-m) at depths varying from 10 to 50 m is inferred to be associated with the base of the unconsolidated alluvium, gravel, and float. The next lower conductive unit (10–15 ohm-m) is interpreted to represent Percha Shale at a depth of about 200 m. Conductive units on the southwest half of the traverse probably reflect interfaces between andesitic volcanic units. A discontinuity in these units indicates the southward continuation of the Lake Valley fault. Apparent eastward dip of the inferred interfaces between andesitic volcanic units indicates graben development along the fault. An unmapped fault is suggested about 2 km east of the Lake Valley fault based on various contrasts in resistivity near the northeast end of the traverse. Deep units detected had high resistivities that may be associated with either limestone, dolomite, or igneous-metamorphic rocks. Proterozoic basement could not be separately identified. Vertical offset across the deep resistive unit provided the chief evidence of vertical throw across the Lake Valley fault. Dip of strata, which is known only in the Lake Valley mining district and to the north, was a factor in interpretation of throw. Using a geologic estimate of 20° dip to the southwest gave the minimum displacement of 50 m to the west. The largest displacement that can be inferred is 250 m, based on comparing resistivity structure east of Monument Peak with that on line 100 to establish an apparent dip of 8°.

Measurements north of Lake Valley on a traverse along Berrenda Creek were influenced by power lines and intersecting faults. Shallower penetrating data affected least by these complications provide hints on the northward extension of the Lake Valley fault. The upper 500 m of the model suggests an apparent westward dip of strata of about 20° that may be associated with multiple faults having a combined throw of 100–150 m.

Mineral Deposits of the Lake Valley Mining District

By V.T. McLemore *and* C. J. Nutt

With a Geochemistry Appendix *by* V.T. McLemore *and* J.R. Herring

U.S. Geological Survey Professional Paper 1644–C

Description of the mining history and selected mines of the district

GEOLOGIC INVESTIGATIONS IN THE LAKE VALLEY AREA, SIERRA COUNTY, NEW MEXICO

U.S. Department of the Interior
U.S. Geological Survey

Contents

Figures

Tables

Note: Combined references list begins on page 76.

Mineral Deposits of the Lake Valley Mining District

By V.T. McLemore[1] *and* C.J. Nutt

Abstract

Lake Valley historic mining district contains carbonate-hosted silver-manganese deposits from which more than 6,000,000 troy ounces of silver were extracted. The district is most famous for the discovery in 1881 of the Bridal Chamber, one of the richest silver ore bodies ever to be mined in the United States. Ore is in fault- and fracture-controlled and stratabound replacements at and near the contact between the thick-bedded Alamogordo and thin-bedded Nunn Members of the Mississippian Lake Valley Limestone. The southeast-dipping wedge of Mississippian rocks hosting the Lake Valley mining district is bounded on the southwest by the recurrently active Lake Valley fault, which places unmineralized Oligocene Mimbres Peak Formation rhyolite against Lake Valley Limestone. Ore is most abundant near, but not along, the Lake Valley fault, and lessens in abundance along strike to the southeast. The deposits are spatially associated with an overlying Quaternary(?) gravel.

Introduction

The historic Lake Valley mining district, in the southern part of the map area of plate 1 (in pocket), contains small, high-grade silver-manganese deposits in carbonate rock (figs. 1, 2). The deposits were exploited for silver, primarily in the 1890's (table 1*A*); interest in manganese corresponded with concern for the supply of strategic metals during and after World Wars I and II (table 1*B*). The ore is restricted to an inlier of Mississippian Lake Valley Limestone that is surrounded by volcanic rocks near the southeast edge of the Emory cauldron. The Lake Valley fault is the most prominent structure in the area and is the southwestern boundary of the mining district.

Lake Valley is one of 11 mining districts in the Black Range (figs. 2, 3; tables 2, 3). The Black Range is largely underlain by volcanic rocks of the middle Tertiary Mogollon-Datil volcanic field and is on the northeast edge of the major Laramide copper porphyry belt in Arizona and New Mexico. Deposit types identified in the Black Range include Cretaceous Laramide porphyry, Laramide skarns, Laramide veins, gold placer, carbonate-hosted, volcanic-epithermal, and rhyolite tin (table 2); classification is from McLemore (1998). The most productive deposit types in the Black Range are Tertiary epithermal-volcanic veins, Laramide porphyry, and Cretaceous to Tertiary carbonate-hosted veins and replacements (McLemore, 1998). This report is primarily descriptive and is about Lake Valley; see McLemore (1998) and Nutt and others (1998) for discussion on the mining districts of the Black Range and assessment of mineral potential at Lake Valley.

[1] New Mexico Bureau of Geology and Mineral Resources, Socorro, NM 87801. (Formerly New Mexico Bureau of Mines and Mineral Resources (NMBMMR).)

Lake Valley

Mining History

Lake Valley is a small but well-known mining district in southwestern Sierra County. So much has been written about this district with little preserved documentation, it is hard to separate fact from fiction. The district is most famous for the discovery in 1881 of the Bridal Chamber, one of the richest silver ore bodies ever to be mined (Eveleth, 1986), although actual production from the Bridal Chamber is unknown. Clark (1895) estimated that 2.5 million ounces of silver were produced from the ore pocket, but production estimated from company reports of the time suggest that total production may have been less than 1 million ounces (NMBMMR file data, newspaper accounts). The Bridal Chamber and nearby workings were ore pockets of silver chlorides and bromides—mostly chlorargyrite (cerargyrite)—a couple of hundred feet long and 25 feet thick (about 100 m long and 7 m thick), with assays as high as 20,000 oz/short ton (MacDonald, 1909). Samples, the largest of which was 640 lb of chlorargyrite, were sent to the National Mining Exposition at Denver, Colo., in 1882.

The district was discovered in August 1876 by Mr. McEverts, a rancher (Keyes, 1908). However, many accounts credit the discovery to George W. Lufkin in 1878. Lufkin, probably with McEverts, staked the first mining claims and named them after the nearby small lake. Lufkin soon took on a partner, Chris Watson, and began working the claims. Later, Lufkin borrowed money from John A. Miller, the post trader at Fort Bayard, and made him a third partner. In April 1881, Miller obtained the claims and sold them to George Daly. George Daly found a group of investors that formed four companies in July 1881: Sierra Grande, Sierra Bella, Sierra Plata, and Sierra Apache. The Sierra Grande group includes the Twenty-Five cut, Thirty stope, Bridal Chamber, and Carolina workings. The Sierra Bella includes the Emporia incline, Harrison, Bella Chute, Bunkhouse, Columbia, Last Chance and Strieby workings. The Sierra Apache includes the Apache and Bacon claims. The Sierra Plata includes the Plata claim. Mining claims, which encompass workings mentioned in text, are listed in table 4. The Sierra Grande Co. operated and administrated all the

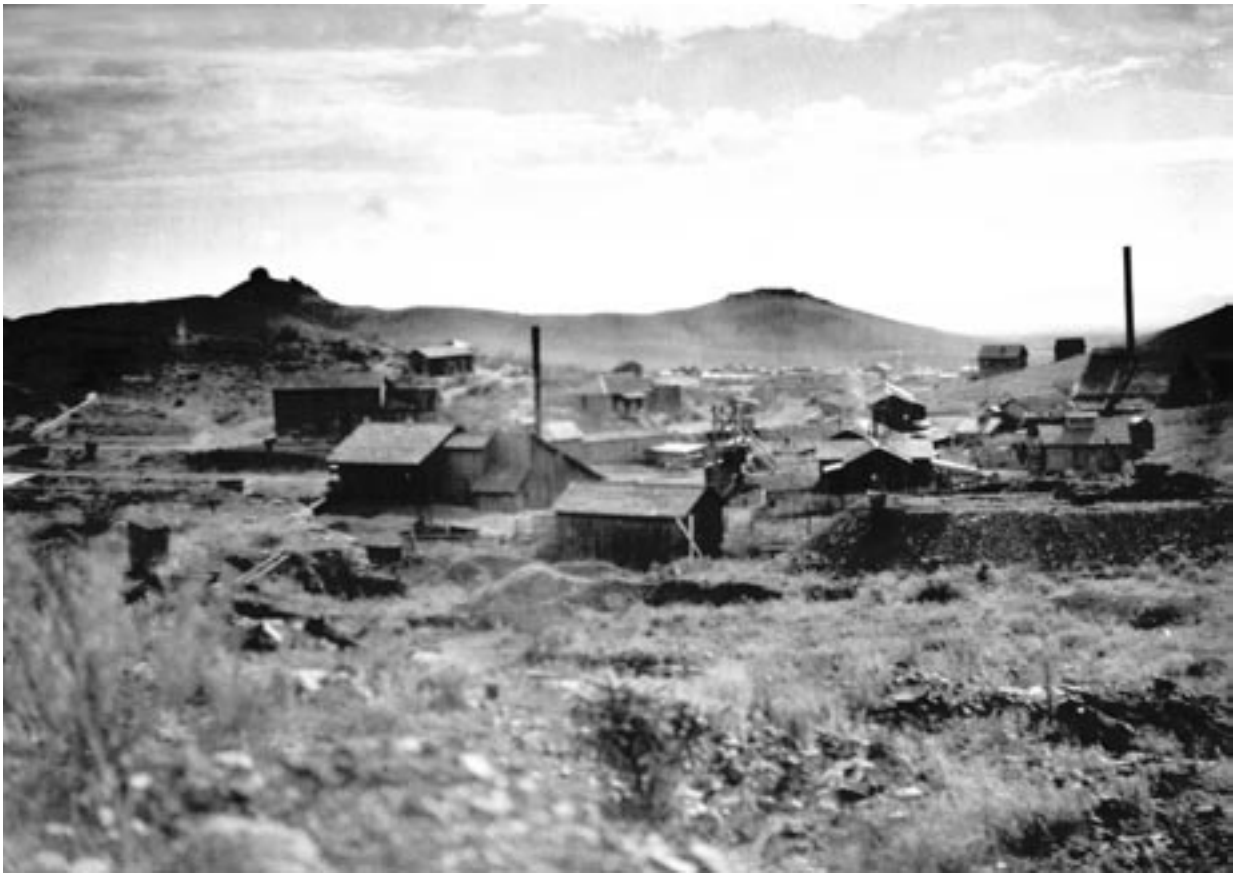

Figure 1. Lake Valley mining district townsite in 1908. Photograph by C.H. Gordon, #45, U.S. Geological Survey.

companies from 1881 to 1893. John Leavitt held a lease on one of the claims and is credited with discovering the Bridal Chamber (Jones, 1904). Mining in the district ceased in 1893, following the dramatic decline in silver prices as a result of the Federal Government's abandonment of silver as a monetary standard.

From 1893 to 1900, various individuals and companies leased the mines periodically. In 1900, the entire property administrated by the former Sierra Grande Company was sold to Lucius G. Fisher, who organized it under the Lake Valley Mines Company (Jones, 1904). From 1910 to 1931, shipments of silver-flux ore were made. During World Wars I and II, manganese was produced. The last production from the district was probably in 1958 or 1959. Total production from the district (tables 1, 2) is estimated as 5,000,000–6,126,000 oz silver, 500,000 pounds lead, 45,540 long tons 23 percent manganese ore, and 57,800 long tons 25 percent manganese concentrates (Farnham, 1961).

Geologic Setting

The Lake Valley mining district is southeast of the Emory cauldron and near the intersection of the Lake Valley and Berrenda faults at the south end of the Animas basin (fig. 3, pl. 1).

Table 1*A*. Precious- and base-metal production from the Lake Valley district.

[Harley (1934); NMBMMR file data; —, no data]

Year	Ore (short tons)	Copper (lb)	Gold (oz)	Silver (oz)	Lead (lb)	Value in dollars during year of production
1878–1893	—	—	—	5,000,000	—	5,000,000
1893–1910	—	—	—	500,000	—	100,000
1910–1931	46,261	—	—	275,000	—	137,500
1934	352	100	1.8	4,616	1,000	3,092
1935	56	—	—	1,550	400	1,130
1936	60	120	6.6	488	1,200	675
1938	29	100	—	215	1,100	200
1939	119	100	—	1,572	300	1,091
1940	132	100	—	1,499	800	1,117
Estimated total 1878–1957	—	100,000	10	6,126,000	>500,000	5,400,000

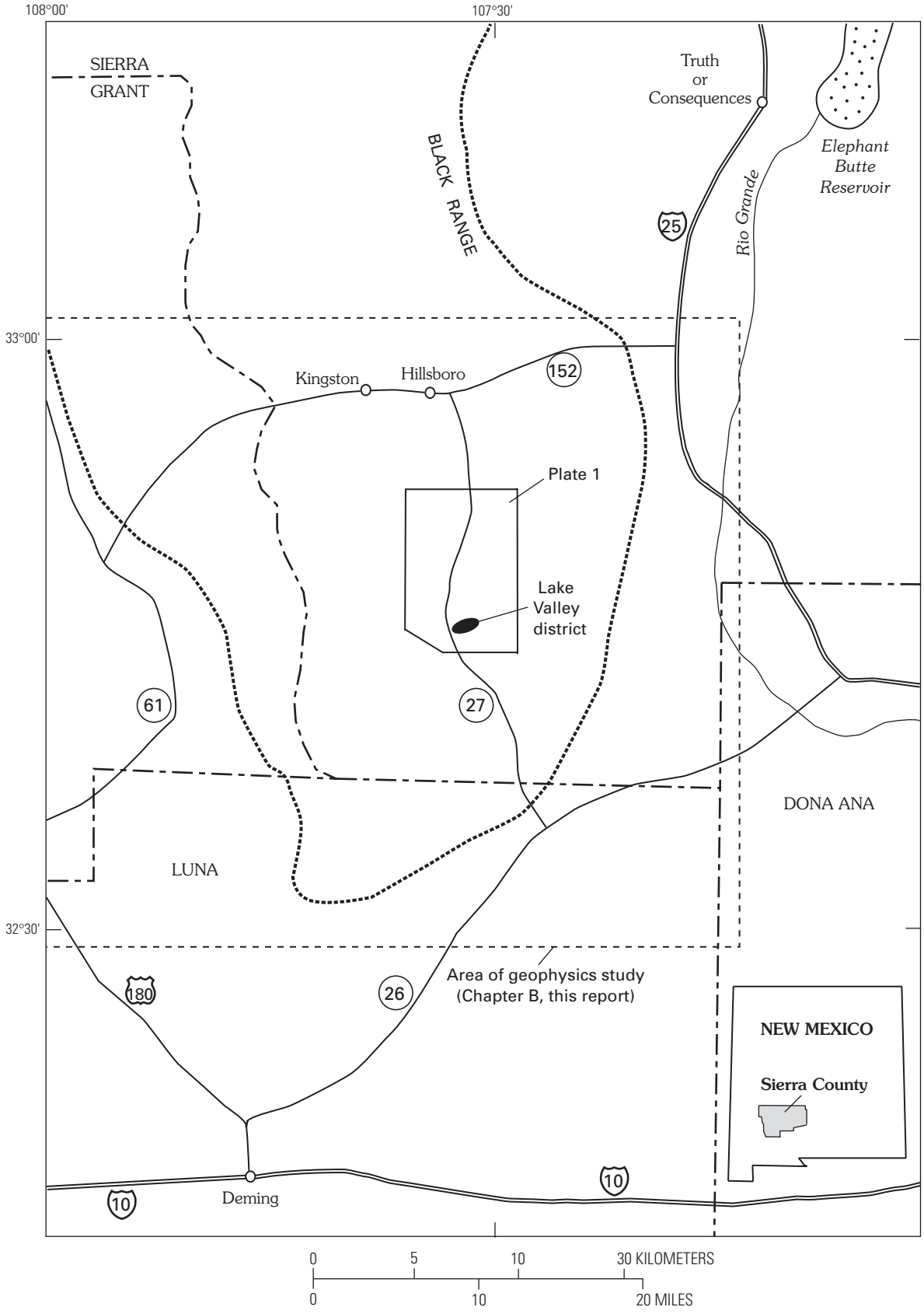

Figure 2. Lake Valley mining district in Black Range and within area of plate 1.

Table 1*B*. Manganese production from mines from the Lake Valley district.

[Farnham (1961); —, no data]

	Long tons ore	Long tons concentrate
Prior to 1942	8,000	—
1942–1943	37,224	—
Good Luck 1953	316	—
1953–1955	—	57,301
1958–1959	2,000	500
Total	45,540	57,801

Table 2. Mining districts other than Lake Valley in Black Range area.

[Volcanic-epithermal refers to shallow, hydrothermal base- and precious-metal veins hosted by volcanic rocks. Pb, lead; Zn, zinc; Ag, silver; Mn, manganese; classification of deposit types from McLemore (2001)]

Mining district	Type of deposit
Chloride	Volcanic-epithermal, placer gold, carbonate-hosted Pb-Zn
Carpenter	Carbonate-hosted Pb-Zn-Ag
Kingston	Carbonate-hosted Ag-Mn
Taylor Creek	Placer tin and tin vein deposits
Tierra Blanca	Carbonate-hosted Ag-Mn, volcanic-epithermal
Hermosa	Carbonate-hosted Pb-Zn
Macho	Volcanic-epithermal, carbonate-hosted Pb-Zn-Ag
Cuchillo	Carbonate-hosted Pb-Zn-Ag, placer tin and tin vein deposits, sedimentary copper, replacement Fe
Georgetown	Carbonate-hosted Ag
Hillsboro	Laramide vein, porphyry copper, carbonate-hosted Pb-Zn and Ag-Mn, Laramide skarn, placer gold

Table 3. Production from mining districts near Lake Valley.

[NMBMMR file data; —, no data]

District	Mn	Cu (lb)	Au (oz)	Ag (oz)	Pb (lb)	Zn (lb)
Carpenter	—	310,000	300	60,000–180,000	6,000,000	12,500,000
Chloride	—	10,127,097	25,253	3,647,763	1,300,000	1,500
Cuchillo	—	withheld	—	27,525	withheld	withheld
Hermosa	—	1,850	3	1,250,000	47,600	8,000
Kingston	2,520 long tons of 34–39% Mn ore plus 1,651 long tons of 35–40% Mn concentrate	111,950	124	6,126,000	676,820	566,900
Macho	—	—	61.4	20,000	679,000	11,000
Tierra Blanca .	—	92,784	97	165,000	318,687	464,055
Hillsboro	withheld	24,000,000	270,000	78,000	153,387	withheld
Lake Valley	57,800 tons of 25% Mn concentrate plus 45,224 long tons at 23 % Mn ore	100,000	10	6,126,000	>500,000	—

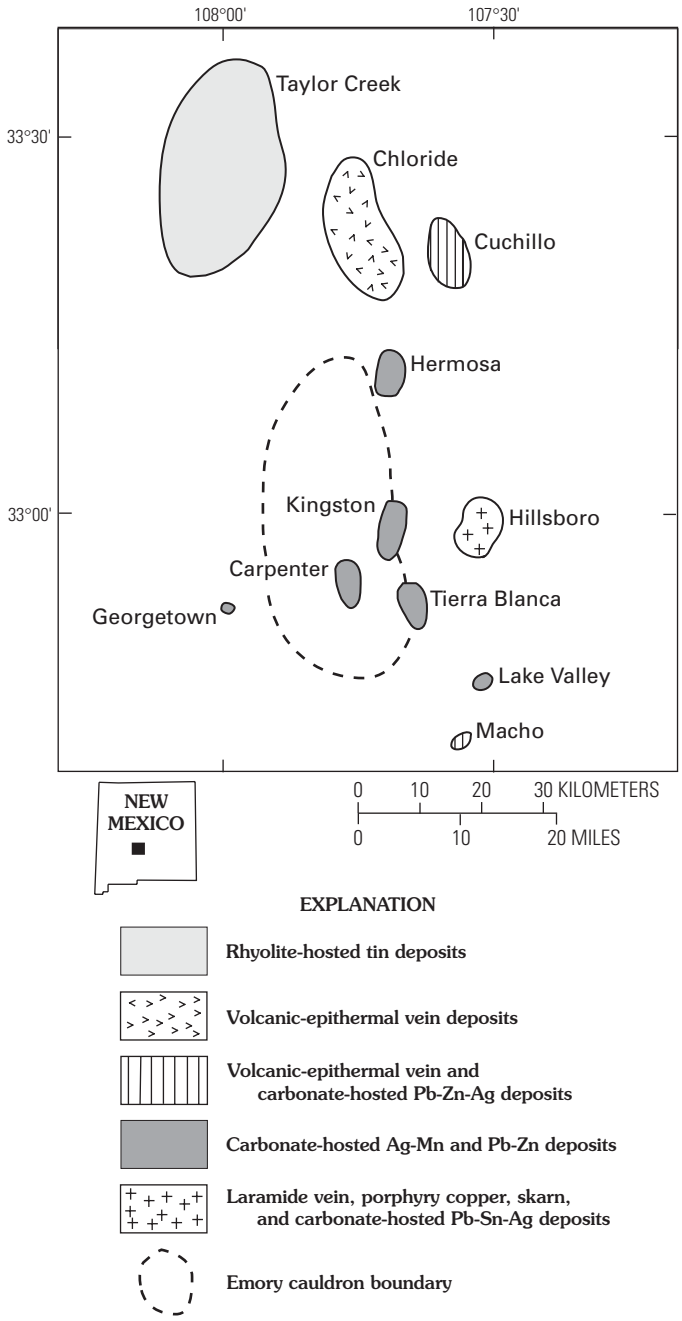

Figure 3. Mining districts in Black Range and in vicinity of Lake Valley mining district and their spatial relationship to approximate boundary of Emory cauldron. Modified from McLemore (1996).

Paleozoic rocks, in most of the map area covered by Tertiary volcanic rocks, host the ore. Ore is confined to veins and replacements in the Mississippian Lake Valley Limestone along a strike distance of about 1.6 km. Outcrop in and near the district includes Paleozoic rocks, Paleocene to Eocene Love Ranch Formation, Eocene to Oligocene Rubio Peak Formation volcanic rock, Oligocene Mimbres Peak Formation rhyolite, and Quaternary and late Tertiary unconsolidated or poorly consolidated material (Chapter A, pl. 1). The Lake Valley fault is the southwestern boundary of the district and drops Mimbres Peak Formation rhyolite against the mineralized Paleozoic rocks.

The Mississippian Lake Valley Limestone that hosts the district is part of a moderately disrupted sequence of southeast-dipping Ordovician, Silurian, Devonian, and Mississippian rocks exposed south of Berrenda Creek (pl. 1). The Ordovician El Paso and Montoya Groups and the Silurian Fusselman Dolomite underlie Quartzite Ridge, which is capped by a dip slope of silicified Fusselman. Devonian Percha Shale and landslide material that slid on the ductile Percha make up the strike valley southeast of Quartzite Ridge. Overlying the Percha Shale at Apache Hill, in ascending order, are the more resistant Mississippian Caballero Formation, the Lake Valley Limestone, small patches of Love Ranch Formation, and the oldest volcanic rocks in the study area. The ore-hosting Lake Valley Limestone makes up the dip slope of the ridge including Apache Hill and adjacent low ridges.

The Lake Valley Limestone consists of four members in the map area: the Andrecito, the Alamogordo, the Nunn, and the Tierra Blanca (Chapter A). The lowermost Andrecito is slope-forming, thin-bedded, argillaceous limestone containing abundant fenestelloid bryozoans and minor crinoid columnals. The overlying Alamogordo is ledge-forming, finely crystalline limestone, and the Nunn is slope-forming, marly, coarse-crystalline limestone with abundant crinoid fragments. The uppermost Tierra Blanca Member is ledge-forming, medium-bedded, and medium to coarsely crystalline limestone that contains abundant white to very light gray chert nodules and lenses.

In the district area, a thin remnant of Paleocene to Eocene Love Ranch Formation conglomerate, siltstone, and shale disconformably overlies the Tierra Blanca Member of the Lake Valley Limestone. Conglomerate clasts are commonly Tierra Blanca chert, and therefore locally derived. At the top of Apache Hill, a silicified crinoid was observed as a clast in the conglomerate.

Eocene to Oligocene Rubio Peak Formation volcanic rocks lie unconformably on Love Ranch Formation and Lake Valley Limestone. In this area, the dark-colored volcanics consist of flows and flow breccias and include both hornblende- and pyroxene-bearing rocks. Rubio Peak volcanic rocks make up much of the topography south and east of the district. The Rubio Peak is only locally oxidized and (or) deuterically altered, and it is not ore bearing.

A thick rhyolite dike at the southwest edge of the Lake Valley district underlies a low hill between two strands of the Lake Valley fault (Chapter A, pl. 1). The rhyolite and related intrusion breccia are interpreted as part of the Town Mountain rhyolite dome of Oligocene Mimbres Peak Formation that crops out southwest of the district and on the downthrown side of the Lake Valley fault. The rhyolite of the hill is characterized by delicate banding and vertical foliation, abundant altered pumice aligned along foliation, very fine grain size, a paucity of phenocrysts, and numerous lithic fragments. Lithic fragments include Kneeling Nun Tuff, Rubio Peak Formation, and Proterozoic basement rocks. Brecciated Rubio Peak and Kneeling Nun occur along the edges of the rhyolite. A very fine grained rhyolite sill and associated veinlets cut the rhyolite. The lithic fragments, altered pumice fragments, sills, and breccia suggest explosive activity related to intrusion. Pieces of abandoned core drilled in brecciated rhyolite along the Lake Valley fault just northwest of the district are barren of mineralized rock. The rhyolite is not mineralized except for minor manganese-oxide veinlets and pockets. (See Appendix, samples Lake 62, 63.)

Table 4. Mining claims in Lake Valley district.

[ac, acres; —, no data. To convert acres to hectares, multiply by 0.40]

Mine name/alias	Size	Ownership	Mineral survey No.	Patent No.	Date patented
Annie P	19.67 ac	Lake Valley Mines Co. (estate of Lucius G. Fisher)	532A	14982	5/17/1889
Apache	—	Lake Valley Mines Co. (estate of Lucius G. Fisher)	894	22958	5/13/1893
Arizona	18.71 ac	Lake Valley Mines Co. (estate of Lucius G. Fisher)	717C	—	11/20/1891
Bacon (Francis Bacon)	18.29 ac	Lake Valley Mines Co. (estate of Lucius G. Fisher)	892	22385	2/19/1932
Carolina (originally Lincoln)	17.733 ac	Lake Valley Mines Co. (estate of Lucius G. Fisher)	657	17027	1/10/1891
Columbia	13.65 ac	Lake Valley Mines Co. (estate of Lucius G. Fisher)	893	22959	5/13/1893
Compromise	—	Lake Valley Mines Co. (estate of Lucius G. Fisher)	1810	832415	11/15/1921
Comstock (Looney shaft)	8.08 ac	Lake Valley Mines Co. (estate of Lucius G. Fisher)	717E	—	11/20/1891
Emporia	17.04 ac	Lake Valley Mines Co. (estate of Lucius G. Fisher)	717H	—	11/20/1891
Good Luck	—	Central Mining Co., Santa Fe (1960)	—	none	—
Jim Finch	—	D. S. Miller ptd, F. H. Perry (1947)	1746	654504	11/25/1918
Last Chance	20.14 ac	Lake Valley Mines Co. (estate of Lucius G. Fisher)	717F	—	11/20/1891
Little Boy	18.46 ac	Lake Valley Mines Co. (estate of Lucius G. Fisher)	717D	—	11/20/1891
Little One	no application	Lake Valley Mines Co. (estate of Lucius G. Fisher)	134	none	—
New Era	—	—	246	none	—
North Carolina (originally Stanton)	19.74 ac	W. C. Hadley-Lake Valley Mines Co	656	17028	1/10/1891
Plata	20.42 ac	Lake Valley Mines Co. (estate of Lucius G. Fisher)	717A	18945	11/20/91
Sierra Grande millsite	4.9 ac patent	Lake Valley Mines Co. (estate of Lucius G. Fisher)	532B	21009	4/23/1892
Silver Reef (Silver Rut)	17.94 ac	Lake Valley Mines Co. (estate of Lucius G. Fisher)	717B	—	11/20/1891
South Carolina	19.99 ac	W. C. Hadley-Lake Valley Mines Co	658	16976	12/26/1890
Stone Cabin	18.741 ac	J. H. Winslow (1967)	425, 1122	—	—
Strieby (Bella)	12.93 ac	Lake Valley Mines Co. (estate of Lucius G. Fisher)	717G	—	11/20/1891

A paleochannel filled with poorly consolidated gravel cuts across the mining district and overlies the Bridal Chamber (Creasey and Granger, 1953). The gravels, as mapped by Creasey and Granger (1953), lie in the present-day topographic low that generally follows the contact between the Alamogordo and Nunn Members of the Lake Valley Limestone. Clasts include pebbles and cobbles of jasperoid, rhyolite, and limestone; porphyry near the base of the paleochannel may be part of a large boulder or a flow. The lower part of the gravels is locally cemented by calcite and silica. The deposits in the paleochannel were described as an igneous "porphyrite" by Clark (1895), who noted a spatial relationship between the "porphyrite" and underlying ore. Creasey and Granger (1953) mapped the unit as an early Tertiary conglomerate that predated Eocene volcanic rocks, but Jicha (1954) mapped the unit as Quaternary gravels. We consider the paleochannel as younger than the Santa Fe Group and deposited about the same time as nearby Quaternary terrace (Qtg) and pediment (Qpy) gravels (Chapter A, pl. 1). The gravels probably extended southward and were continuous with pediment gravels on the southeast, but the intervening gravels have since been stripped by erosion.

The district is in a wedge of rocks bounded on the southwest by the northwest-striking Lake Valley fault and on the north by westerly-striking faults (Chapter A, pl. 1). As explained in Chapter A, the Lake Valley fault in the area of the district is interpreted as having multiple movements, including a component of right-lateral strike-slip in the Laramide and normal movement in the Tertiary. The map pattern shows that in the mining area, near the Lake Valley fault, the beds have a slightly more easterly strike than elsewhere in the map area; this bend in strike may relate to drag along the Lake Valley fault. In the district itself, west-striking faults of small offset and associated fractures are the dominant structures. These faults are about parallel to a larger west-striking fault that approximately bounds the district on the north and cuts Quartzite Ridge (pl. 1). West-striking faults are rare in the map area outside the district.

Mineralized Rock

Small and irregular zones of mineralized rock are localized at and near the contact between the Alamogordo and Nunn Members of the Lake Valley Limestone. Cross sections by Clark (1895) across the district emphasize the stratabound character of the ore. The Alamogordo Member is thick- to medium-bedded, fine-grained to aphanitic limestone that shows a conchoidal fracture. In contrast, the overlying Nunn Member is thin bedded, contains abundant clays, and breaks along bedding planes. The contact between the members is exposed in the old workings, where slickensides indicate bedding plane slippage of the ductile Nunn Member over the rigid and fractured Alamogordo Member. Jasperoid replaces fractured Alamogordo, and is itself brecciated. Harley (1934) reported 0.3–0.6 m of jasperoid at the top of the Alamogordo. In the western part of the district, the jasperoid is brecciated and hosts ore, whereas in the eastern part it is less disrupted and forms the footwall of mineralized rock in the lower part of the Nunn Member.

The richest ore in the Lake Valley mining district is near the Lake Valley fault. Jicha (1954) stated that the ore is in the drag zone of normal movement on the fault. The detailed map of the mining district and underground workings by Creasey and Granger (1953) shows that although ore is concentrated near the Lake Valley fault, it is not along the fault. However, minor faults northeast of the Lake Valley fault contain mineralized rock (Creasey and Granger, 1953).

Ore in the district is spatially associated with the Quaternary gravels, as shown on the map by Creasey and Granger (1953). Clark, who referred to the paleochannel gravels as porphyrite, noted that all the deposits, with exception of a small one in the Apache group of claims, are near the gravel unit and that the largest, the Bridal Chamber and Bunkhouse, are directly under it. Both the Bridal Chamber and Bunkhouse deposits are in caverns and consist largely of cerargyrite. Clark also stated that the overlying gravel carried up to an ounce of silver per ton.

Jasperoid occurs not only in the Lake Valley Limestone, but also in the upper part of the Fusselman Dolomite and in the Montoya Group north and northeast of the mining area. The best developed and most extensive jasperoid is in the Fusselman Dolomite (fig. 4). In the map area, jasperoid in the Fusselman Dolomite is overlain by unaltered Rubio Peak Formation and

Figure 4. Jasperoid in the Fusselman Dolomite. Photograph from Lovering (1972).

Sugarlump Tuff; therefore the jasperoid is Eocene or older and predates caldera magmatism. The jasperoid in the Fusselman Dolomite that holds up Quartzite Ridge is aphanitic and white to gray colored, and is in places brecciated and recemented by aphanitic silica. Jigsaw puzzle textures are found locally. However, large areas of red to brown to white jasperoid are unbrecciated and aphanitic. Locally, manganese oxide and crystalline quartz veinlets cut the jasperoid, and drusy quartz and iron and manganese oxides fill vugs. Visible pyrite is rare to absent except where the jasperoid is cut by faults, but microscopic finely disseminated pyrite, in many places altered to hematite and goethite, is common. Lovering and Heyl (1989) reported these jasperoids to be barren except where cut by the Lake Valley fault.

Table 5. Silver production from mines in Lake Valley district, 1878–1893.

[Clark (1895)]

Mine	Production (oz of silver)
Bridal Chamber	2,500,000
Thirty stope	1,000,000
Emporia incline	200,000
Bunkhouse	300,000
Bella	500,000
Twenty-five cut	200,000
Apache area	300,000
Total	5,000,000

Description of Deposits

Descriptions of the mine workings at Lake Valley are from Clark (1895), Harley (1934), Creasey and Granger (1953), and this study. Major workings, many of which are discussed in the text, are shown in figure 5 and table 5. Following Creasey and Granger (1953), the district is separated into four areas: Grande, Bella-Strieby, Apache, and Stone Cabin areas (fig. 5); most of the ore was extracted from the Grande and Bella-Strieby areas.

The mineral deposits occur in two forms: (1) fault- and fracture-controlled replacements and (2) stratabound replacement bodies. The fracture- and fault-controlled deposits are in irregular, steeply dipping zones locally at the intersection of northeast- and northwest-striking fractures and faults (Creasey and Granger, 1953) and along west-striking faults. Mineralized rock is most common in crosscutting structures in the western part of the mining district and in the Alamogordo Member of the Lake Valley Limestone. Deposits at the Daly shaft (fig. 5) and at the No. 14 surface cut (near the Boiler shaft northwest of the Bridal Chamber) are typical of fault- and fracture-controlled deposits. Locally, the lower 0.3–0.9 m of the Nunn Member is mineralized and, in underground workings at the Daly shaft, the Andrecito Member is mineralized for approximately 0.6–0.9 m from the controlling structure.

Tabular, stratabound replacement deposits are adjacent to the fault- and fracture-controlled deposits. These deposits are typically in the upper Alamogordo Member, near the contact with the overlying Nunn Member. The silver ore bodies were thin, irregular tabular zones 0.9–2 m thick that were underlain and laterally surrounded by larger manganese replacement bodies 1–9 m thick. The high-grade silver zones were mined out in the 1880's, leaving only manganese replacements, some of which contain low-grade silver. Thinner and smaller manganese-silver deposits, 1–3 m thick, are in the Apache and Stone Cabin area workings.

A high-grade silver pocket was mined from the Bridal Chamber, and smaller silver bonanza pockets from the Emporia incline and Bunkhouse shaft (Clark, 1895). The Bridal Chamber consisted of nearly pure cerargyrite in a pocket about 100 m long and 7 m thick (MacDonald, 1909). A streak of pure cerargyrite or chlorargyrite (AgCl) was 1 m thick, and assays as high as 20,000 oz/short ton were common. Silver pockets in the Emporia incline contained 200–500 oz/short ton silver and 50–60 percent lead as galena (Clark, 1895). Ore from the Bunkhouse mine contained 200–500 oz/short ton silver. A 5-ton shipment from the Columbia mine contained 3,600 oz/short ton silver (Silliman, 1882).

Primary silver minerals, since mined out, were stephanite, proustite, pyrargyrite, and argentiferous galena (Harley, 1934). Oxidized minerals (cerargyrite, embolite, native silver, cerussite, vanadinite, wulfenite, endlichite, descloizite, iodyrite) were either deposited as primary minerals when the fluid evolved to a more oxidizing state or were formed by later supergene fluids. Other minerals found in the district include pyrolusite, manganite, psilomelane, limonite, hematite, calcite, anderite, and apatite (Silliman, 1882; Genth and von Rath, 1885; Clark, 1895; Lindgren and others, 1910).

Alteration minerals at Lake Valley are primarily quartz , calcite, and clay. The quartz is mostly jasperoid occurring in aphanitic veins. The calcite-clay assemblage is at and near the contact between the Alamogordo and Nunn Members; in addition, several faults and fracture zones in the underground workings are filled with calcite and clay minerals. Locally, clay zones, overlying or adjacent to mineralized jasperoids, contain elevated silver, lead, and other metals. (See Appendix, samples Lake 74, 83, 98.) Elsewhere, a zone consisting of fine-grained white calcite and clay overlies the manganese deposits.

At the Bridal Chamber, a 0.3–1 m silicified zone overlies the Ag-Mn deposit at the top of the Alamogordo Member. This silicified zone is low in metals concentration (Appendix, samples Lake 89, 90) and is unconformably overlain by the paleochannel-filling gravels. A sample of clay from between the Nunn Member and the poorly consolidated gravel at the Bridal Chamber contains elevated silver, lead, and other metals (Appendix, sample Lake 91) and is interpreted as a supergene enrichment zone; the paleochannel may have eroded part of the ore deposits in the Bridal Chamber area.

A crude zonation that exists in the district is predominantly a reflection of the abundance of silver and jasperoid in the western part of the area. The western deposits, known as the Grande area workings (Clark, 1895; Apell and others, 1947; Creasey and Granger, 1953), contain the largest and highest grade deposits (Clark, 1895; Creasey and Granger, 1953) and consisted of predominantly siliceous ore. Early ore mined from these workings averaged 65 percent silica, 6 percent iron, 12 percent manganese, and 20 oz/short ton silver (Clark, 1895). High-grade

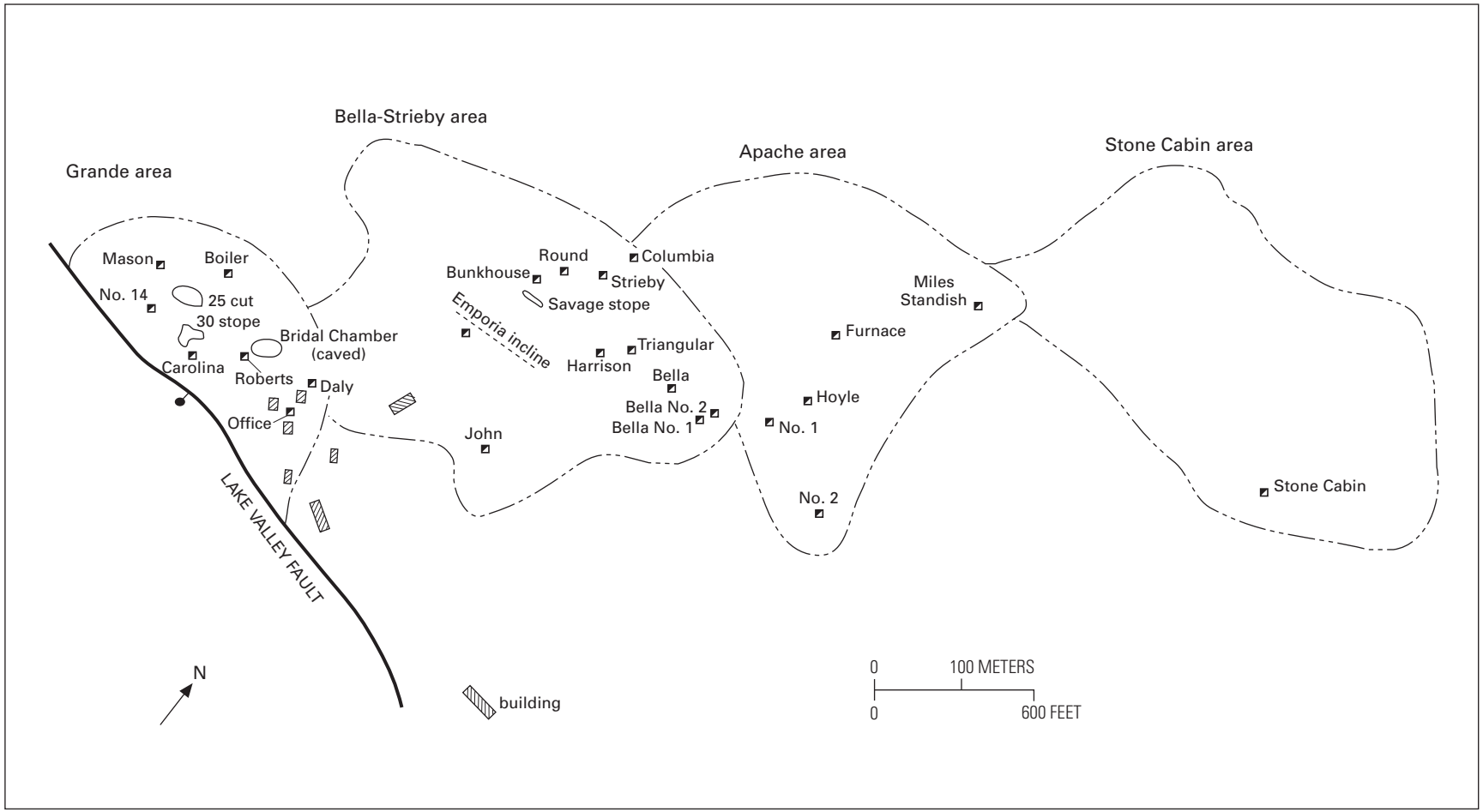

Figure 5. Lake Valley mining district showing major workings. Minor workings, not shown, are within area boundaries. Modified from Creasey and Granger (1953).

silver bodies were common. Manganese ore assayed in the 1940's averaged 42.7 percent silica, 8 percent iron, and 20.8 percent manganese (Creasey and Granger, 1953). The Bella workings and Emporia incline in the Bella-Strieby area were intermediate in silica composition. Early ores mined from these workings averaged 30 percent silica, 12 percent iron, 18 percent manganese, and 30–50 oz/short ton silver (Clark, 1895). Manganese ore assayed in the 1940's averaged 45.6 percent silica, 8 percent iron, and 20.2 percent manganese (Creasey and Granger, 1953). Ore from the Bunkhouse and Columbia mines (Bella-Strieby area) and from the Apache area consisted of more manganese, and typically, less silica and silver. Early ore from these deposits averaged 8 percent silica, 12 percent iron, 24 percent manganese, and 20–30 oz/short ton silver (Clark, 1895). Manganese ore assayed in the 1940's averaged 38.2 percent silica, 6 percent iron, and 21.4 percent manganese (Creasey and Granger, 1953).

All the deposits are shallow. The Boiler shaft was sunk to a depth of 53 m, and the deepest mineralized area was 49 m (Clark, 1895). Most of the other workings in the Grande area are less than 37 m deep. The John shaft, in the Bella-Strieby area, is 49 m deep; a drift connects it to the Emporia incline. Several replacement deposits are intersected by the drifts at the John shaft, but silver concentrations are low (Appendix, samples Lake 32, 33). Harley (1934) reported that a drilling program in 1928–1929, exploring the potential for deeper deposits in the lower Lake Valley Limestone and Fusselman Dolomite, was unsuccessful. The exact locations of these holes are unknown.

Several episodes of brecciation and silicification affected the Lake Valley Limestone in the district. Clark (1885) reported that in the western part of the district, the jasperoid at the top of the Alamogordo Member was cut by silver-bearing jasperoid. Observations from near the Bridal Chamber reveal several periods of jasperoid deposition followed by brecciation and dissolution of the host limestone. The first event consisted of deposition of banded green and gray jasperoid in replacement pods. The green and gray jasperoid is brecciated and cemented by red and light-brown jasperoid, which is in turn brecciated and cemented by manganese-iron oxides, black jasperoid, and calcite that formed both fissure and bedded deposits. These deposits were brecciated and cemented locally by chocolate-brown, gray, green, black, and red jasperoid, and then cut by manganese-quartz veins. The final event was deposition of white boxwork quartz. White, clear, crystalline quartz and calcite occur in veinlets, and white to brown crystalline calcite fills vugs. Vanadinite occurs as very fine grained hexagonal prisms and thin coatings (Silliman, 1882; Genth and von Rath, 1885) and probably formed during a late oxidation or supergene stage. Iodyrite is within calcite crystals (Genth and vom Rath, 1885). Deposits northeast of the Bridal Chamber are lower grade, contain less silica, and exhibit only one or two stages of brecciation. Delicate banded manganese oxide, typical of epithermal deposition, occurs locally in the district.

Placing the silver mineralization in a paragenetic sequence is difficult because the silver minerals were mined out. Silliman (1882) suggested silver, as embolite, occurred with the green jasperoid (also called flint or vein stone), and Clark's (1885) observation of early barren jasperoid cut by veins of silver-bearing jasperoid supports this idea. Chemical analyses indicate that manganese and silver content correlate positively, suggesting that at least some silver was deposited during the manganese event.

Geochemistry

Korzeb and others (1995; 61 samples) and V. T. McLemore (this report; 84 samples, Appendix) collected samples of the carbonate-hosted replacement deposits, jasperoids, and igneous and sedimentary rocks within the district. Chemical analyses of jasperoids are also reported in Young and Lovering (1966) and Lovering and Heyl (1989).

Trace element analysis of the mineralized samples from the Lake Valley deposits indicates that many of these deposits are enriched in silver (0.6–>300 ppm), lead (10–14,900 ppm), manganese (28–118,000 ppm), and zinc (4–92,500 ppm) and are relatively low in copper (1–79 ppm) and gold (<2–175 ppb). The highest gold concentration (175 ppb) is from a sample collected in the deeper underground workings of the Shelby shaft located between the Savage and Strieby mines (Appendix, sample Lake 25). Silver (in mineralized samples collected from the district) has a high Pearson correlation coefficient with lead (0.50), bromine (0.51), arsenic (0.31), and vanadium (0.45). These data reflect the predominant mineralogy of manganese and iron oxides and silver halides and bromides in a gangue of quartz and calcite.

One select sample collected along the Lake Valley fault northwest of the district, where the fault separates the Mimbres Peak rhyolite that underlies Town Mountain from the Fusselman Dolomite, contains elevated silver (59 ppm), lead (3,050 ppm), zinc (3,580 ppm), and manganese (79,890 ppm) (Appendix, sample Lake 101). This sample is from a small prospect that exposes thin manganese-calcite veins in rhyolite and Fusselman Dolomite. Another prospect along the fault contained a small carbonate-hosted replacement in Fusselman Dolomite; the metal concentrations were low (Appendix, sample Lake 102). Samples of thin manganese veins cutting the rhyolite southwest of the main district are also low in metals (Appendix, samples Lake 62, 63).

The jasperoids, with a few exceptions, are low in metal concentrations. The highest gold concentrations (100–230 ppb) are from three jasperoid samples collected along a splay of the northeast-trending Berrenda fault zone (Appendix, samples Lake 65, 66, 67). These samples also contain elevated lead (601–4,750 ppm), zinc (24–509 ppm), molybdenum (37–331 ppm), arsenic (42–399 ppm), and vanadium (186–1,900 ppm).

Discussion

Age constraints on mineralization are uncertain. In the Black Range, known base- and precious-metal mineralization is related to Cretaceous porphyry or middle Tertiary volcanic epithermal events (McLemore, 1998). Jasperoid clasts in the early Tertiary Love Ranch Formation conglomerate and the occurrence of in-place Fusselman jasperoid overlain by unaltered Rubio Peak Formation and Sugarlump Tuff indicate that some silicification in the area was Eocene or earlier, but this

silicification is not proven to be the same generation as jasperoid that occurs at Lake Valley. The Oligocene Mimbres Peak Formation at Town Mountain is not mineralized, with the exception of rare manganese veinlets; however, offset along the Lake Valley fault could have obscured mineralized rhyolite.

We suggest that regardless of the timing of early mineralization, supergene enrichment produced the large orebodies at the Bridal Chamber and Bunkhouse. Clark (1895) described them as being in caverns and as consisting largely of cerargyrite (horn silver), which typically forms during supergene processes. The Lake Valley Limestone in the area was at or close to the surface in Paleocene to Eocene time and Quaternary time. Quaternary paleochannel gravels are spatially associated with the deposits. This association may reflect easier erosion of the supergene altered rock, or indicate that the paleochannel played some role as a conduit of fluids.

Note: A combined list of references for all chapters of this Professional Paper is located at the end of this volume, beginning on page 76.

Appendix. Chemical analyses of samples collected in and near the Lake Valley district, Sierra County, New Mexico. Method of analysis: INAA, neutron activation (U.S. Geological Survey); ICP, inductively coupled plasma spectrometry (U.S. Geological Survey); XRF, X-ray fluorescence spectrometry (New Mexico Bureau of Geology and Mineral Resources). V.T. McLemore and (or) Connie Nutt collected samples. Sample preparation by Jim Herrring and V.T. McLemore; USGS analyses arranged by Jim Herring. Blank spaces, not analyzed; *, sample collected from underground workings; **, XRF not analyzed because of analytical interference; ppm, parts per million; ppb, parts per billion; %, weight percent; <, less than. Latitude (N.), longitude (W.) in degrees, minutes, seconds.

Field No.	Type of sample	Mine	Latitude	Longitude	Au ppb	Sc ppm	Ta ppm	Th ppm	U ppm	Be ppm
Method of analysis					INAA					
Ore samples										
LakeV1	Mn oxide with red jasperoid		32 43 15	107 34 19	<2	0.4	<0.5	<0.5	11	<2
LakeV2	mill tails	mill tails	32 43 13	107 34 20	27	1.3	<0.5	0.8	5.4	3
Lake22*	chip of rib	Shelby	32 43 10	107 34 10	<5	2	< 40	17	< 100	< 1
Lake35*	grab of pillar	Emporia	32 43 13	107 34 10	6	< 2	< 40	< 6	< 100	< 1
Lake36*	grab of Mn stope	Daly	32 43 7	107 34 10	8	< 2	< 40	17	< 100	< 1
Lake37*	grab of chert	Office	32 43 6	107 34 13	<5	< 2	< 40	8	< 100	< 1
Lake38*	grab of rib	Office	32 43 6	107 34 13	<5	< 2	< 40	15	< 100	< 1
Lake20*	grab of muck	Savage mine	32 43 14	107 34 8	6	5	< 40	< 6	< 100	< 1
Lake21*	chip of rib	Strieby shaft	32 43 14	107 34 5	6	< 2	< 40	21	< 100	< 1
Lake22*	chip of rib	Shelby	32 43 10	107 34 10	<5	2	< 40	17	< 100	< 1
Lake25*	2 inch chip	Shelby-lower	32 43 10	107 34 10	175	3	< 40	< 6	< 100	< 1
Lake26*	dump of Mn stope	Shelby	32 43 10	107 34 10	18	< 2	< 40	< 6	< 100	< 1
Lake27*	grab of clay altered fault zone	Shelby	32 43 10	107 34 10	<5	8	< 40	< 6	< 100	< 1
Lake30*	grab of back	Emporia	32 43 13	107 34 10	<5	3	< 40	14	< 100	< 1
Lake31*	grab of pillar	Emporia	32 43 13	107 34 10	5	< 2	< 40	16	< 100	2
Lake32*	4 ft chip	John shaft	32 43 10	107 33 58	<5	< 2	< 40	< 6	< 100	1
Lake33*	4 ft chip	John shaft	32 43 10	107 33 58	<5	3	< 40	13	< 100	< 1
Lake36*	grab of Mn stope	Daly	32 43 7	107 34 1	<5	< 2	< 40	22	< 100	< 1
Lake37*	grab of chert	Office	32 43 6	107 34 3	<5	< 2	< 40	10	< 100	< 1
Lake38*	grab of rib	Office	32 43 6	107 34 3	6	< 2	< 40	20	< 100	< 1
Lake40*	4 ft vertical chip	Daly	32 43 7	107 34 10	12	< 2	< 40	16	< 100	< 1
Lake41*	4 ft vertical chip	Daly	32 43 7	107 34 10	<5	< 2	< 40	15	< 100	< 1
Lake42a*	chip of rib	Daly	32 43 7	107 34 10	<5	< 2	< 40	11	< 100	< 1
Lake74	clay above jasperoid	Roberts	32 43 10	107 34 5	10	13	<40	<6	<100	2
Lake75	6 ft chip across vertical jasperoid, under Alamogordo	Daly	32 43 7	107 34 10	24	<2	60	40	880	<1
Lake81	green chert, select	Shaft 14	32 43 6	107 34 30	6	<2	<40	<6	147	<1
Lake82	Mn black chert, select	Shaft 14	32 43 6	107 34 30	14	<2	49	33	783	<1
Lake83	altered white zone along fault, 5 ft chip	Shaft 14	32 43 10	107 34 15	5	<2	<40	<6	<100	<1
Lake84	5 ft chip of wall, muddy breccia	No. 14	32 43 20	107 34 20	28	<2	57	41	882	<1
Lake86	green, gray, red jasperoid	N Boiler	32 43 22	107 34 25	31	<2	<40	<6	271	<1
Lake88	gray altered ?, Bridal Chamber, grab of wall	Bridal Chamber	32 43 7	107 34 25	17	11	<40	<6	<100	1

Field No.	Type of sample	Mine	Latitude	Longitude	Au ppb	Sc ppm	Ta ppm	Th ppm	U ppm	Be ppm
Lake89	chip of 1 ft silicified gravel, Bridal Chamber	Bridal Chamber	32 43 7	107 34 25	<5	3	<40	<6	<100	<1
Lake90	green-brown sandstone, chip, Bridal Chamber	Bridal Chamber	32 43 7	107 34 25	<5	11	<40	<6	<100	1
Lake91	orange-black altered fault gouge, Bridal Chamber	Bridal Chamber	32 43 7	107 34 25	<5	9	<40	15	198	1
Lake94*	grab of rib, Mn ore	Near Office	32 43 6	107 34 13	16	3	<40	11	<100	3
Lake95*	grab of rib of bladed Mn ore	Near Office	32 43 6	107 34 13	18	<2	62	39	909	1
Lake96*	grab of red jasperoid with white talc	Near Office	32 43 6	107 34 13	7	5	<40	<6	<100	<1
Lake97*	4 ft vertical chip of pillar	Bridal Chamber	32 43 7	107 34 25	<5	2	<40	<6	189	<1
Lake98*	grab of white talc	Bridal Chamber	32 43 7	107 34 25	8	3	<40	<6	<100	<1
Lake99*	chip of rib, Mn ore	adit	32 43 35	107 33 55	<5	<2	<40	14	509	<1
Lake100	select dump of gray jasperoid	John shaft	32 43 10	107 34 0	38	<2	<40	<6	<100	1
Lake92	dump grab, green, gray, yellow chert	Bella	32 43 10	107 34 10	14	<2	50	31	868	<1
Igneous rocks										
Lake60	rhyolite dike	SW hill	32 43 5	107 34 23	<5	<2	<40	23	<100	2
Lake61	rhyolite	SW hill	32 43 10	107 34 28	<5	<2	<40	34	<100	3
Lake64	rhyolite dike	SW hill	32 42 56	107 34 19	22	2	<40	21	<100	2
Lake78	Town Mt rhyolite	Sec 20	32 43 30	107 35 21	<5	2	<40	20	<100	3
TB 100	McClede Mt rhyolite		32 51 00	107 36 00						
TB 101	McClede Mt tuff		32 50 59	107 36 00						
TB 102	Deer Mt rhyolite		32 50 35	107 38 25						
TB 106	rhyolite		32 51 19	107 40 50						
TB 112	rhyolite		32 49 58	107 40 25						
Jasperoids outside district										
Lake50	30 ft chip of jasperoid	Sec 20	32 43 13	107 34 55	<5	< 2	< 40	< 6	< 100	< 1
Lake53	chip of jasperoid	Sec 21	32 43 40	107 34 25	10	< 2	< 40	< 6	< 100	1
Lake54	chip of jasperoid	North of Lake Valley	32 46 27	107 32 34	<5	< 2	< 40	< 6	< 100	< 1
Lake65	jasperoid Fusselman, dump grab	Sec 4	32 46 0	107 33 25	230	<2	<40	<6	<100	<1
Lake66	altered limestone Fusselman, calcite, Fe, dump grab	Sec 4	32 46 0	107 33 25	100	<2	<40	<6	<100	7
Lake67	6 ft chip across jasperoids	Sec 4	32 45 59	107 33 28	227	<2	<40	<6	<100	<1
Lake69	10 ft chip across jasperoid in Alamogordo	Sec 16	32 44 46	107 33 29	12	<2	<40	<6	<100	<1
Lake70	select of gray banded jasperoid	Sec 16	32 44 46	107 33 29	7	<2	<40	<6	<100	<1

Field No.	Type of sample	Mine	Latitude	Longitude	Au ppb	Sc ppm	Ta ppm	Th ppm	U ppm	Be ppm
Lake71	altered Fusselman limestone, chip	Sec 17	32 44 29	107 34 50	<5	<2	<40	<6	<100	<1
Lake79	Montoya gray-red jasperoid, dump	Sec 20	32 43 42	107 35 10	7	<2	<40	<6	<100	<1
Lake80	Montoya jasperoid, 40 m chip	Sec 20	32 43 53	107 35 17	6	<2	<40	<6	<100	<1
Lake400	10 ft chip of jasperoid	Sec 35	32 47 0	107 32 0	<5	<2	<40	<6	<100	<1
Lake401	chip of jasperoid	Sec 35	32 47 0	107 32 0	<5	<2	<40	<6	<100	<1
Lake402	dump grab Fusselman jasperoid	Sec 34	32 47 0	107 32 0	6	<2	<40	<6	217	<1
Lake403	gray-green jasperoid Fusselman, dump grab	Sec 34	32 47 0	107 32 0	6	<2	<40	7	282	2
Lake103	select of red jasperoid with calcite veins	Lake Valley fault	32 43 6	107 34 50	8	<2	<40	<6	<100	2
TB 105	jasperoid		32 51 30	107 40 50						
TB 107	jasperoid		32 51 10	107 40 45						
TB 109	jasperoid		32 51 15	107 40 40						
TB111	jasperoid, purple		32 50 00	107 40 15						
TB113	jasperoid, purple		32 49 57	107 40 20						
TB115	jasperoid		32 49 55	107 40 17						
Ore samples outside district										
Lake42b	dump	unknown	32 42 56	107 33 48	<5	< 2	< 40	15	< 100	2
Lake62	Mn veins in rhyolite	SW hill	32 42 59	107 34 17	5	3	<40	14	<100	3
Lake63	6 inch chip of Mn-Si-Fe vein in rhyolite	SW hill	32 42 57	107 34 18	<5	4	<40	8	<100	3
Lake76	silicified Berrenda fault breccia, chip sample across 3 feet	Sec 1	32 46 40	107 36 55	<5	2	<40	<6	<100	<1
Lake85	dump grab, Fe-Mn oxides, jasperoid	Sec 11	32 45 5	107 32 28	22	9	63	<6	<100	8
Lake101	Mn oxides on rhyolite	Lake Valley fault	32 43 5	107 34 50	<5	4	43	42	648	2
Lake102	calcite veinlets, recrystallized limestone	Lake Valley fault	32 43 7	107 34 50	<5	<2	<40	<6	<100	<1
Sedimentary rocks										
Lake68	grab of Alamogordo limestone	Sec 16	32 44 35	107 33 35	<5	<2	<40	<6	<100	<1
Lake73	Fusselman limestone, chip	Sec 71	32 44 19	107 34 44	26	<2	<40	<6	<100	<1
Lake51	chip of black Percha shale	Sec 21	32 43 40	107 34 25	<5	13	< 40	9	< 100	3
Lake52	chip of red Percha shale	Sec 21	32 43 40	107 34 25	8	6	< 40	< 6	< 100	< 1

Field No.	Ag ppm	Cu ppm	Pb ppm	Zn ppm	Mo ppm	Ni ppm	Co ppm	Cd ppm	Bi ppm	As ppm	Fe %	Mn ppm	Ba ppm	Cr ppm
Method of analysis	ICP	ICP	ICP	ICP	ICP	ICP	ICP	ICP	ICP	ICP	ICP	ICP	ICP	ICP
Ore samples														
LakeV1	15.1	68	915	4425	13	7	1	36.9	<5	6.1	37.2	8259	190	380
LakeV2	65.3	28	1024	1045	6	19	3	7.9	<5	<0.5	0.24	72078	4600	67
Lake22*	< 2	< 2	387	78300	< 2	37	15	740	23	13	8.9	101000	5	6
Lake35*	258	22	12300	16200	< 2	12	3	103	10	28	8.1	72500	12	65
Lake36*	157	3	2970	2670	< 2	11	< 2	21	24	62	9.5	104000	21	28
Lake37*	257	13	2230	1010	44	185	4	4	10	64	5.9	75000	149	157
Lake38*	56	< 2	1870	665	16	10	3	< 2	15	63	4.2	98800	38	29
Lake20*	11	7	605	1410	14	48	3	7	< 10	39	2.9	33500	47	30
Lake21*	< 2	< 2	670	24800	26	218	9	748	27	112	11	118000	< 1	152
Lake22*	< 2	< 2	374	81500	< 2	30	15	725	21	22	8.9	99600	4	5
Lake25*	245	41	9900	4100	7	10	2	96	14	628	9.7	71500	67	11
Lake26*	6	< 2	691	92500	< 2	20	< 2	8	< 10	59	2.8	52700	5	4
Lake27*	< 2	22	28	354	< 2	34	17	< 2	< 10	< 10	3.4	4550	468	19
Lake30*	60	18	889	25200	< 2	231	9	291	15	21	6.1	93400	63	200
Lake31*	59	13	756	889	< 2	165	4	6	19	117	6.5	98600	12	160
Lake32*	38	5	317	265	< 2	19	3	< 2	< 10	94	2.9	48600	32	45
Lake33*	9	8	136	410	< 2	290	6	7	10	17	3.4	91700	37	219
Lake36*	143	< 2	3110	2740	< 2	9	< 2	23	26	68	10	116000	24	32
Lake37*	222	6	2180	978	44	185	5	5	< 10	67	6.2	81200	110	136
Lake38*	53	< 2	1890	686	12	16	3	< 2	18	75	4.4	108000	43	27
Lake40*	219	59	14900	16400	< 2	15	3	702	21	50	9.2	103000	39	70
Lake41*	11	< 2	589	4690	< 2	11	3	13	18	32	6.1	102000	23	67
Lake42a*	48	13	882	2140	< 2	359	7	12	13	25	2.6	95800	1250	202
Lake74	26	17	628	1350	<2	32	11	5	17	<10	3.24	8000	347	32
Lake75	77	6	1760	1180	<2	<3	3	10	17	42	7.06	102700	40	28
Lake81	291	10	2290	764	<2	7	<2	2	<10	33	1.42	16110	28	44
Lake82	188	25	2460	1200	<2	<3	3	3	12	99	4.23	93500	20	86
Lake83	51	10	585	190	<2	12	<2	8	<10	<10	1.29	8240	75	35
Lake84	186	17	3130	3590	<2	<3	3	25	18	117	7.9	103130	527	17
Lake86	229	32	3830	859	24	483	8	60	<10	52	6.38	31890	71	241
Lake88	3	11	35	3980	<2	42	11	181	13	<10	3.57	1610	414	15
Lake89	<2	37	<4	201	2	15	3	<2	<10	<10	0.78	1720	208	4
Lake90	<2	18	20	767	<2	41	12	<2	16	<10	3.75	888	405	27
Lake91	5	16	2370	5880	<2	36	20	<2	18	69	6.67	31010	821	22
Lake94*	<2	16	41	53	<2	5	<2	<2	<10	<10	2.25	4050	474	12
Lake95*	12	7	733	402	<2	<3	3	<2	15	112	5.63	103110	17	66
Lake96*	3	13	75	70	<2	5	<2	<2	<10	<10	0.39	1990	125	<2
Lake97*	16	17	342	1000	5	13	3	16	<10	<10	1.15	17220	898	18
Lake98*	22	18	730	314	<2	7	3	<2	<10	<10	0.69	1660	140	<2
Lake99*	<2	4	128	178	<2	5	<2	<2	<10	59	1.52	58210	26	98
Lake100	<2	19	120	35	31	760	11	<2	<10	40	1.65	1980	43	151
Lake92	89	16	1490	8430	<2	277	12	200	12	52	3.23	97260	118	350

Field No.	Ag ppm	Cu ppm	Pb ppm	Zn ppm	Mo ppm	Ni ppm	Co ppm	Cd ppm	Bi ppm	As ppm	Fe %	Mn ppm	Ba ppm	Cr ppm
Method of analysis	ICP	ICP	ICP	ICP	ICP	ICP	ICP	ICP	ICP	ICP	ICP	ICP	ICP	ICP
Igneous rocks														
Lake60	<2	<2	24	27	<2	<3	<2	<2	<10	<10	0.47	249	110	<2
Lake61	<2	4	18	13	<2	7	<2	<2	<10	<10	0.78	266	243	11
Lake64	<2	<2	23	31	<2	5	<2	<2	<10	<10	0.5	208	118	11
Lake78	<2	<2	21	36	<2	<3	<2	<2	<10	<10	0.53	172	94	18
TB 100														
TB 101														
TB 102														
TB 106														
TB 112														
Jasperoids outside district														
Lake50	< 2	< 2	138	17	3	4	48	< 2	< 10	< 10	0.67	40	106	< 2
Lake53	< 2	< 2	27	16	< 2	5	45	< 2	< 10	< 10	0.14	28	34	< 2
Lake54	< 2	< 2	10	4	2	9	9	< 2	< 10	< 10	1.9	381	59	< 2
Lake65	<2	7	636	24	37	13	2	<2	<10	146	2.01	78	125	42
Lake66	<2	41	4750	509	331	94	26	<2	11	399	18.7	956	72	30
Lake67	<2	14	601	75	86	362	7	<2	<10	42	2.21	180	309	105
Lake69	<2	7	8	14	<2	11	<2	<2	<10	<10	0.44	76	82	26
Lake70	<2	7	<4	4	3	13	<2	<2	<10	<10	0.38	172	42	51
Lake71	<2	11	24	49	<2	8	27	<2	<10	<10	0.98	459	151	3
Lake79	<2	11	613	17	109	445	6	<2	<10	142	0.74	114	61	95
Lake80	<2	4	54	24	18	8	<2	<2	<10	42	0.73	117	39	24
Lake400	<2	7	70	24	<2	<3	54	<2	<10	13	0.38	212	107	<2
Lake401	<2	20	147	54	23	634	10	<2	<10	36	1.24	592	81	117
Lake402	<2	16	64	102	<2	20	25	<2	<10	23	0.98	24590	2440	61
Lake403	<2	10	162	125	<2	15	19	<2	<10	29	0.51	33440	6170	64
Lake103	<2	10	33	83	10	260	5	<2	<10	<10	0.95	559	84	39
TB 105														
TB 107														
TB 109														
TB111														
TB113														
TB115														
Ore samples outside district														
Lake42b	< 2	< 2	24	26	< 2	< 3	< 2	< 2	< 10	< 10	0.55	630	270	13
Lake62	<2	13	40	51	<2	6	<2	<2	<10	<10	0.84	3880	505	10
Lake63	<2	11	19	55	<2	9	3	<2	<10	<10	2.39	703	167	23
Lake76	<2	18	6	25	9	232	6	<2	<10	<10	0.93	271	114	44
Lake85	<2	3	12	119	5	77	32	<2	26	<10	>30	4220	60	43
Lake101	59	33	3050	3580	<2	11	17	80	12	70	2.22	79890	1520	29
Lake102	<2	7	7	8	<2	4	<2	<2	<10	<10	0.14	460	103	7

Field No.	Ag ppm	Cu ppm	Pb ppm	Zn ppm	Mo ppm	Ni ppm	Co ppm	Cd ppm	Bi ppm	As ppm	Fe %	Mn ppm	Ba ppm	Cr ppm
Method of analysis	ICP	ICP	ICP	ICP	ICP	ICP	ICP	ICP	ICP	ICP	ICP	ICP	ICP	ICP
Sedimentary rocks														
Lake68	<2	18	<4	14	2	<3	<2	<2	<10	<10	0.06	183	6	<2
Lake73	<2	8	<4	20	<2	<3	<2	<2	<10	<10	0.06	133	2	<2
Lake51	< 2	6	20	62	< 2	30	12	< 2	< 10	11	3.4	296	237	28
Lake52	< 2	< 2	34	35	< 2	15	7	< 2	< 10	< 10	2.1	309	1660	5

Field No.	V ppm	Sn ppm	La ppm	Al%	Mg%	Ca%	Na%	K%	Sr ppm	Y ppm	Ga ppm	P%	Ti%	Nb ppm
Method of analysis	ICP	ICP	ICP	ICP	ICP	ICP	ICP	ICP	ICP	ICP	ICP	ICP	ICP	ICP
Ore samples														
LakeV1	226		1.8	0.18	0.01	0.08	0.01	0.04	41	5		0.012	0.01	
LakeV2	205		7.9	0.48	0.06	9.14	0.03	0.21	242	18		0.002	0.01	
Lake22*	166	< 5	4	4	< 0.005	0.29	0.06	0.13	275	16	129	0.04	0.006	< 4
Lake35*	1300	< 5	6	0.37	0.05	7.7	0.05	0.14	305	29	100	0.03	0.01	< 4
Lake36*	469	< 5	7	0.29	< 0.005	0.55	0.06	0.21	1040	13	138	0.009	0.01	< 4
Lake37*	232	< 5	5	0.42	0.02	1.5	0.01	0.18	208	10	108	0.02	0.01	< 4
Lake38*	328	< 5	3	0.85	< 0.005	0.21	0.01	0.23	86	8	142	0.008	0.02	< 4
Lake20*	170	5	10	1	0.28	26	0.03	0.56	193	19	49	0.009	0.12	< 4
Lake21*	594	< 5	24	0.28	0.03	0.86	0.1	0.29	1340	53	163	0.03	0.01	< 4
Lake22*	156	< 5	4	4	< 0.005	0.3	0.06	0.12	278	15	134	0.04	0.005	< 4
Lake25*	807	< 5	4	1.5	0.22	16	< 0.005	0.51	279	9	95	0.03	0.04	< 4
Lake26*	181	< 5	8	0.13	0.24	20	0.007	0.02	92	16	76	0.03	< 0.005	< 4
Lake27*	109	6	17	4.9	1.3	7.3	0.03	1.3	109	14	23	0.06	0.26	< 4
Lake30*	271	< 5	12	1.3	0.11	0.47	0.14	0.71	662	22	125	0.02	0.04	< 4
Lake31*	236	< 5	9	0.41	0.008	1.3	0.05	0.13	547	17	133	0.01	0.02	< 4
Lake32*	182	< 5	7	0.53	0.11	0.92	0.04	0.23	118	28	71	0.04	0.02	< 4
Lake33*	331	< 5	19	0.97	0.18	0.79	0.14	0.49	153	34	131	0.05	0.04	< 4
Lake36*	489	< 5	8	0.3	< 0.005	0.6	0.06	0.22	1090	14	161	0.008	0.02	< 4
Lake37*	222	< 5	5	0.42	0.02	1.7	0.01	0.18	206	10	109	0.02	0.02	< 4
Lake38*	334	< 5	4	0.88	< 0.005	0.23	0.01	0.24	87	8	149	0.007	0.02	< 4
Lake40*	498	< 5	6	0.35	< 0.005	3.8	0.13	0.09	480	31	139	0.03	0.01	< 4
Lake41*	186	< 5	9	0.65	0.02	2.9	0.09	0.31	726	14	139	0.01	0.02	< 4
Lake42a*	161	< 5	4	0.33	0.02	6.5	0.02	0.14	150	14	126	0.02	0.01	< 4
Lake74	193	39	22	7.623	1.1	5.75	0.019	3.24	88	18	26	0.083	0.5	11
Lake75	452	<5	11	0.63	0.087	4.788	0.079	0.38	924	17	85	0.025	0.042	<4
Lake81	310	<5	6	0.378	0.031	0.574	0.013	0.12	24	14	18	0.027	0.016	<4
Lake82	643	<5	3	0.143	<0.005	0.37	0.009	0.04	100	12	88	0.021	0.006	<4
Lake83	321	<5	7	1.05	0.104	10.2	0.021	0.35	65	9	8	0.014	0.033	<4
Lake84	592	<5	11	0.949	0.032	4.388	0.019	0.33	462	21	84	0.028	0.051	<4
Lake86	620	<5	6	0.239	0.029	2.364	0.007	0.06	77	8	33	0.044	0.011	<4
Lake88	125	35	27	7.349	1.724	9.28	0.12	1.87	101	22	15	0.078	0.455	12
Lake89	42	<5	11	1.254	0.459	28.1	0.018	0.25	219	16	<4	0.029	0.056	<4
Lake90	143	44	28	7.165	1.451	10.3	0.049	1.86	88	22	13	0.082	0.481	11
Lake91	306	16	41	7.117	0.698	1.244	0.065	2.59	362	24	40	0.077	0.382	5
Lake94*	21	<5	33	4.051	0.148	0.776	0.934	0.04	342	15	13	0.01	0.09	16
Lake95*	272	<5	4	0.209	<0.005	3.729	0.031	0.06	171	12	85	0.018	0.008	<4
Lake96*	57	<5	11	2.368	0.368	26.3	0.04	0.91	241	18	8	0.024	0.061	5
Lake97*	187	<5	9	0.67	0.242	21	0.084	0.29	213	19	19	0.034	0.037	<4
Lake98*	68	<5	6	1.446	0.269	30.6	0.058	0.56	152	13	5	0.026	0.048	<4

Field No.	V ppm	Sn ppm	La ppm	Al%	Mg%	Ca%	Na%	K%	Sr ppm	Y ppm	Ga ppm	P%	Ti%	Nb ppm
Method of analysis	ICP	ICP	ICP	ICP	ICP	ICP	ICP	ICP	ICP	ICP	ICP	ICP	ICP	ICP
Ore samples														
Lake99*	162	<5	10	0.408	0.035	0.79	0.013	0.14	43	23	57	0.039	0.02	<4
Lake100	125	<5	12	0.521	0.031	1.177	0.014	0.11	19	19	5	0.026	0.015	12
Lake92	145	<5	4	0.273	<0.005	4.054	0.089	0.18	256	14	81	0.02	0.011	<4
Igneous rocks														
Lake60	6	<5	32	6.971	0.127	0.326	2.209	3.96	25	19	15	<0.005	0.076	26
Lake61	9	<5	35	6.421	0.09	0.49	2.494	3.12	61	12	13	0.014	0.093	20
Lake64	6	<5	34	6.354	0.091	0.31	2.065	3.98	24	19	13	<0.005	0.07	24
Lake78	17	<5	29	5.712	0.072	0.153	1.024	4.68	28	18	15	<0.005	0.065	23
TB 100														
TB 101														
TB 102														
TB 106														
TB 112														
Jasperoids outside district														
Lake50	27	< 5	2	0.23	0.03	0.07	0.006	0.04	16	< 2	< 4	0.03	0.006	< 4
Lake53	7	< 5	2	0.21	0.25	1.3	0.008	0.03	18	< 2	8	0.02	< 0.005	< 4
Lake54	28	< 5	20	0.62	0.59	26	0.02	0.41	230	20	8	0.11	0.05	< 4
Lake65	223	<5	<2	0.05	0.023	0.094	<0.005	0.01	13	<2	<4	<0.005	<0.005	<4
Lake66	1900	<5	28	0.422	3.527	5.144	0.009	0.05	34	18	28	0.025	0.049	<4
Lake67	186	<5	13	0.383	0.037	0.142	0.005	0.02	36	16	<4	0.053	0.013	<4
Lake69	124	<5	11	0.66	0.069	0.177	0.018	0.24	17	21	<4	0.06	0.027	<4
Lake70	26	<5	<2	0.152	0.01	0.072	0.012	0.04	10	4	<4	0.015	0.005	<4
Lake71	38	<5	4	0.839	0.807	1.692	0.028	0.11	14	3	<4	0.01	0.036	<4
Lake79	12	<5	33	0.128	0.039	0.1	0.007	0.05	65	4	<4	0.025	0.011	<4
Lake80	21	<5	<2	0.069	0.01	0.037	<0.005	0.01	7	<2	<4	0.015	<0.005	<4
Lake400	104	<5	4	0.334	0.255	0.285	0.012	0.09	24	5	<4	0.162	0.012	<4
Lake401	191	<5	4	0.29	0.031	0.133	0.009	0.11	17	4	<4	0.06	0.015	9
Lake402	110	<5	3	0.178	0.064	0.564	0.008	0.06	26	2	26	0.015	0.011	<4
Lake403	56	<5	2	0.192	0.026	0.087	0.006	0.1	74	<2	36	0.006	0.01	<4
Lake103	41	<5	11	1.359	0.71	4.114	0.018	0.38	33	9	7	0.023	0.079	7
TB 105														
TB 107														
TB 109														
TB111														
TB113														
TB115														

Field No.	V ppm	Sn ppm	La ppm	Al%	Mg%	Ca%	Na%	K%	Sr ppm	Y ppm	Ga ppm	P%	Ti%	Nb ppm
Method of analysis	ICP	ICP	ICP	ICP	ICP	ICP	ICP	ICP	ICP	ICP	ICP	ICP	ICP	ICP
Ore samples outside district														
Lake42b	10	< 5	31	5.9	0.13	4.1	2.1	3.5	591	18	16	< 0.005	0.05	14
Lake62	23	<5	31	4.895	0.151	0.781	1.05	2.42	366	16	14	0.01	0.091	17
Lake63	32	<5	17	2.772	0.114	0.27	0.529	1.08	64	12	14	0.103	0.041	8
Lake76	30	<5	37	0.774	0.354	18.9	0.016	0.05	204	30	<4	0.027	0.041	6
Lake85	420	<5	21	0.874	0.271	11.3	0.006	0.02	75	110	<4	0.164	0.031	<4
Lake101	34	<5	25	5.089	0.053	0.202	0.129	4.78	598	27	89	0.041	0.15	<4
Lake102	3	<5	<2	0.151	0.076	11.5	0.007	0.03	52	<2	7	<0.005	<0.005	<4
Sedimentary rocks														
Lake68	4	<5	4	0.128	0.279	38.1	0.015	0.05	281	16	<4	0.022	0.006	<4
Lake73	<2	<5	<2	<0.005	13.2	20.8	0.017	<0.01	27	<2	<4	<0.005	<0.005	14
Lake51	154	7	23	7.4	3.1	1.7	0.06	3.6	47	12	29	0.02	0.33	4
Lake52	66	< 5	13	3.8	3.6	13	0.05	1.8	207	12	20	0.04	0.17	< 4

Field No.	Ce ppm	Nd ppm	Eu ppm	Yb ppm	Ho ppm	Li ppm	Si%	Total S %	SiO_2 %	TiO_2%	Al_2O_3 %	Fe_2O_3T%	MnO%	MgO %
Method of analysis	ICP	ICP	ICP	ICP	ICP	ICP			XRF	XRF	XRF	XRF	XRF	XRF
Ore samples														
LakeV1	4	<5	<0.2	<0.2										
LakeV2	8	6	0.3	0.8										
Lake22*	11	< 9	< 2	< 1	< 4	50								
Lake35*	< 5	< 9	< 2	< 1	< 4	11			**					
Lake36*	9	< 9	< 2	< 1	< 4	11								
Lake37*	5	< 9	< 2	< 1	< 4	29								
Lake38*	6	< 9	< 2	< 1	< 4	20								
Lake20*	7	< 9	< 2	< 1	< 4	7				<0.01		0.28	6.17	
Lake21*	24	17	2	< 1	< 4	6			**					
Lake22*	10	< 9	< 2	< 1	< 4	48								
Lake25*	< 5	< 9	< 2	< 1	< 4	3								
Lake26*	< 5	< 9	< 2	< 1	< 4	4			**					
Lake27*	33	13	< 2	1	< 4	61				0.45		4.58	0.73	
Lake30*	14	9	< 2	< 1	< 4	18			**					
Lake31*	10	< 9	< 2	< 1	< 4	12			**					
Lake32*	5	< 9	< 2	< 1	< 4	27			**					
Lake33*	17	12	< 2	< 1	< 4	33			**					
Lake36*	11	< 9	< 2	< 1	< 4	11								
Lake37*	6	< 9	< 2	< 1	< 4	27								
Lake38*	7	< 9	< 2	< 1	< 4	20								
Lake40*	< 5	< 9	< 2	< 1	< 4	16			**					
Lake41*	12	< 9	< 2	< 1	< 4	19			**					
Lake42a*	< 5	< 9	< 2	< 1	< 4	27			**					
Lake74	42	19	<2	1	<4	64	27.1	0.02		0.65		3.85	0.73	
Lake75	19	<9	<2	<1	<4	24	14.7	0.01	**					
Lake81	9	<9	<2	<1	<4	16	>30	0.02		<0.01		0.36	3.08	
Lake82	10	<9	<2	<1	<4	43	>30	0.02	**					

Field No.	Ce ppm	Nd ppm	Eu ppm	Yb ppm	Ho ppm	Li ppm	Si%	Total S %	SiO_2%	TiO_2%	Al_2O_3 %	Fe_2O_3T %	MnO%	MgO %
Method of analysis	ICP	ICP	ICP	ICP	ICP	ICP			XRF	XRF	XRF	XRF	XRF	XRF
Ore samples														
Lake83	15	<9	<2	<1	<4	18	>30	0.02		0.05		1.36	1.08	
Lake84	18	<9	<2	<1	<4	11	13.7	0.01	**					
Lake85	35	57	7	4	<4	15	4.51	0.02						
Lake86	10	<9	<2	<1	<4	18	>30	0.03	**					
Lake88	51	21	<2	2	<4	20	22.9	0.06		0.72		5.14	0.24	
Lake89	21	<9	<2	1	<4	10	9.56	0.02		0.12		1.32	0.23	
Lake90	56	21	<2	2	<4	20	23	0.03						
Lake91	75	35	<2	2	<4	11	>30	0.02	**					
Lake94*	49	14	<2	2	<4	35	9.9	0.02	**					
Lake95*	13	<9	<2	<1	<4	27	18.4	0.03	**					
Lake96*	18	<9	<2	1	<4	17	10.4	0.02		0.13		0.62	0.25	
Lake97*	15	<9	<2	1	<4	12	19.6	0.03		0.03		0.99	2.41	
Lake98*	13	<9	<2	<1	<4	9	7.61	0.02		0.09		1.09	0.25	
Lake99*	16	<9	<2	<1	<4	11	>30	0.02	**					
Lake100	13	<9	<2	<1	<4	129	>30	0.26		0.03		1.83	0.27	
Lake92	14	<9	<2	<1	<4	11	20.8	0.04	**					
Igneous rocks														
Lake60	63	18	<2	2	<4	13	>30	<0.01	75.41	0.11	12.66	0.70	0.03	0.46
Lake61	56	10	<2	2	<4	36	>30	<0.01	78.18	0.15	11.19	1.11	0.05	0.66
Lake64	68	21	<2	2	<4	34	>30	0.01	77.66	0.10	11.37	0.71	0.03	0.41
Lake78	59	17	<2	2	<4	80	>30	<0.01	79.40	0.09	10.76	0.76	0.02	0.20
TB 100									76.30	0.13	12.09	0.88	0.05	0.26
TB 101									77.24	0.13	12.02	0.87	0.07	0.18
TB 102									69.99	0.41	14.44	2.51	0.05	1.36
TB 106									90.86	0.05	4.59	0.31	<0.01	0.08
TB 112									80.10	0.11	10.04	0.74	0.01	0.07
Jasperoids outside district														
Lake50	< 5	< 9	< 2	< 1	< 4	56				0.03		0.09	0.01	
Lake53	< 5	< 9	< 2	< 1	< 4	79				0.17		2.90	0.06	
Lake54	53	21	< 2	1	< 4	7				0.02		0.25	0.01	
Lake65	7	<9	<2	<1	<4	17	>30	0.03		0.02		2.50	0.01	
Lake66	54	14	<2	<1	<4	63	20.7	0.02		0.12		21.92	0.13	
Lake67	22	<9	<2	<1	<4	48	>30	0.05		0.03		2.96	0.03	
Lake69	15	<9	<2	1	<4	25	>30	0.02		0.06		0.64	0.01	
Lake70	7	<9	<2	<1	<4	8	>30	0.02		0.02		0.49	0.02	
Lake71	17	<9	<2	<1	<4	10	>30	0.06		0.09		1.47	0.07	
Lake79	61	18	<2	<1	<4	31	>30	0.11		0.03		0.99	0.01	
Lake80	8	<9	<2	<1	<4	18	>30	0.03		0.02		1.02	0.02	
Lake400	11	<9	<2	<1	<4	37	>30	0.04		0.03		0.51	0.03	
Lake401	12	<9	<2	<1	<4	11	>30	0.01		0.04		1.51	0.08	
Lake402	9	<9	<2	<1	<4	10	>30	0.04		<0.01		<0.01	3.81	
Lake403	11	<9	<2	<1	<4	5	>30	0.03		<0.01		<0.01	4.03	
Lake103	31	<9	<2	1	<4	71	>30	0.01		0.15		1.23	0.07	
TB 105										0.03		0.50	0.01	
TB 107										0.05		0.59	0.01	

Field No.	Ce ppm	Nd ppm	Eu ppm	Yb ppm	Ho ppm	Li ppm	Si%	Total S %	SiO_2 %	TiO_2%	Al_2O_3 %	Fe_2O_3T %	MnO%	MgO %
Method of analysis	ICP	ICP	ICP	ICP	ICP	ICP			XRF	XRF	XRF	XRF	XRF	XRF
TB 109									94.76	0.07	1.04	0.69	0.02	1.29
TB111									98.79	0.02	0.38	0.22	<0.01	0.06
TB113									50.00	0.91	18.76	7.65	0.14	3.67
TB115										0.02		0.24	<0.01	
Ore samples outside district														
Lake42b	64	18	< 2	2	< 4	32				0.09		0.74	0.07	
Lake62	59	17	<2	2	<4	39	>30	0.05		0.10		1.13	0.49	
Lake63	34	<9	<2	1	<4	48	>30	0.03		0.07		3.58	0.1	
Lake76	48	21	<2	2	<4	9	23.8	0.06		0.09		1.34	0.04	
Lake101	69	28	<2	3	<4	10	27.1	0.02	**					
Lake102	8	<9	<2	<1	<4	44	>30	0.01		0.02		0.21	0.06	
Sedimentary rocks														
Lake68	10	<9	<2	1	<4	3	0.93	0.02		0.02		0.17	0.02	
Lake73	6	<9	<2	<1	<4	<2	4.74	<0.01		0.01		0.17	0.02	
Lake51	53	20	< 2	1	< 4	40				0.77		5.40	0.05	
Lake52	31	13	< 2	< 1	< 4	27				0.48		3.44	0.05	

Field No.	CaO %	Na_2O %	K_2O %	P_2O_5%	LOI%	TOTAL %	As ppm	Ba ppm	Cr ppm	Cu ppm	Ga ppm	Mo ppm	Nb ppm	Ni ppm
Method of analysis	XRF	XRF	XRF	XRF	XRF	XRF	XRF	XRF	XRF	XRF	XRF	XRF	XRF	XRF
Ore samples														
LakeV1														
LakeV2														
Lake22*														
Lake35*														
Lake36*														
Lake37*														
Lake38*														
Lake20*							43	24	189	13	4	14	1	38
Lake21*														
Lake22*														
Lake25*														
Lake26*														
Lake27*							3	540	162	30	13	<1	4	37
Lake30*														
Lake31*														
Lake32*														
Lake33*														
Lake36*														
Lake37*														
Lake38*														
Lake40*														
Lake41*														
Lake42a*														
Lake74							7	321	114	17	20	<2	6	36
Lake75														

Field No.	CaO %	Na_2O %	K_2O %	P_2O_5%	LOI%	TOTAL %	As ppm	Ba ppm	Cr ppm	Cu ppm	Ga ppm	Mo ppm	Nb ppm	Ni ppm
Method of analysis	XRF	XRF	XRF	XRF	XRF	XRF	XRF	XRF	XRF	XRF	XRF	XRF	XRF	XRF
Ore samples														
Lake81							10	13	340	12	4	1	<2	9
Lake82														
Lake83							2	69	196	8	3	<1	<1	11
Lake84														
Lake85														
Lake86														
Lake88							2	514	120	12	15	<1	6	47
Lake89							3	226	63	20	4	<2	<2	18
Lake90														
Lake91														
Lake94*														
Lake95*														
Lake96*							3	133	38	6	6	<2	<2	6
Lake97*							5	921	153	12	4	2	<1	17
Lake98*							8	176	28	9	5	<1	<1	9
Lake99*														
Lake100							40	39	1100	13	3	14	12	343
Lake92														
Igneous rocks														
Lake60	0.24	3.06	5.28	0.01	1.29	99.247	<1	108	47	4	17	2	21	4
Lake61	0.17	3.30	4.07	0.03	0.43	99.337	<1	226	153	11	14	2	18	6
Lake64	0.17	2.82	4.79	<0.01	1.08	99.14	<1	112	81	4	14	2	19	4
Lake78	0.18	1.46	6.01	0.02	1.21	100.11	4	94	81	4	16	2	16	3
TB 100	0.16	3.78	4.78	<0.01	0.79	99.23	1	11	63	<1	19	4	28	4
TB 101	0.16	3.77	4.75	0.02	0.57	99.78	<1	44	41	4	18	2	27	3
TB 102	0.45	3.41	4.70	0.11	2.49	99.92	<1	26	29	6	19	2	28	3
TB 106	0.08	0.11	3.39	0.01	0.50	99.98								
TB 112	0.04	0.28	7.84	0.03	0.66	99.91	10	36	7	5	12	<2	19	2
Jasperoids outside district														
Lake50							11	112	18	5	<2	5	<2	3
Lake53							2	69	19	5	<2	<2	2	6
Lake54							2	38	9	4	7	2	<2	3
Lake65							115	103	224	8	4	21	<2	8
Lake66							428	48	89	44	54	179	<2	101
Lake67							45	300	625	13	6	46	6	192
Lake69							7	75	307	8	3	3	<2	8
Lake70							1	37	367	7	<2	4	<2	9
Lake71							15	161	17	15	4	2	2	9
Lake79							150	57	646	11	<2	69	7	244
Lake80							39	43	161	5	<2	11	<2	5
Lake400							13	92	8	9	3	<2	<2	4
Lake401							37	76	888	16	<2	12	10	278
Lake402							26	1200	470	13	<2	3	<2	16
Lake403							16	2600	460	10	<2	4	<2	10
Lake103							3	72	406	9	6	6	7	138

Field No.	CaO %	Na_2O %	K_2O %	P_2O_5%	LOI%	TOTAL %	As ppm	Ba ppm	Cr ppm	Cu ppm	Ga ppm	Mo ppm	Nb ppm	Ni ppm
Method of analysis	XRF	XRF	XRF	XRF	XRF	XRF	XRF	XRF	XRF	XRF	XRF	XRF	XRF	XRF
TB 105							2	40	174	9	<2	4	<2	6
TB 107							<2	48	259	7	3	3	<2	7
TB109							207	14	217	487	<2	326	<2	10
TB111	0.22	0.02	0.05	0.03	0.92	99.11	21	28	15	30	4	80	<2	6
TB113	0.04	0.06	0.05	0.01	0.27	99.90	16	15	10	33	3	16	<2	7
TB115	7.50	2.42	4.76	0.54	3.95	100.29	18	24	5	8	<2	3	<2	3
Ore samples outside district														
Lake42b							3	290	89	6	15	<1	14	5
Lake62							3	460	75	16	12	2	13	7
Lake63							2	163	149	12	13	2	7	8
Lake76							<2	91	361	10	<2	4	4	110
Lake101														
Lake102							<2	91	106	4	8	<2	<2	3
Sedimentary rocks														
Lake68							<2	15	15	6	<2	<2	<2	4
Lake73							<2	4	29	<2	<2	<2	<2	<2
Lake51							10	248	90	11	17	1	16	33
Lake52							2	1200	55	8	9	<2	9	19

Field No.	Pb ppm	Rb ppm	Sr ppm	Th ppm	U ppm	V ppm	Y ppm	Zn ppm	Zr ppm
Method of analysis	XRF	XRF	XRF	XRF	XRF	XRF	XRF	XRF	XRF
Ore samples									
LakeV1									
LakeV2									
Lake22*									
Lake35*									
Lake36*									
Lake37*									
Lake38*									
Lake20*	546	37	200	<1	11	858	24	1500	22
Lake21*									
Lake22*									
Lake25*									
Lake26*									
Lake27*	17	94	121	1	1	190	19	365	106
Lake30*									
Lake31*									
Lake32*									
Lake33*									
Lake36*									
Lake37*									
Lake38*									
Lake40*									
Lake41*									
Lake42a*									
Lake74	648	277	43	5	3	306	22	1800	151
Lake75									
Lake81	2200	8	24	8	2	1300	17	468	13
Lake82									
Lake83	588	28	61	2	1	582	10	200	13
Lake84									
Lake85									
Lake86									
Lake88	30	93	107	3	2	152	27	5000	142
Lake89	4	14	208	3	<2	55	17	240	23
Lake90									
Lake91									
Lake94*									
Lake95*									
Lake96*	82	68	119	<2	1	72	21	83	30
Lake97*	369	17	193	1	3	544	21	1100	15
Lake98*	733	36	145	2	<1	73	15	353	20
Lake99*									
Lake100	123	15	19	<2	2	137	21	32	7
Lake92									

Field No.	Pb ppm	Rb ppm	Sr ppm	Th ppm	U ppm	V ppm	Y ppm	Zn ppm	Zr ppm
Method of analysis	XRF	XRF	XRF	XRF	XRF	XRF	XRF	XRF	XRF
Igneous rocks									
Lake60	23	196	12	22	2	6	23	27	114
Lake61	17	224	30	35	5	10	16	15	92
Lake64	23	186	24	18	4	8	24	31	103
Lake78	21	498	13	14	2	21	24	28	95
TB 100	29	214	1	25	5	10	32	46	143
TB 101	34	208	<1	25	4	4	27	35	141
TB 102	44	213	6	26	3	4	23	127	145
TB 106									
TB 112	20	529	64	20	3	8	24	20	110
Jasperoids outside district									
Lake50	132	3	19	<2	2	26	<2	17	5
Lake53	9	14	116	8	1	30	26	12	376
Lake54	23	3	7	<2	<2	12	2	19	8
Lake65	628	<2	5	<2	<2	191	2	23	5
Lake66	4900	<2	14	2	32	1450	26	775	29
Lake67	629	<2	17	<2	4	173	21	79	9
Lake69	5	21	6	<2	1	119	23	14	13
Lake70	2	3	2	<2	1	26	5	5	5
Lake71	26	12	6	<2	<2	39	6	53	31
Lake79	635	<2	72	<2	<2	10	9	16	8
Lake80	55	<2	7	<2	<2	21	<2	24	<2
Lake400	65	4	23	<2	1	83	6	22	7
Lake401	146	7	17	<2	3	175	6	57	9
Lake402	71	2	25	<2	2	550	3	101	6
Lake403	246	4	58	<2	<2	332	3	102	7
Lake103	29	31	33	4	2	38	12	93	122
TB 105	21	7	9	<2	<2	11	4	22	8
TB 107	4	56	9	<2	<2	10	<2	11	19
TB109	811	<2	7	<2	<2	7	3	2800	8
TB111	270	<2	7	<2	2	22	4	488	36
TB113	330	4	6	<2	3	31	4	451	23
TB115	42	4	4	<2	<2	7	<2	306	4
Ore samples outside district									
Lake42b	20	169	616	16	2	12	21	32	93
Lake62	41	117	289	13	3	32	18	57	92
Lake63	21	56	66	6	5	25	14	62	48
Lake76	9	<2	94	<2	2	30	33	29	28
Lake101									
Lake102	10	3	51	<2	<2	7	<2	9	<2
Sedimentary rocks									
Lake68	3	<2	134	<2	1	9	17	18	13
Lake73	3	<2	9	<2	1	10	<2	15	<2
Lake51	12	218	28	11	8	159	23	70	169
Lake52	7	113	107	8	3	75	19	45	147

Geochemistry of Mine Dump Material from the Lake Valley Mining District

By J.R. Herring *and* V.T. McLemore

U.S. Geological Survey Professional Paper 1644–D

GEOLOGIC INVESTIGATIONS IN THE LAKE VALLEY AREA, SIERRA COUNTY, NEW MEXICO

U.S. Department of the Interior
U.S. Geological Survey

Contents

Figures

Tables

Note: Combined references list begins on page 76.

Geochemistry of Mine Dump Material from the Lake Valley Mining District

By J.R. Herring *and* V.T. McLemore[1]

Abstract

This report characterizes rocks and soils from the surfaces of mine dumps in the Lake Valley mining district, Sierra County, south-central New Mexico, as to their concentrations and ranges of several geoenvironmentally significant trace elements (GSTE). The study focuses on implications of possible release of these trace elements into the environment. The mine dumps are remnants of silver and manganese underground mining operations and consist of heterogeneous mixtures of low-grade ore and waste rock.

The considered set of GSTE (Ag, As, Ba, Bi, Cd, Co, Cr, Cu, Hg, Mn, Mo, Ni, Pb, Sb, Sn, V, and Zn) is selected for the notable enrichment of its various elements relative to average shale and (or) for geoenvironmental significance of the various elements in terms of known toxicity or environmental mobility. Trace element enrichments above a baseline significance level are combined into a single GSTE score for each dump that ranks the collective presence of elevated element concentrations above baseline concentrations. Although the score itself does not indicate the potential for these trace elements to move into the environment, it can be combined with other criteria, such as water leach data, to indicate those mine dumps that have high collective presence of GSTE in significant amounts that are easily releasable into the environment. Finally, the score can also be considered with other criteria of the dump composition, such as the presence of sulfide or carbonate minerals, that can increase or decrease the release of GSTE into the environment.

The dumps with highest potential impact on the environment are those with high GSTE scores, low abundance of carbonate minerals, and high abundance of sulfide minerals. Dumps with these criteria are enriched in zinc and secondarily in antimony. Lead enrichments upwards of 20,000 ppm also occur in dumps with high GSTE scores, but these dumps also have relatively abundant carbonate and only minor sulfide, which argues for limited acid water generation and, hence, low potential for mobilization of the lead. Elements with the greatest enrichments above a significant baseline concentration, notably lead, antimony, and zinc, have low solubility fractions of their bulk solid concentrations, which reduces the amounts that might be released into the environment. Conversely, manganese, molybdenum, and to a lesser extent arsenic have much greater solubility fractions and will solubilize proportionally more of their bulk concentrations from the mine dump solids. pH concentrations of the 24-hour leachate samples are alkaline and do not indicate acid-generation potential of the minerals and water.

Introduction

Background

The Lake Valley mining district lies within the Caballo Resource Area, which is a Bureau of Land Management (BLM)-administered region including all of Sierra and Otero Counties, south-central New Mexico. At the request of the BLM, the U.S. Geological Survey (USGS), in cooperation with the New Mexico Bureau of Mines and Mineral Resources, undertook a geologic and mineral resource evaluation of six BLM-designated Areas of Critical Environmental Concern. In addition to these studies, the USGS sampled abandoned mine dumps throughout the Resource Area in an effort to characterize the base- and precious-metal composition of the mined deposits. This report consists of geochemical characterization of mine dump material in one of those areas mined for silver, lead, zinc, and manganese in southwestern New Mexico during the past century. The intent is to provide information to aid decisions for subsequent reclamation of some or all of these mine dumps.

Lake Valley District—Location, Geology, Ore Deposits, and Mining History

The Lake Valley mining district is located about 25 km south of Hillsboro in south-central New Mexico. The locations of Lake Valley and neighboring mining districts in Sierra County are shown in figure 1. No current mining takes place in Lake Valley.

Two styles of mineralization have occurred, resulting in (1) fissure replacement bodies along fracture zones and faults, and (2) tabular, bedded replacement deposits. The fissure replacement bodies along faults and fracture zones are irregular, steeply dipping deposits that cut across bedding planes. Adjacent to the mineralized fault zones, tabular, stratabound deposits have replaced the upper Alamogordo Member near its contact with

[1] New Mexico Bureau of Geology and Mineral Resources, Socorro, NM 87801. (Formerly New Mexico Bureau of Mines and Mineral Resources.)

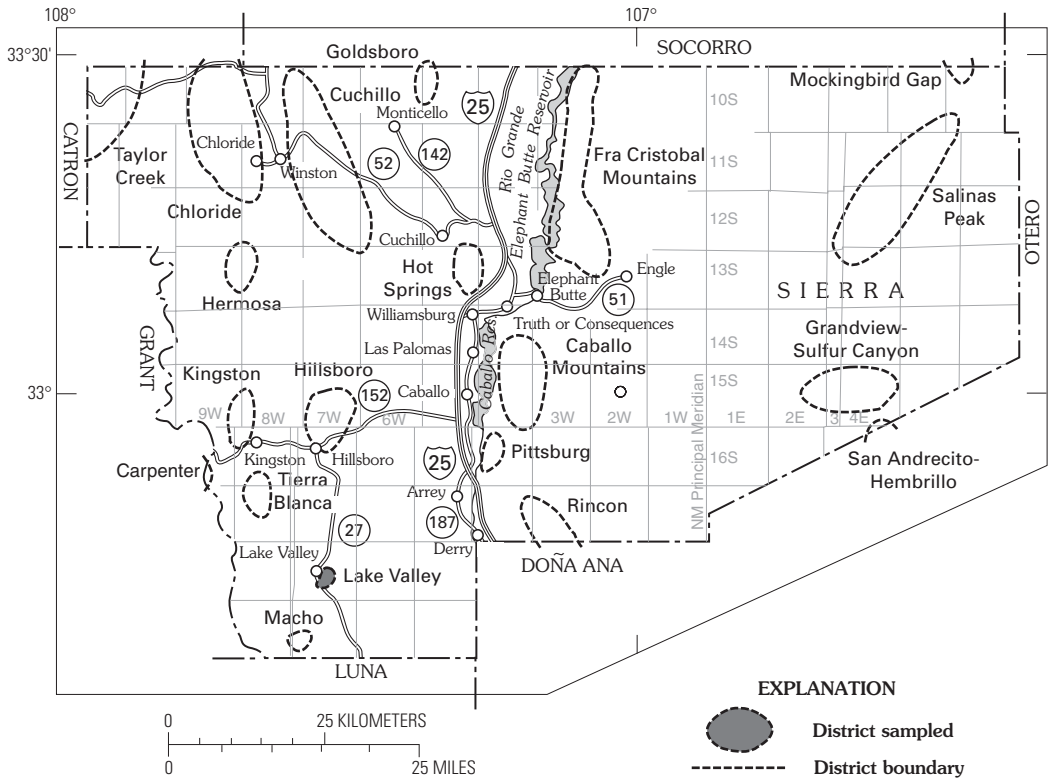

Figure 1. Location of the Lake Valley mining district, southwestern Sierra County, N. Mex., and neighboring mining districts.

the overlying Nunn Member of the Mississippian Lake Valley Limestone (Chapter C). These deposits are also irregular in shape and grade into the fissure replacement bodies. The fissure replacement bodies are most likely the feeder zones for the bedded deposits. The silver ore bodies were thin, irregular tabular zones 1–2 m thick that were underlain and laterally surrounded by larger Mn-Ag replacement bodies 1.5–9 m thick. Only the manganese replacement bodies, some containing low-grade silver, remain; the high-grade silver zones were mined out in the 1880's.

The primary silver minerals, since mined out, were stephanite, proustite, pyrargyrite, and argentiferous galena (Harley, 1934, and references therein). Oxidized minerals (cerargyrite, embolite, native silver, cerussite, vanadinite, wulfenite, endlichite, descloizite, iodyrite) either were deposited as primary minerals when the mineralizing fluid evolved to a more oxidizing fluid or were oxidized by later supergene fluids. The Bridal Chamber consisted of nearly pure cerargyrite in a pocket 100 m long and 7.6 m thick. A streak of pure cerargyrite or chlorargyrite (AgCl) was 1 m thick. Assays as high as 20,000 oz/short ton were common. Other, smaller silver bonanza pockets were also found in the district. Other minerals found in the district include pyrolusite, manganite, psilomelane, limonite, hematite, calcite, ankerite, and apatite. Silica occurs mostly as jasperoid and aphanitic veins, although late-stage drusy quartz is common filling open spaces. Calcite occurs throughout the deposits. Clay minerals are common along the Alamogordo-Nunn contact and local faults. White, clear, crystalline quartz and calcite veinlets and white to brown, crystalline calcite fill vugs. Vanadinite occurs as minute hexagonal prisms and thin coatings and was probably formed during a late oxidation or supergene stage. Iodyrite occurs within calcite crystals, indicating a late stage of deposition. Visible pyrite is rare to absent. Pyrite occurs in jasperoid where the jasperoid is cut by faults. In thin section, many jasperoids contain trace amounts of finely disseminated pyrite that is commonly altered to hematite and goethite. Rare pyrite is also found as visible cubes with the manganese oxide minerals and as small disseminations within limestone adjacent to Ag-Mn replacement deposits.

Neighboring mining districts are different from Lake Valley in terms of their geology, mined minerals, and mine dump compositions. Lovering and Heyl (1989), and Harley (1934) gave brief descriptions of the mining history, ore occurrence, and geology. Northrop (1959 and 1996) has provided detailed listings of various minerals found in Lake Valley and neighboring districts. North and McLemore (1986, 1988), McLemore (2001), and Harley (1934) provided additional discussion of the Lake Valley and neighboring mining districts.

The mine dumps are a group of piles of rock waste and gangue brought to the surface from the underground mining operations. Most lie near adit or shaft openings (see fig. 1 in Chapter C). In a few places they are associated with processing sites, such as mills, in the district. Most of the several dozen piles throughout the district are < 2,000 m^3 in volume, although a few large piles range in volume up to about 20,000 m^3. Sizes of the sampled piles are listed in table 1.

Table 1. Trace element concentrations, means, ranges and GSTE scores for composited mine dump samples.

Field No.-type-approximate volume (m^3)	Ag, ppm	As, ppm	Ba, ppm	Bi, ppm	Cd, ppm	Co, ppm	Cr, ppm	Cu, ppm	Hg, ppm	Mn, ppm	Mo, ppm	Ni, ppm	Pb, ppm	Sb, ppm	Sn, ppm	V, ppm	Zn, ppm	CO2, %	Total S, %	Leachate pH, 24 or 24/48 hr	Leachate conductivity, µS/cm
1AX-dump base-8000	67	59	220	<10	10.5	3	27	40	0.34	66000	<2	15	1320	27	<5	299	1150	10	0.04		
1C-dump top-2000	69	67	301	<10	8	4	28	54	0.39	70100	2	19	1420	31	<5	342	1160	8	0.04		
1D-dump runoff sediment	31	72	291	10	7	4	34	38	0.62	71300	<2	17	1390	31	<5	431	1450	8	0.11		
2-shaft dump-200	43	65	65	<10	<2	2	14	44	0.16	47600	<2	8	752	39	<5	358	470	16	0.12		
3-headworks dump-1000	84	58	302	<10	84	6	48	75	0.51	63100	4	24	1760	24	<5	323	8030	11	0.04	9.29/8.81	45/57
4X-shaft dump-200	174	237	151	12	49	5	28	96	1.34	44700	6	14	17850	31	<5	711	6325	17	0.10	9.31	38
5-shaft dump-600	208	93	88	<10	23	4	10	133	0.74	61100	<2	12	4820	62	<5	758	3010	13	0.12		
6-shaft dump-300	1	3.5	301	<10	<2	7	10	51	0.45	1100	<2	21	65	1	<5	77	101	20	0.04		
7-shaft dump-900	146	160	283	16	113	9	30	47	0.80	63400	13	20	6500	18	12	425	7330	4	0.21	9.05	93
8-shaft dump-500	52	181	397	11	79	6	21	46	1.63	60600	<2	21	9430	29	<5	802	7740	14	0.05	9.38/8.85	42/47.6
9X-shaft dump-4000	113	64	83	10	26	4	14	30	0.67	66600	<2	13	2440	39	<5	509	3480	17	0.10		
10-shaft dump-1000	3	40	404	<10	<2	13	37	29	0.52	7100	12	40	171	4	14	191	373	7	0.43	8.64	176
11-adit dump-800	1	4	192	<10	<2	11	12	20	0.14	400	<2	21	20	1	<5	69	74	27	0.04		
Means and Ranges																					
Arithmetic mean	76	85	237	9	31	6	24	54	1	47900	4	19	3688	26	5	407	3130	13	0.11		
Geometric mean	34	53	204	9	11	5	21	48	1	25700	2	17	1193	15	4	327	1396	12	0.08		
Upper central range	189	181	369	11	57	9	35	78	1	137400	6	25	7874	63	7	690	6536	19	0.17		
Lower central range	6	15	113	6	2	3	13	29	0	4800	1	12	181	4	3	155	298	7	0.04		
Upper expected range	971	588	650	14	272	14	57	124	2	685500	12	37	48210	248	11	1416	28766	31	0.36		
Lower expected range	1	5	64	5	0	2	8	18	0	1000	0	8	29	1	2	75	68	4	0.02		
Geoenvironmentally significant trace element (GSTE) component, total, and scaled scores																				Total score	Scaled score
Average shale	0.07	13	580	0.4	0.3	19	90	45	0.4	850	2.6	68	20	1.5	6	130	95				
Significance factor	100	1	1	25	10	2	2	1	1	20	2	1	1	1	1	1	1				
Significant concentration	7	13	580	10	3	38	180	45	0.4	17000	5.2	68	20	1.5	6	130	95				
Baseline significance (factor of 3 above significant concentration)	0.5	0.5	0.5	0.5	0.5	0.5	0.5	0.5	0.5	1	0.5	0.5	0.5	0.5	0.5	0.5	0.5			8.1	18
Log maximum enrichment (to 1 %, 10 % for Mn)	3.2	2.9	1.2	3.0	3.5	2.4	1.7	2.3	4.4	0	3.3	2.2	2.7	3.8	3.2	1.9	2.0			44.6	100
Sample																					
1AX	1.0	0.7			0.5					1			1.8	1.2		0.4	1.1			7	16
1C	1.0	0.7			0.4			0.1		1			1.9	1.3		0.4	1.1			7	17
1D	0.6	0.7			0.4				0.2	1			1.8	1.3		0.5	1.2			7	17
2	0.8	0.7								0			1.6	1.4		0.4	0.7			6	14
3	1.1	0.6			1.4			0.2	0.1	1			1.9	1.2		0.4	1.9			10	22
4X	1.4	1.3		0.1	1.2			0.3	0.5	0	0.1		3.0	1.3		0.7	1.8			12	27
5	1.5	0.9			0.9			0.5	0.3	1			2.4	1.6		0.8	1.5			11	24
6								0.1	0.1				0.5				0.0			0.6	1
7	1.3	1.1		0.2	1.6			0.0	0.3	1	0.4		2.5	1.1	0.3	0.5	1.9			12	27
8	0.9	1.1		0.0	1.4			0.0	0.6	1			2.7	1.3		0.8	1.9			11	26
9X	1.2	0.7			0.9				0.2	1			2.1	1.4		0.6	1.6			9	21
10		0.5							0.1		0.4		0.9	0.4	0.4	0.2	0.6			3	8
11																				0	0

Acknowledgments

All sample preparation was performed in the Denver labo ratories of the U.S. Geological Survey, assisted by Dave Firewick. We acknowledge XRAL Laboratories, Inc., for ICP AES analysis and R. Knight of the Denver laboratories of the U.S. Geological Survey for INAA analyses. We acknowledge the Bureau of Land Management for help and assistance in accessing sampling sites and providing background information about past mine development and current reclamation interests. Finally, we acknowledge comments on the manuscript by J.M. O'Neill, J.C. Ratté, W.R. Miller, and G.A. Desborough.

Methods

Field Methods

Study Site Identification and Sampling Strategy

Most of the mines in the various districts are shaft or adit openings with the mine spoil piled around or near the openings. In the initial phase of this study, random mine dump piles were selected and two samples consisting of a surficial sample and a sample about 30 cm depth were collected from each mine dump. This sampling allows comparison of surface material, presum ably more subject to weathering and leaching, with slightly deeper material, presumably subject to less exposure and weath ering. In addition, each sample was sieved into three size frac tions, with size intervals at 2 mm and 0.15 mm (8 and 100 mesh, respectively), in order to examine partitioning of trace elements into the various size fractions (Herring and others, 1998). The second phase of the project included resampling of the Lake Val-ley district, where again randomly selected mine dump piles—including some of the same piles that were sampled initially—were sampled but only for surficial material. This time, the sam pling design was altered to ensure representative sampling of the entire surface of the pile in a single sample, which requires obtaining at least thirty, 30-g incremental sub-samples taken ran domly over the surface of the pile. These are combined into a single sample that is statistically representative of the material at the surface of the dump pile. Obviously, it provides no charac terization of material in the inside of the pile. Prior to analysis, the sample was sieved to separate the < 2 mm fraction for analysis. The coarser material was discarded. The strategy behind this type of analysis is to concentrate on this finer grained material, assuming that this material with its large total particle surface area has a greater potential for geoenvironmental interaction compared to the coarser material.

Analysis

Samples were analyzed for 40 elements using inductively coupled plasma–atomic emission spectrometry (ICP-AES). Other analytical techniques were used for As, Cr, Hg, Sb, total S, and CO_2. Herring and others (1998) presented analytical methodology and complete analytical results.

Water Leach Studies

Aqueous extracts of splits of the analyzed samples were obtained using a 20:1 deionized water:rock leach ratio. Leach ing time was 24 hours, and the leach experiments were passive except for a single inversion with return to original position after 1 hour. The leachate was filtered at 0.2 µm, and the pH and conductivity were measured immediately on the filtered sample. The filtrate was acidified to pH 1 and subsequently analyzed by ICP Mass Spectrometry (ICP-MS).

Statistical Techniques and Central and Expected Ranges of Occurrence

Statistical analyses require numeric data sets. When some, but less than or equal to one-half, of the reported values are non-numeric (censored) and below their lower limit of detection (LLD), these censored values have been replaced with arbitrary values equal to 70 percent of their LLD. For the elements with censored distributions, the geometric means and deviations were estimated by the technique of Cohen (1959) for singly truncated distributions. Mineralized samples are unique among crustal rocks in that they represent highly enriched concentra tions of some otherwise minor or trace elements. These concen tration distributions include some enormously elevated concentrations, which greatly skew the arithmetic mean toward higher values. For that reason, the geometric means of sample concentrations are also reported. These log-transformed con centrations remove the weighting bias caused by a few largely elevated concentrations against a field of otherwise much lower values. Further discussion of data treatment is included in the report by Herring and others (1998).

Mine dumps are frustratingly heterogeneous. They are composed of a variety of rock types, including soil, gangue, wall rock, and bedrock. The material can range from weathered to nonweathered and can vary in size. Consequently, the task of modeling the distribution of elements within mine dumps tran scends the enormous past effort expended in attempts to under-stand and model more well behaved distributions of elements, such as lognormal, in rocks and soils that occur in an undis turbed (unmined) environment (Miesch, 1976). Nonetheless, the initial approach used here is to compare concentration data that are based on assumed log normal distributions of various elements. Herring and others (1998) noted that several of the trace elements from the Lake Valley area have concentration distributions that exhibit apparent single- or multi-modal geo metric mean normal distributions. Geometric means are reported along with their arithmetic counterparts in table 1. In the case of a few extremely high concentrations, the geometric mean will always be lower than the arithmetic mean and moder ate the effect of those few extreme concentrations.

Estimates of the distributions about the geometric mean (GM) are provided by the geometric deviation (GD). The

distributions are listed in table 1 and depicted in figure 2*A*. The estimated central range of element concentrations, in which about Ä 68 percent of the population is estimated to occur, is given by Ä GM/GD to GM × GD. The expected range, estimated to contain about 95 percent of the population of concentrations, is given by $GM/GD^{1.96}$ to $GM \times GD^{1.96}$. The listed geometric deviations Ä bear no resemblance to the often-used standard deviation, a linear quantity that is added to or subtracted from the arithmetic mean to estimate distribution of a normal population. The GD is a multiplier or divisor to the GM and, as such, has a compelling advantage over the arithmetic standard deviation. The central and expected ranges encompass only positive numbers, whereas arithmetic (standard) deviations often result in meaningless negative numbers for the lower part of the distribution range.

Results

Trace Elements of the Lake Valley District Mine Dumps and Water Leach Studies

On average, all mine dump samples from the district are Ä enriched in the following economic and geoenvironmentally sig-Ä nificant trace elements: Ag, As, Cd, Mn, Pb, and Zn. Less signif icant enrichments of Sr and V also occur. For Ag, As, Ba, Cd, Cu, Cr, Mn, Pb, V, and Zn, there are several individual mine dumps that are enriched well above the district geometric mean concentration for each of these elements (table 1). Consistent correlation is generally exhibited for these elements in most

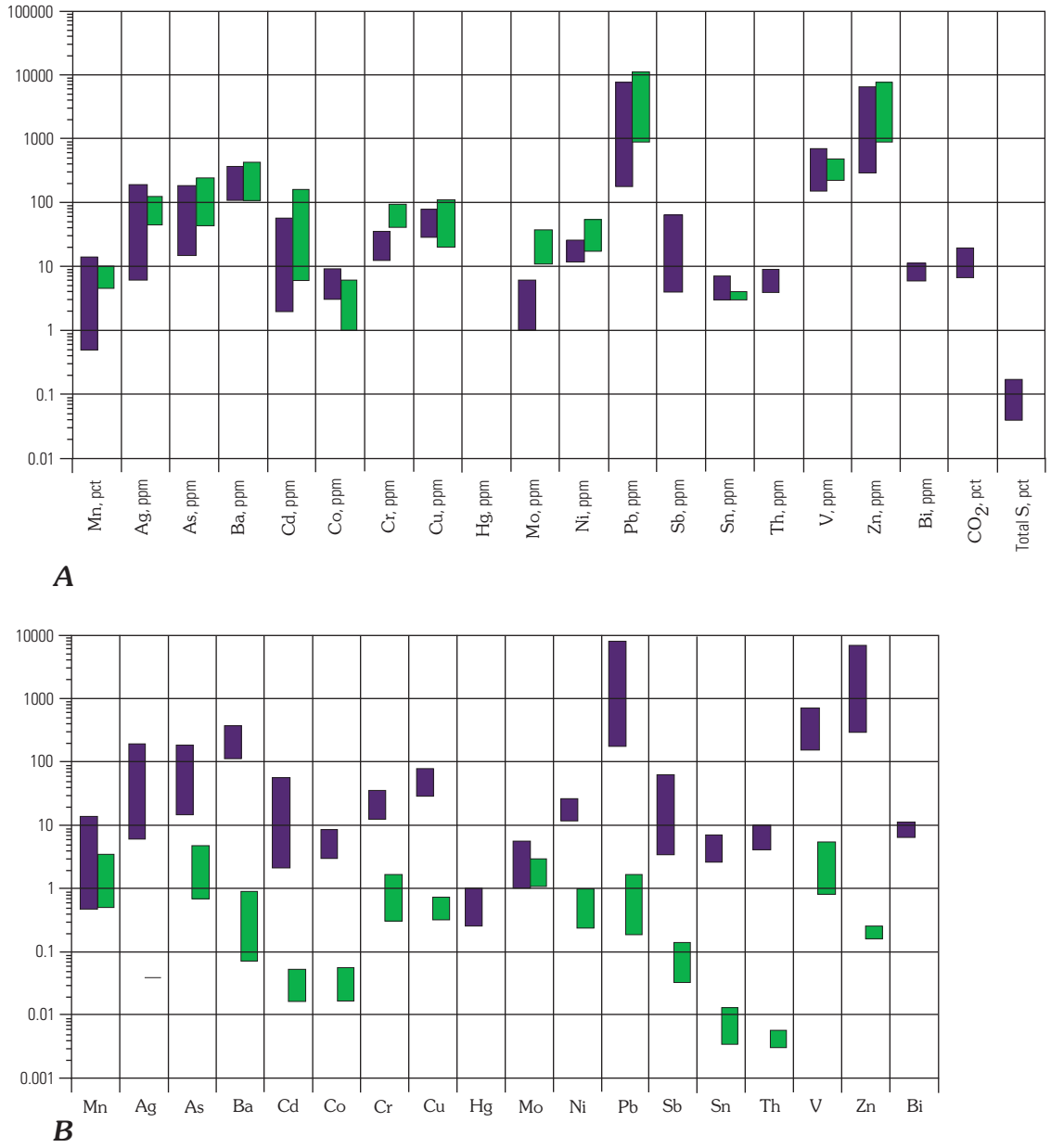

Figure 2. Central ranges of concentrations of trace elements, symmetrically distributed about the geometric mean, for *A*, Composited (blue bar) and grab (green bar) samples of < 2 mm material on mine dumps in Lake Valley; *B*, Composited solid samples (in parts per million) (blue bar) and water leachate concentrations (in parts per billion) (green bar) for < 2 mm material on mine dumps in Lake Valley.

samples within the district—when one trace element is enriched, typically most others are as well. Among neighboring districts, Lake Valley has the highest mean concentrations of Ag, Mn, As, and Cd (Herring and others, 1998). Throughout the district, notable correlations exist within the group of Ag, As, Cd, Pb, and Zn and also within a second group of Co, Cr, and Cu.

In the Lake Valley district, many trace elements have con centrations in several individual samples that lie above the upper central range and therefore are considered notable (table 1). Only one or two concentrations lie above the upper expected range for Bi, Cu, Ni, Sn, and total S. However, the lack of sig nificant concentration enrichment should be viewed in the context that for many trace elements, such as Pb and Zn, the all-sample GM is one to two orders of magnitude greater than average crustal concentrations. In other words, all mine dumps within the district are greatly enriched in many trace elements relative to their crustal abundance.

When the < 2 mm fractions of the rock samples are leached in water, elements with largest concentrations in the leachate are Mn, As, Cr, Mo, Pb, and V, whereas Cd, Co, Sb, Sn, and Th exhibit the least concentrations. The remaining GSTE show intermediate concentrations. Mn, Ba, Cr, Pb, and V exhibit the greatest range of concentrations, whereas Cd, Cu, Mo, Th, and Zn have the least. The GM and central ranges of the water leach concentration data are given in figure 2*B*. The water leach con centration data, in ppb, is shown alongside the bulk rock sample concentration data in ppm. The solubility or relative aqueous availability of the trace elements relative to bulk rock concentra tions can be readily discerned by comparing the separation of the central ranges between the bulk and leach concentrations on the log-scaled chart of figure 2*B*. Those central ranges of rock and leach concentration that are farthest apart, such as for Pb or Th, indicate relative insolubility or unavailability of the dissolved element compared to its concentration in the solid sample. Ele ments where the two central ranges are close together, for exam ple Mn and Mo, have relative aqueous availability of their solid fractions greater than the other elements. pH concentrations of the 24-hour leachate samples are around 9 and do not indicate immediate acid-generation potential based on interaction between the minerals and water.

Discussion

Particle Size Effects; Correlations; Weathering

In a previous study, Herring and others (1998) noted an apparent but modest particle-size effect in the concentration data wherein greatest enrichments often occur in the finest size por tion of the sample, < 0.15 mm. For the trace elements, notable concentration enrichment occurs in the finest fraction compared to the bulk sample concentration for most samples for As, Ba, Co, Cr, Cu, Mo, Ni, Pb, V, and Zn. This suggests that the ore is more friable than other material, such as wall rock, on the waste dumps and concentrates in the finer fraction with continued weathering and disaggregation. Another possible explanation for this phenomenon is that during mining the ore is handled more extensively than the waste rock. This additional handling results in comminution of the ore or sub-grade ore rock com pared to waste rock or gangue that is minimally handled and tends to have larger pieces on dump piles.

Not surprisingly, notable ($0.75 < r^2 < 0.9$) to significant ($r^2 > 0.9$) correlations appear among the transition metals Co, Cr, Cu, and Ni and between the metals of this set and Mo. Zinc, another transition metal, does not associate with this set and, instead, has notable to significant correlation with a significantly intercorrelated set of Ag, As, Cd, and Pb. Manganese exhibits no notable or significant correlation with any of the other geoen vironmentally significant set of trace elements. Restricting the correlations to the smallest size fraction samples (< 0.15 mm) retains all the significant correlations and improves these nota ble correlations to significant levels. In addition, V notably cor relates with the Ag, As, Cd, and Pb set, and Sn notably correlates with the transition metal and Mo set.

Surficial samples of some dumps were compared with those about $^1/_2$ m deeper at the same locality to examine whether compositional differences provide some insight into weathering processes. Presumably, compositional differences are, in part, due to greater exposure of the surface sample to weathering con ditions leading possibly to greater leaching and removal of trace elements. Only minor compositional difference exists between the surface and deeper samples at a locality, which is to say that compositional differences that might be attributable to weather ing differences are small. These minor differences may also reflect compositional heterogeneity of the dump.

Acid Water Production Potential

Acid water production potential refers to the likelihood of generation of acidic water when certain minerals in the dump pile react with surface or ground water. Acidic water results from oxidation principally of sulfide minerals to form sulfate, either dissolved or recombined into a new mineral form. Sulfide minerals must be exposed to oxygen in an aqueous medium, either permanent or ephemeral, for this acid water production and metal release to occur. The presence of all three components—reduced mineralized sulfur, oxygen, and water—is necessary. Conversely, the presence of some minerals, com monly carbonate present as calcite or the less soluble dolomite along with mafic minerals or calcium plagioclase, lessens the release of metals from sulfide minerals through titration of the acid waters that are produced and counteracts the enhanced sol ubility of most metals through acid reactions. In simplest terms, metal release via acid water generation is facilitated by the reac tion between water and sulfide minerals within the dump and, in turn, is inhibited by the presence of carbonate minerals.

Sulfide minerals are noted to occur in the district but are rare and confined to only the deepest workings (Lovering and Heyl, 1989). Nonetheless, they do occur on the dump piles. Northrop (1959) observed the presence of pyrite in western Sierra County and specifically in the Lake Valley district. He further noted that calcite also is common here. Consequently, the mine dumps of Lake Valley can be examined individually for enhanced presence of pyrite that may enhance acidic

weathering and transport of GSTE, suggested by elevated con centrations of total S. Conversely, the presence of enhanced concentrations of carbonate, suggested by elevated concentra tions of CO_2 (as noted in table 1), serves to titrate against acidic weathering. For CO_2, the entire concentration is assumed to represent carbonate minerals as little organic carbon is present in these rocks. If the CO_2 is assumed to be present entirely as calcite, the calcite mass will be 2.3 times the listed percentages of CO_2 in table 1. The sampled dumps have a GM concentration of total S 0.08 percent. If the total S were present entirely as sul fide, the maximum concentration, 0.43 percent, would require 1 percent calcite (0.5 percent CO_2) for neutralization. The minimum CO_2 content for all samples is 4 percent, more than suffi cient to titrate against any produced acidity from sulfide oxidation.

Based on composition, the dump samples from Lake Valley would not be expected to show extensive potential for acid gen eration during interaction with water. Indeed, this is demon strated by the water leach data. However, increasing the leach time to 48 hours on two samples results in a drop of $^1/_2$ pH unit, which suggests the possibility of continued and relatively slow oxidation of pyrite. The extent to which this reaction could lower the pH is unknown, but presumably the minor carbonate would preclude other than circum-neutral pH.

Geoenvironmentally Significant Trace Elements (GSTE) and GSTE Score

Geoenvironmentally significant trace elements (GSTE) are defined to be those trace elements that normally occur at trace concentrations in the Earth's crust, but that are known to be bio logically active and, depending on their abundance and avail-ability, may have a detrimental effect on the environment. The biologic activity includes bioessential metabolism, bioconcen tration without apparent use, and bioconcentration with known toxicities ranging from mild to acute among various trophic lev els of organisms. In this study, those elements that are poten tially enriched in the area and that are known to be biologically active are Ag, As, Ba, Bi, Cd, Co, Cr, Cu, Hg, Mo, Ni, Pb, Sb, Sn, V, and Zn.

Combining concentrations of GSTE into a single number for evaluation can be done in many ways. One candidate for evaluating the GSTE is to calculate a score based on the collec tive presence of the elements combined with the geoenviron mental significance of elements in a given sample. This score becomes a screening tool to identify mine dumps that warrant further scrutiny in terms of potential geoenvironmental effects. The principal utility of such a score is to reduce a complex set of multiple element concentrations and potential geoenvironmental significances into a single quantity that permits comparison among samples. The challenge here is to combine concentration data into a single number that retains the collective significance of those components, even when the several elements have enor mous ranges in their concentrations and varying degrees of geoenvironmental significance.

Two considerations are important in creating such an enrichment score of GSTE. First, the score must indicate enrichment relative to a familiar standard, preferably one in which elemental concentrations are relatively benign in terms of their geoenvironmental significance. Second, the score must be relatively insensitive to widely ranging concentrations among the different elements such that elements with typically larger abundance do not dominate the score relative to those elements with lesser abundance but which still have important geoenvi ronmental significance.

The GSTE score resolves the first consideration by calcu lating enrichment of the set of trace elements relative to average shale (Turekian and Wedepol, 1961). This choice is reasonable because the host rocks to the mineralized deposits within the Lake Valley area are sedimentary strata and because a shale unit immediately underlies the mineralized strata. In addition, aver-age shale has concentrations of most trace elements that are gen erally considered benign in terms of their geoenvironmental significance. The choice of a standard is arbitrary, but it should satisfy the criteria of being relatively abundant, being well known, and having comparatively low (environmentally benign) concentrations of GSTE. Other choices, for example, other so-called standard shales besides that chosen, would work equally well. More importantly, these other choices would not apprecia bly change the calculated score. Another possibility is to use the crustal abundance and calculate enrichment in the sample rela tive to that value (the clarke of concentration). That choice, too, would not significantly alter the calculated score using the tech nique in this study.

As noted, concentrations of elements in the standard should be typically low, but they should not be so low that misleading scores can result. This can happen because enrichment relative to the standard is calculated as a ratio. Elements with very low concentrations in the standard can overweight their influence on a calculated score when enriched in samples to concentrations that are well beyond those of the standard but still are not geoen vironmentally significant. Consequently, the ratio must be adjusted for the geoenvironmental significance of concentrations of individual elements in the standard material. For example, average shale concentrations—or even average crustal concen trations for that matter—are so low for Ag, Bi, and Cd that a GSTE score would be greatly influenced by just these three ele ments with the substantial increases in their abundance that could accompany only minor mineralization. Moreover, in this mining district, these elements have extremely large and consis tent enrichments relative to average shale, and these enriched concentrations, if not adjusted in significance, would otherwise dominate the score. Their very low concentration in average shale is well below geoenvironmental significance, so a cor rected significance factor, which uses an increased concentration over the standard, has been applied to these elements. Similarly, Mn has such significant enrichment in all mine dumps through-out the Lake Valley district that it also would have a dominating influence on the GSTE score. Manganese has its GM enriched above the average shale concentration by a factor of 40. Conse quently, its significance value has been increased from its con centration in standard shale using a significance factor of 20. This significance factor, when multiplied times the average shale concentration of 850 ppm, yields a significant concentration for Mn of 17,000 ppm. Just over one-half of the elements considered here are assigned significance factors of 1 (table 1),

which means no increase is needed in the average shale concen tration of that element to produce its geoenvironmentally signifi cant concentration. For the other elements, significance factors range from 2 to a high of 100 for Ag.

In order to resolve the second consideration—that of mean ingfully comparing elements with widely ranging abundance—the raw score is computed using log values of concentration enrichments relative to the standard or modified values. This desensitizes the score to those elements with consistently large concentrations, such as Zn. This is but one among many tech niques that desensitizes a population descriptor to a few aber rant, large concentrations. For example, the square root of the sums of the squares also could be used. Here, the sum of the logs of the significance values is then taken as 0, and enrich ments are calculated relative to this 0 value. Summing logs of the concentrations for the initial calculation of the score is simi lar to calculating the GM concentration. In departure from GM calculation, however, the score calculation excludes log concen trations < 0. Negative log concentration values, resulting from concentrations less than that in average shale, would lower the overall score. Obviously as an element's concentration becomes progressively lower than some level of significance, it cannot continue to decrease the score, which would mean that the over-all sample becomes less significant geoenvironmentally. Hence, negative values cannot be included. Cobalt and nickel are an example in this data set, with both elements always present at concentrations less than in average shale. Once elements with relative log concentration of 0 or less are removed, the raw score is computed by summing the remaining log concentrations.

Finally, the raw score is then scaled against the maximum reasonable enrichment that might occur relative to average shale. This assumes that the maximum reasonable enrichment is to 1 percent abundance in the whole standard for each trace element. For Mn, with its exceptional abundance, the maximum reason-able enrichment value is set to 10 percent abundance in the whole standard. The raw maximum reasonable enrichment score for average shale is then 44.6, a number that represents a maximum enrichment of each GSTE abundant at 1 percent and Mn at 10 percent. The raw scores of mine dump samples in this data set are scaled against this latter number set to 100 (table 1). This score of 100 represents the maximum attainable abundance for the combined set of GSTE.

In order to calculate a score for minimal or baseline signifi cance, one assumes an enrichment by a factor of 3 over each ele ment's significant concentration. The computed raw score of baseline significance is 8.1, which scales to 18 (table 1) against the maximum reasonable enrichment set to 100. This baseline score can be considered as that score above which the mine dumps have geoenvironmentally significant enrichments of a few or several trace elements.

GSTE Scores for Lake Valley Mine Dumps

Table 1 includes a list of GSTE scores for the mine dumps. Of the 13 mine dump samples, 7 have GSTE scores less than the scaled baseline significance score (18). Based on score alone, these dumps are not considered geoenvironmentally significant. However, before these dumps are dismissed as nonsignificant, their scores need to be examined in case there is an enhanced presence of just one or a few significant elements. In five of the dumps, scores for each of three elements, Pb, Sn, and Zn, range from about 1 to 2, reflecting enrichments from about 10 to 100 above the significant concentrations for these elements. These five dumps might be considered for further scrutiny, such as solubility levels or the presence of factors that could enhance release of these particular trace elements into the environment. Otherwise the GSTE in seven dumps are not considered important.

Six dumps (3, 4X, 5, 7, 8, 9X) have GSTE scores above the baseline value of 18. Their scores range from 21 to 27.3. The metals with consistently highest concentration scores in these dumps are Pb, Sn, and Zn, each element with enrichment scores >1 for the six dumps. Silver, arsenic, and cadmium exhibit lesser enrichments, with some values >1 but not in all samples. No other GSTE have individual element scores greater than 1. For Pb, Sn, and Zn, average enrichment scores are 2.4, 1.3, and 1.8, respectively, indicating modest enrichment in Sn and espe cial enrichment in Pb and Zn for all six dumps. The highest value for Pb, occurring in sample 4X, is 3.0, which constitutes an enrichment value of 1,000 above the significant concentra tion of 20 ppm. All six dumps are candidates for further scrutiny for the presence of factors that could enhance release of these trace elements into the environment.

In summary, the score is a single number that represents the collective presence of substantially enriched elements above a baseline significance level. It is not highly skewed by very large enrichments of just one or a few elements. At the low end of the GSTE scores, there is some nominal, baseline score that indicates nonsignificant enrichment relative to average shale or whatever value is taken as significant enrichment; increasingly higher values of the score signify progressive enrichment of one or more GSTE. The score is simply a measure of the collective presence of a set of trace elements in the dump samples. It does not signify the potential for these trace elements to release into the environment. On the other hand, a utility of the score is that it can be compared to other criteria, such as water leach data, to indicate those mine dumps that have high collective presence of GSTE in forms that are easily releasable into the environment. Finally, the score can also be compared to other criteria of the dump composition, such as the presence of sulfide or carbonate minerals, that could enhance or lessen the release of GSTE into the environment.

Combining Other Factors with GSTE Score

Mine dumps with the highest GSTE scores can be com pared with other criteria of the dump composition, such as the presence of sulfide or carbonate minerals, that enhance or decrease the release of GSTE into the environment. Figure 3 shows the GSTE score plotted along with total S, CO_2, and the concentrations of the three elements that exhibit greatest enrich ment in these samples (Pb, Sb, and Zn). Those dumps that have the greatest potential for release of GSTE into the environment have high scores, high total S, low CO_2, and high concentrations

of GSTE. Of the six dumps shown in the figure, dump 7 with its enrichment in Zn best fits these criteria. Other dumps with rela tively higher concentrations of total S are 4, 5, and 9. However, these three dumps also have significant carbonate contents to mitigate against the acid-generated leaching of their various enriched trace elements.

A better approach can be used to evaluate mine dumps by combining the highest GSTE scores, the presence of sulfide or carbonate, and solubility data generated from the leaching experiments. This approach has the advantage of using actual solubility information rather than inferred environmental release of GSTE based on bulk concentration in the mine dump solids. Figure 4 shows these results for the four highest GSTE score samples that also have water leachate data. Of the three mine dumps with relatively similar GSTE scores, high CO_2, and low total S (dumps 3, 4, and 8), the only GSTE that have solubility enhancement relative to most other samples are As, Pb, and Sb (dump 4), and Cd (dump 3). Dump 8 has no particular enrich ment of any soluble GSTE. All samples showed no particular enrichment of Ag or Zn, elements whose bulk concentrations in the solid fractions are always significantly enriched. Note that for GSTE with large enrichment in the solid fraction, specifi cally Pb, Sb, and Zn, the leachable amounts, expressed as a frac tion of solid concentration, are all low (fig. 2*B*). Nonetheless,

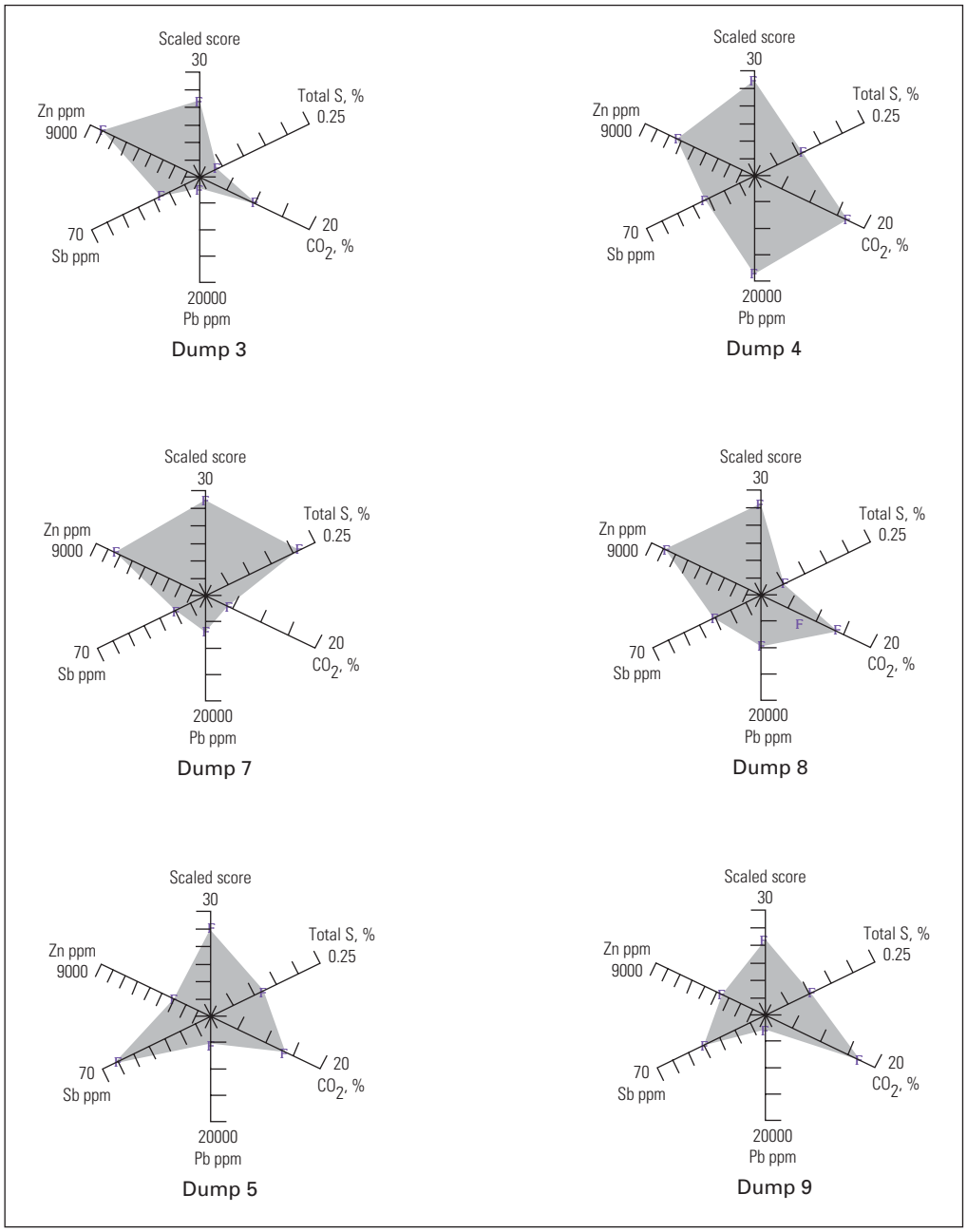

Figure 3. Spider diagrams combining geoenvironmentally significant trace element (GSTE) highest scores, total S as a measure of acid generation potential, CO_2 as a measure of carbonate to counteract acid generation, and concentrations of Pb, Sb, and Zn.

even small leachable fractions can still result in the release of significant quantities of an element when many tons of material at the dump surface are exposed to and leached by natural waters, especially if these waters are acidified by oxidation of sulfide minerals.

Finally, we consider something not otherwise considered in this study—the Cu to Mo ratio. Generally, the ratio in forage plants must exceed 1, or there is risk of molybdenosis (Erd man, 1990). Initially it would seem as if this is not an issue, for the bulk concentrations of Cu always well exceed those of Mo in the bulk concentrations of the dump samples. However, Mo has much greater solubility and, hence, mobility into the environment at these circum-neutral to slightly alkaline pH val ues of the leachates (fig. 2*B*). Although the data here are sim ply the solubility concentrations and not those of plants, we should note that the leachate Cu:Mo ratio is always < 1 and tends to get lower with additional leaching—for dump sample 3, the ratio is 0.81 in 24 hours and 0.45 in 48 hours. If local forage plant species do not discriminate in their uptake of these two elements from their dissolved ratio, they could acquire problematic concentrations of Mo that could become geoenvironmentally detrimental.

Summary and Conclusions

The dumps with largest potential release of trace elements and consequent negative impact on the environment are those with high GSTE scores, low abundance of carbonate minerals, and high abundance of sulfide minerals (table 1; figs. 3 and 4). Dumps with these criteria are enriched in Zn and secondarily in Sb; consequently, these two have the greatest potential for release into ground water within the district. Maximum

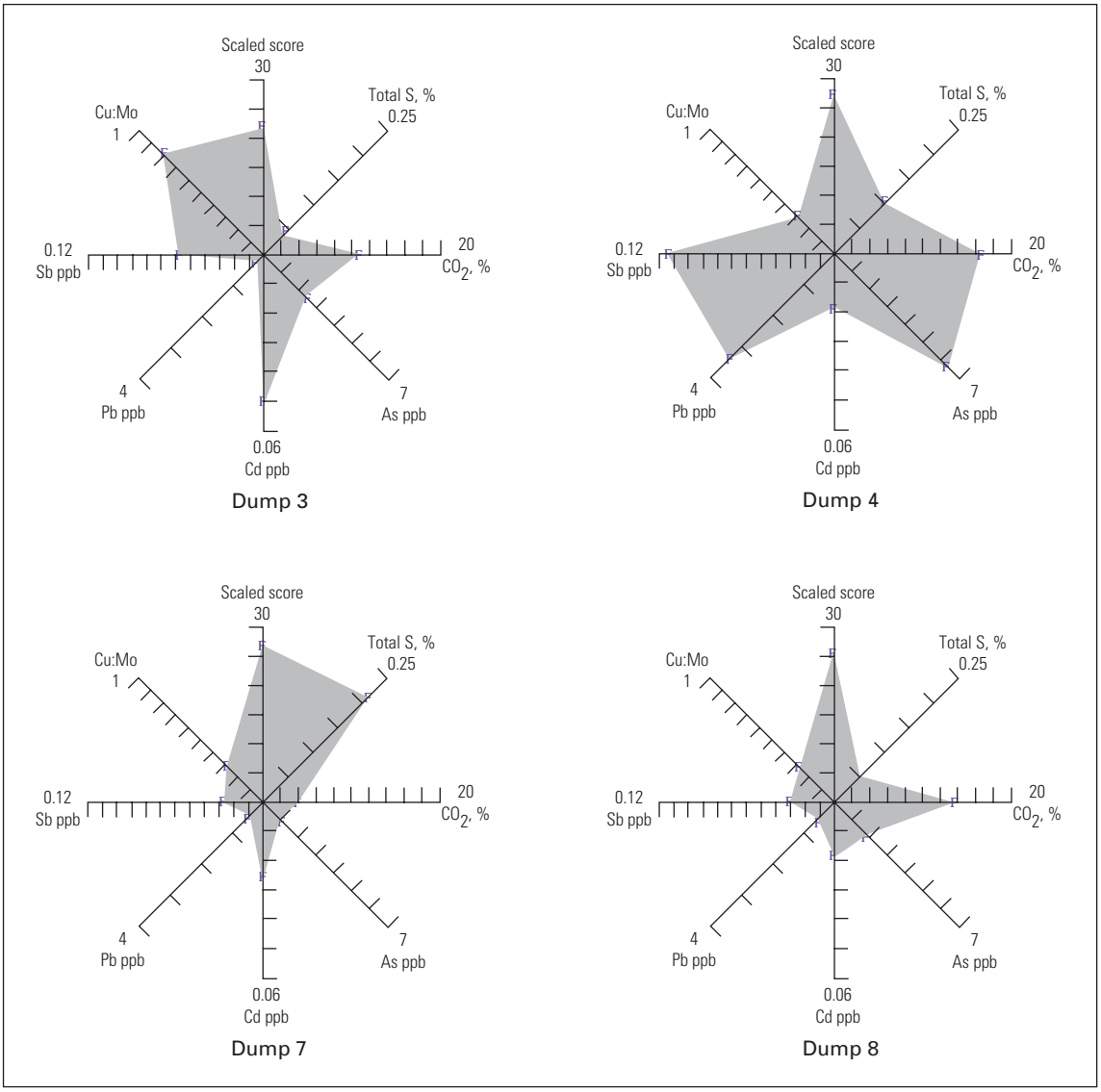

Figure 4. Spider diagrams combining geoenvironmentally significant trace element (GSTE) highest scores, total S as a measure of acid generation potential, CO_2 as a measure of carbonate to counteract acid generation, and concentrations of As, Cd, Pb, Sb, and the Cu:Mo ratio.

enrichments of Pb approaching 20,000 ppm also occur in dumps with high GSTE scores, but these dumps also have relatively abundant carbonate and depleted sulfide presence and, hence, low potential for acid water mobilization of the Pb. The elements with the greatest enrichments above their significant baseline concentrations, notably Pb, Sb, and Zn, also have low solubility fractions of their bulk solid concentrations relative to other elements that will lessen release into the environment. Conversely, Mn, Mo, and to a lesser extent As, have much greater solubility fractions and will solubilize proportionally more of their bulk concentrations from the mine dump solids.

In conclusion, the approach used in this report—combining bulk composition as a GSTE score of the solid material from mine dumps—easily screens for enrichment of various GSTE. Combining the GSTE score with solubility and acid-generation mineral abundance data subsequently identifies those dumps most likely to release GSTE into the environment and identifies the specific GSTE likely to be released.

Note: A combined list of references for all chapters of this Professional Paper is located at the end of this volume, beginning on page 76.

References Cited

[All Chapters]

Adams, D.C., and Keller, G.R., 1994, Crustal structure and basin geometry in south-central New Mexico, *in* Keller, G.R., and Cather, S.M., eds., Basins of the Rio Grande Rift—Structure, stratigraphy, and tectonic setting: Geological Society of America Special Paper 291, p. 241–255.

Apell, G.A., Hazen, S.W., and Howe, E.G., 1947, Lake Valley manganese deposits, Sierra County, New Mexico: U.S. Bureau of Mines Report of Investigations RI-4099, 9 p.

Bankey, Viki, and Kleinkopf, M.D., 1988, Bouguer gravity anomaly map and four derivatives of Idaho: U.S. Geological Survey Geophysical Investigations Map GP-978.

Bartsch-Winkler, Susan, ed., 1997, Geology, mineral and energy resources of the Mimbres Resource Area, New Mexico: U.S. Geological Survey Open-File Report 97-521, CD-ROM.

Brant, A.A., 1966, Geophysics in the exploration for Arizona porphyry coppers, *in* Titley, S.R., and Hicks, C.L., eds., Geology of the porphyry copper deposits, southwestern North America: Tucson, Ariz., University of Arizona Press, p. 87–110.

Callender, J.F., Seager, W.R., and Swanburg, C.A., 1983, Late Tertiary and Quaternary volcanism: Geothermal Resources of New Mexico Scientific Map Series, scale 1:500,000.

Clark, E., Jr., 1895, The silver mines of Lake Valley, New Mexico: American Institute of Mining and Metallurgy Engineering Transactions, v. 24, p. 138–167.

Cohen, A.C., Jr., 1959, Simplified estimators for the normal distribution when samples are singly censored or truncated: Technometrics, v. 1, p. 217–237.

Constable, S.C., Parker, R.L., and Constable, C.G., 1987, Occam's inversion; a practical algorithm for generating smooth models from electromagnetic sounding data: Geophysics, v. 52, no. 3, p. 289–300.

Cordell, Lindrith, 1983, Composite residual total intensity aeromagnetic map of New Mexico—Geothermal Resources of New Mexico Scientific Map Series (prepared by National Geophysical Data Center, NOAA): Las Cruces, N.Mex., New Mexico State University Energy Institute. Scale 1:500,000.

Cordell, L.E., and Grauch, V.J.S., 1985, Mapping basement and magnetization zones in the San Juan basin, New Mexico, *in* Hinze, W.J., ed., The utility of regional gravity and magnetic maps: Society of Exploration Geophysicists, p. 181–197.

Creasey, S.C., and Granger, A.E., 1953, Geologic map of the Lake Valley manganese district, Sierra County, New Mexico: U.S. Geological Survey Field Studies Map MF-9, scale 1:24,000.

Dobrin, M.B., and Savit, C.H., 1988, Introduction to geophysical prospecting, 4th Edition: New York, McGraw-Hill, 867 p.

Elston, W.E., 1957, Geology and mineral resources of the Dwyer quadrangle, Grant, Luna, and Sierra Counties, New Mexico: New Mexico Bureau of Mines and Mineral Resources Bulletin 38, 86 p.

Elston, W.E., 1989, Overview of the Mogollon-Datil volcanic field, *in* Chapin, C.E., and Zidek, Jiri, eds., Field excursions to volcanic terranes in the western United States—Volume I, southern Rocky Mountain region: New Mexico Bureau of Mines and Mineral Resources Memoir 46, p. 43–46.

Elston, W.E., Seager, W.R., and Clemmons, R.E., 1975, Emory cauldron, Black Range, New Mexico—Source of the Kneeling Nun Tuff, *in* Seager, W.R., Clemmons, R.E., and Callender, J.F., eds., Las Cruces Country: New Mexico Geological Society Guidebook 26, p. 283–292.

Erdman, J.A., 1990, Copper-molybdenum imbalances and the incidence of nutritional diseases in livestock and humans, *in* Doe, B.R., ed., Proceedings of a U.S. Geological Survey workshop on environmental geochemistry: U.S. Geological Survey Circular 1033, p. 179–181.

Ericksen, G.E., Wedow, Helmuth Jr., Eaton, G.P., and Leland, G.R., 1970, Mineral resources of the Black Range Primitive area, Grant, Sierra, and Catron Counties, New Mexico: U.S. Geological Survey Bulletin 1319–E, 162 p.

Eveleth, R.W., 1986, Lake Valley's famed Bridal Chamber—"a beautifully large and solid looking streak": New Mexico Geological Society Guidebook 37, p. 293–296.

Farnham, L.L., 1961, Manganese deposits of New Mexico: U.S. Bureau of Mines Information Circular IC–8030, 176 p.

Futa, Kiyoto, and Ratté, J.C., 1989, Petrogenetic implications of Rb-Sr and Sm-Nd isotopes related to post-caldera volcanism in the western Mogollon-Datil volcanic field, New Mexico: New Mexico Bureau of Mines and Mineral Resources Bulletin 131, p. 100.

Genth, F.A., and von Rath, G., 1885, On the vanadates and iodyrite from the Lake Valley, Sierra County, New Mexico: Proceedings of the American Philosophical Society, Philadelphia, v. 22, p. 363–375.

Harley, G.T., 1934, The geology and ore deposits of Sierra County, New Mexico: New Mexico Bureau of Mines and Mineral Resources Bulletin 10, 220 p.

Harrison, R.W., 1990, Cenozoic stratigraphy, structure, and epithermal mineralization of the north-central Black Range, New Mexico, in the regional geologic framework of south-central New Mexico: Socorro, N.Mex., New Mexico Institute of Mining and Technology Ph. D. dissertation, 402 p.

Hedlund, D.C., 1974, Age and structural setting of base-metal mineralization in the Hillsboro–San Lorenzo area, southwestern New Mexico [abs.], *in* Siemers, C.R., Woodward, L.A., and Callender, J.F., eds., Silver Anniversary Guidebook; Ghost Ranch; North-Central New Mexico: New Mexico Geological Society Guidebook 25, p. 378–379.

Hedlund, D.C., 1977a, Geologic map of the Hillsboro and San Lorenzo quadrangles, Sierra and Grant Counties, New Mexico: U.S. Geological Survey Miscellaneous Field Studies Map MF–900–A, scale 1:48,000.

Hedlund, D.C., 1977b, Mineral resources map of the Hillsboro and San Lorenzo quadrangles, Sierra and Grant Counties, New Mexico: U.S. Geological Survey Miscellaneous Field Studies Map MF–900–B, scale 1:48,000.

Herring, J.R., Marsh, S.P., and McLemore, V.T., 1998, Major and trace element concentrations and correlations in mine dump samples from mining districts in Sierra, Socorro, and Otero counties, south-central New Mexico—Mockingbird Gap, Lava Gap, Salinas Peak, Goodfortune Creek, Bearden Canyon, and Sulfur Canyon mining districts of the northern San Andres Mountains, Sierra and Socorro County; Lake Valley mining district of Sierra County; and Tularosa and Orogrande mining districts of Otero County: U.S. Geological Survey Open-File Report 98-486, 21 p.

Hildenbrand, T.G., 1983, FFTFIL—A filtering program based on two-dimensional Fourier analysis of geophysical data: U.S. Geological Survey Open-File Report 83-237, 30 p.

International Association of Geodesy, 1971, The Geodetic Reference System, 1967: International Association of Geodesy Special Publication 3, 116 p.

Jicha, H.L., Jr., 1954, Geology and mineral deposits of Lake Valley quadrangle, Grant, Luna, and Sierra Counties, New Mexico: New Mexico Bureau of Mines and Mineral Resources Bulletin 37, 93 p.

Jones, F.A., 1904, New Mexico mines and minerals: Santa Fe, N. Mex., New Mexican Printing Company, 349 p.

Keller, G.V., and Frischknecht, F.C., 1966, Electrical methods in geophysical prospecting: New York, Pergamon Press, 519 p.

Kelly, S.A., and Chapin, C.E., 1997, Cooling histories of mountain ranges in the southern Rio Grande rift based on apatite fission-track analysis—A reconnaissance survey: New Mexico Geology, v. 19, no. 1, p. 1–14.

Kelly, V.C., and Silver, Caswell, 1952, Geology of the Caballo Mountains: University of New Mexico Publications in Geology 4, 286 p.

Keyes, C.H., 1908, Genesis of the Lake Valley, New Mexico, silver deposits: Transactions of the American Institute of Mining and Metallurgical Engineers, v. 39, p. 139–169.

Klein, D.P., and Wise, R.A., 1998, Geoelectric measurements across Lake Valley fault: U.S. Geological Survey Open-File Report 98-334, 74 p.

Kleinkopf, M.D., 1997, Interpretations of regional geophysical anomalies applied to mineral resources studies in southern New Mexico: Geological Society of America Abstracts with Programs, v. 29, no. 2, p. 18.

Korzeb, S.L., Kness, R.F., Geroyan, R.I., and Ward, D.A., 1995, Mineral resource assessment of the Caballo Resource Area, Sierra and Otero Counties, New Mexico: U.S. Bureau of Mines Open-File Report MLA 5-95, 177 p.

Laudon, L.R., and Bowsher, A.L., 1949, Mississippian formations of southwestern New Mexico: Geological Society of America Bulletin, v. 60, p. 1–87.

Le Bas, M.J., LeMaitre, R.O., Streckeisen, A., and Zanetkin, B., 1986, A chemical classification of volcanic rocks based on the Total Alkali-Silica diagram: Journal of Petrology, v. 27, p. 745–750.

Lindgren, W., Graton, L.C., and Gordon, C.H., 1910, The ore deposits of New Mexico: U.S. Geological Survey Professional Paper 68, 361 p.

Lovering, T.G., 1972, Jasperoid in the United States; its character, origin, and economic significance: U.S. Geological Survey Professional Paper 710, 164 p.

Lovering, T.G., and Heyl, A.V., 1989, Mineral belts in western Sierra County, New Mexico, suggested by mining districts, geology, and geochemical anomalies: U.S. Geological Survey Bulletin 1876, 49 p.

MacDonald, G.A., and Katsura, T., 1964, Chemical composition of Hawaiian lavas: Journal of Petrology, v. 5, pt. 1, p. 82–133.

MacDonald, N., 1909, Discussion of the paper of Charles R. Keyes, p. 139: American Institute of Mining Engineers Transactions, v. 39, p. 850–856.

McIntosh, W.C., Kedzei, L.L., and Sutter, J.F., 1991, Paleomagnetism and $^{40}Ar/^{39}Ar$ ages of ignimbrites, Mogollon-Datil volcanic field, southwestern New Mexico: New Mexico Bureau of Mines and Mineral Resources Bulletin 135, 79 p.

McIntosh, W.C., Chapin, C.E., Ratté, J.C., and Sutter, J.F., 1992, Time-stratigraphic framework for the Eocene-Oligocene Mogollon-Datil volcanic field, southwest New Mexico: Geological Society of America Bulletin, v. 104, p. 851–871.

McLemore, V.T., 1996, Volcanic-epithermal, precious-metals deposits in New Mexico, *in* Coyner, A.R., and Fahey, P.L., eds., Geology and Ore Deposits of the American Cordillera: Geological Society of Nevada Symposium Proceedings, Reno/Sparks, Nevada, April 1995, p. 951–969.

McLemore, V.T., 1998, Insights into origin of carbonate-hosted Ag and Pb-Zn replacement deposits in the Black Range, Sierra and Grant Counties, New Mexico [abs.]: New Mexico Geology, v. 20, p. 49.

McLemore, V.T., 2001, Silver and gold occurrences in New Mexico: New Mexico Bureau of Mines and Mineral Resources Resource Map 21. Scale 1:1,000,000.

Miesch, A.T., 1976, Sampling designs for geochemical surveys—Syllabus for a short course: U.S. Geological Survey Open-file Report 76-772, 127 p.

Morelli, Carlo, Gantar, C., Honkasla, Tauno, McKonnel, R.K., Tanner, J.G., Szabo, Bela, Uotila, U.A., and Whalen, G.T., 1974, The international gravity standardization net 1972 (I.G.S.N.): Paris, Bureau Central de l'Association Internationale de Geodesie Special Publication 4, 194 p.

North, R.M., and McLemore, V.T., 1986, Silver and gold occurrences in New Mexico: New Mexico Bureau of Mines and Mineral Resources Resource Map 15, 32 p.

North, R.M., and McLemore, V.T., 1988, A classification of the precious metal deposits of New Mexico, *in* Bulk mineable precious metal deposits of the western United States Symposium Volume: Geological Society of Nevada, Symposium Proceedings Volume, p. 625–659.

Northrop, S.A., 1959, Minerals of New Mexico: Albuquerque, N. Mex., University of New Mexico Press, 665 p.

Northrop, S.A., 1996, Minerals of New Mexico, 3rd Edition: Albuquerque, N. Mex. University of New Mexico Press, 356 p.

Nutt, C.J., O'Neill, J.M., McLemore, V.T., Lindsey, D.A., Ratté, J.C., Hedlund, D.C., Klein, D.P., and Kleinkopf, M.D., 1998, Geology of the Lake Valley area, Sierra County, New Mexico and geophysical evaluation of Lake Valley area: U.S. Geological Survey Open-File Report 98-347, 70 p.

Poole, F.G., Stewart, J.H., Palmer, A.R., Sandberg, C.A., Madrid, R.J., Ross, R.J., Jr., Hintze, L.F., Miller, M.M., and Wrucke, C.T., 1992, Latest Precambrian to latest Devonian time—Development of a continental margin, *in* Lipman, P.W., and Zoback, M.L., eds., The geology of North America: Geological Society of America, v. G–3, p. 9–56.

Schneider, R.V., and Keller, G.R., 1994, Crustal structural of the western margin of the Rio Grande rift and Mogollon-Datil volcanic field, southwestern New Mexico and southeastern Arizona, *in* Keller, G.R., and Cather, S.M., eds., Basins of the Rio Grande rift—Structure, stratigraphy, and tectonic setting: Geological Society of America Special Paper 291, p. 220–226.

Seager, W.R., 1986, Reconnaissance geologic map of the Hillsboro and San Lorenzo 15-minute quadrangles, Grant and Sierra Counties, New Mexico: New Mexico Bureau of Mines and Mineral Resources Open-File Report 400.

Seager, W.R., Clemons, R.E., Hawley, J.W., and Kelley, R.E., 1982, Geology of northwest part of the Las Cruces 1° × 2° sheet (scale 1:250,000), New Mexico: New Mexico Bureau of Mines and Mineral Resources Geologic Map 53, scale 1:250,000.

Seager, W.R., and Hawley, J.W., 1973, Geology of the Rincon quadrangle, New Mexico: New Mexico Bureau of Mines and Mineral Resources Bulletin 101, 42 p.

Seager, W.R., Mack, G.H., Raimonde, M.S., and Ryan, R.G., 1986, Laramide basement-cored uplift and basins in south-central New Mexico, *in* Clemmons, R.E., King, W.E., and Mack, G.H., 1986, eds., Truth or Consequences region: New Mexico Geological Society Guidebook 37, p. 123–130.

Seager, W.R., Shafiqullah, M., Hawley, J.W., and Marvin, R.F., 1984, New K-Ar date from basalts and the evolution of the southern Rio Grande rift: Geological Society of America Bulletin, v. 95, p. 87–99.

Silliman, B., 1882, The mineral regions of southern New Mexico: Transactions of the American Institute of Mining and Metallurgical Engineers, v. 10, p. 440–443.

Strangway, D.W., Swift, C.M., Jr., and Holmer, R.C., 1973, The application of audio-frequency magnetotellurics (AMT) to mineral exploration: Geophysics, v. 38, p. 1159–1175.

Telford, W.M., Geldart, L.P., and Sheriff, R.E., 1990, Applied geophysics, 2nd Edition: Cambridge, United Kingdom, Cambridge University Press, 770 p.

Turekian, K.K., and Wedepohl, K.H., 1961, Distribution of elements in some major units of the Earth's crust: Geological Society of America Bulletin, v. 72, p. 175–192.

Vozoff, Keeva, 1972, The magnetotelluric method in the exploration of sedimentary basins: Geophysics, v. 37, p. 98–141.

Vozoff, Keeva, 1991, The magnetotelluric method, *in* Nabigian, M.N., ed., Electrical methods in applied geophysics, Volume 2, Applications, Part A, Chapter 8: Tulsa, Okla., Society of Exploration Geophysicists, p. 641–712.

Young, E.J., and Lovering, T.G., 1966, Jasperoids of the Lake Valley mining district, New Mexico: U.S. Geological Survey Bulletin 1222–D, p. D1–D27.

USGS
science for a changing world